Theory and Analysis of Thermally Stimulated Discharge Currents in Pure Ice

Robert A Will
Geoscience Department
New Mexico Institute of
Mining and Technology

Faculty Advisor : Dr. Gerardo W. Gross

Table of Contents

APPENDIX I - Test Procedures

APPENDIX II - Inversion Procedures

APPENDIX III - Foil effects

APPENDIX IV - Test Data

ABSTRACT

Theory of Thermally Stimulated Discharge (TSD) is presented. TSD currents from first order dipolar relaxation mechanism and space charge drift are discussed. Methods of experimentation and anylitical determination of trapping parameters E, τ_o , P_o , and dielectric constant ϵ_s are outlined.

Results from pure ice show three to four peaks in the temperature range from 100° K to 200° K. Generalized eigenvalue-eigenvector fitting of these curves yields activation energies 7.24 kcal/mole, 8.23 kcal/mole, and 9.83 kcal/mole for peaks at 128° K, 135° K and 145° K respectively. Anomalous results obtained from a single sample show only two peaks at 125 ° K and 145° K with activation energies 7.03 kcal/mole and 10.4 kcal/mole respectively. Interpretation of discrepancies indicate strong shifting of the 135° K peak in anomalous results. Possible mechanisms are discussed.

1-INTRODUCTION

Thermally Stimulated Discharge (TSD) currents have been utilized as a means of investigating charge transport and storage properties of polymers since the creation and study of the first "electret" by Eguchi (1925). The time temperature superposition theory applied, by Gross (1968), to the well known Debye equation yields solutions which describe TSD response of dielectric mechanisms in terms of the characteristic trapping parameters τ_o, E, and ϵ_s. These parameters may be determined from a single TSD test as opposed to the repeated isothermal electrical bridge measurements required for the same determination.

TSD is particularly useful in studying the dielectric properties of ice at very low temperatures (90K-250K). At these temperatures charge storage mechanisms such as dipolar orientation and space charge migration combine to give ice a large dielectric constant . Data taken from pure ice exhibits 3 to 4 discrete relaxation mechanisms showing high repeatability. Relaxation fre-

quencies in this temperature range however are very low , on the order of .01 Hz and lower. Electrical bridge measurements may not be performed reliably at these frequencies. In addition, the TSD response curves from these mechanisms overlap strongly in most samples tested. Such overlapping makes routine analysis of TSD curves by standard methods impossible. These data require special tests and analytical methods for accurate trapping parameter determination.

In this paper, methods of experimentation and analysis of TSD currents are reviewed. The theory of first order dipole relaxation is presented as well as graphical and analytical methods of determining trapping parameters from TSD curves. Linear inverse fitting has been applied to data from pure ice using methods discussed by Jackson (1972).

2-THEORY

2-1 Dielectric Polarization

Persistent charge may be frozen into an electret as the result of more than a single mechanism. The most prominent mechanisms are dipolar orientation and space charge migration. These two mechanisms differ markedly from each other ; in the case of dipolar orientation the individual molecules in the material act as miniature electric dipoles, while space charge polarization is due to actual migration of free charge carriers accompanied by subsequent build-up at sample boundaries. The latter presents complications to the study of both orientation and migration mechanisms.

Before beginning a discussion of TSD it is instructive to outline a few basic properties of a capacitor filled with a dielectric and to note some of the dynamical properties pertinent to the creation of electrets.

Figure 1 illustrates the distribution of charge induced on

the plates of a capacitor under an electrical potential, and the effect of introducing a dielectric material between the plates. The surface charge density on the capacitor in vacuum is

$$\sigma_o = \frac{Q}{A}$$

where

σ_o = surface charge density

Q = charge on plates

A = surface area of one plate

When the dielectric medium is introduced between the plates and the applied voltage held constant, the surface charge density increases to

$$\sigma = \epsilon_s \sigma_o$$

where

ϵ_s = static dielectric constant

The charge on the plates of the capacitor therefore has components caused by the external field E_p and the internal polarization (P). With the introduction of two more relations in electrostatics

$$E_p = 4\pi\sigma_o$$

and

$$D = 4\pi\sigma$$

where

D = displacement [current] density

polarization can be defined as

$$\sigma_o + P_s = \sigma$$

where

P_s = polarization induced on the plates of the capacitor due to a dielectric medium

It follows that

$$E_p + 4\pi P = D$$

$$D = \epsilon_s E_p$$

then

$$\epsilon_s - 1 = \frac{(4\pi P_s)}{E_p} \qquad (2\text{-}1)$$

Here the dielectric constant is defined in terms of the induced polarization.

It must be pointed out that polarization, as defined above, represents the total charge induced on the plates as the result of a variety of mechanisms. Some polarization mechanisms react to changes of an applied field virtually instantaneously while the mechanisms to be presented here react at a hindered rate due to kinetic effects.

From equation 2-1 it can be seen that changes in applied field must be accompanied by a change in polarization in order to maintain equilibrium. One simple assumption which has been made concerning the rate of change of polarization as it approaches equilibrium is that the speed of approach is proportional to the displacement from equilibrium.

$$\frac{dP(t)}{dt} = \frac{P_s - P(t)}{\tau} \qquad (2\text{-}2)$$

where

τ = relaxation time

This expression was originally derived for constant temperatures, however it has been assumed, with great success, that the temperature dependence of τ may be introduced and the equation solved for non isothermal systems (van Turnhout[1975], p. 27).

As stated above, a portion of the polarization adjusts instantaneously to changes in applied field and cannot be considered in equation 2-2. A modification of equation 2-1 yields

$$\epsilon_s - 1 = \frac{4\pi(P_d - P_\infty)}{E_p}$$

$$\varepsilon_s - \varepsilon_\infty = \frac{4\pi(P_d - P_\infty)}{E_p}$$

where

P_d = static polarization

P_∞ = optical (high frequency) polarization

and

$$\epsilon_\infty - 1 = \frac{4\pi P_\infty}{E_p}$$

where

ϵ_∞ = high frequency limit of dielectric constant

Now equation 2-2 transforms to

$$\tau\frac{dP(t)}{dt} + P(t) = (\epsilon_s - \epsilon_\infty)\frac{E_p(t)}{4\pi} \qquad (2\text{-}3)$$

This is the most useful form of the Debye equation for application to TSD.

2-2 Mechanisms of Polarization

Polarization in a dielectric can be attributed to four processes: electronic and atomic displacement polarization, orientational displacement of dipoles, and space charge migration(Haering and Adams[1960])). Of the four, only the latter two contribute to persistent charge storage in electrets. Both electronic and atomic polarization are due to small-scale distortions and displacements in the molecular structure. Although they may contribute to the bulk polarization, their rates of decay are very high and independent of temperature.

Space-Charge Polarization

Most dielectrics exhibit a low level conductivity even though the number of electrons in the conduction band is negligible. Migration of electrons in response to an applied field is called space charge drift, or space charge limited (SCL) drift. Figure 2 shows a simplistic representation of the bulk effect of space charge migration. This figure should be compared with Figure 1 in which the distribution is more representative of dipole orientation. An important aspect of space charge is illustrated here. Since excess charge accumulates at the boundaries of the dielectric, the local field is altered with respect to the charge carriers. The proximity of like charges in this region becomes, in itself, a driving potential active in the process of accumulation and relaxation of space charge (van Turnhout[1975]). Motion of this excess charge is therefore both time and space dependent.

It is for this reason that the analysis of space charge polarization is somewhat more complex than that of orientational polarization.

Dipole Orientation

In general, the most stringent requirement for a molecule to possess a dipole moment is that it must be charge-assymetrical. If a molecule (or complex polymer chain) presents a high degree of symmetry it will not have a significant dipole moment. This distinction is important in light of the fact that some non-polar molecules, under the influence of a very high electric field, may distort in shape and show electron and atomic polarizability which do not contribute to the electret effect.

Figure 3 shows a water molecule and its simplification as an electric dipole. The simplification of the molecule to an elementary dipole has proven to be valid given certain accompanying assumptions, the most important of which is that dipoles in an electric field do not interact with each other. This is to say that the local electric field is not altered by orientation of the surrounding dipoles. Further, when displaced from equilibrium with respect to an applied field, the dipole will approach equilibrium at a characteristic rate. The relaxation time for a dipole displaced from equilibrium is

$$\tau(T) = \tau_o \exp(\frac{E}{kT})$$

where

E = activation energy of rotation

2-3 Theory

Equation 2-3 will now be discussed under the conditions describing the usual TSD experiment (short circuit and linear temperature increase).

Assume that a dielectric material has been exposed to an external high voltage (on the order of 1 KV/cm) for a time that is much longer than the estimated τ at the temperature of formation. It can then be assumed that all dipoles have reached equilibrium orientation. The dipoles are frozen in and the voltage is removed.

Setting $E_p(t) = 0$, equation 2-3 becomes

$$\frac{dP(t)}{dt} = -s(T)P(t)$$

where

$$s(T) = \frac{1}{\tau(T)}$$

Rearranging

$$\frac{dP(t)}{P(t)} = -s(T)dt \qquad (2\text{-}4)$$

and integrating both sides

$$\ln[P(t)]_o^t = -s_o \int_o^t \exp(\frac{-E}{kT})dt.$$

Let $B = \frac{dT}{dt}$

$$\frac{P(t)}{P_o} = \exp\{\frac{-s_o}{B}\int_o^T \exp(\frac{-E}{kT})dT\}$$

and

$$P(t) = P_o \exp\{\frac{-s_o}{B}\int_o^T \exp(\frac{-E}{kT})dT\} \qquad (2\text{-}5)$$

P_o is also defined by the relation

$$P_o = \frac{N_{dip} p^2 E_p}{3kT_p} \qquad (2\text{-}5a)$$

where

N_{dip} = number of dipoles

p = average dipole moment

E_p = forming field

T_p = forming temperature

The static dielectric constant can also be determined from the relation

$$\epsilon_s = \frac{P_o}{\epsilon_o E_p} + \epsilon_\infty \qquad (2\text{-}5b)$$

where

ϵ_o = permittivity of free space = 8.854×10^{-14} F/cm

E_p = forming field

The discharge current density is equal to the rate of change of polarization.

$$j(t) = \frac{dP(t)}{dt}$$

where

$j(t)$ = discharge current density

Then from equations 2-4 and 2-5

$$j(t) = -P_o s(T) \exp\{\frac{-s_o}{B}\int_o^T \exp(\frac{-E}{kT})dT\} \qquad (2\text{-}6)$$

Some important characteristics of this function have been summarized by Garlick and Gibson (1948).

(i) For given s_o, P_o and B, T_m is proportional to E where T_m is the temperature at which j(T) reaches a maximum

(ii) For given E and P_o, T_m varies with s_o and B

(iii) The area under the discharge curve is proportional to P_o

(iv) The initial rise portion of the curve can be approximated by

$$\ln[i] = \text{Constant} - \frac{E}{kT} \qquad (2\text{-}7)$$

Property (iv) is used commonly in routine TSD analysis.

Figures 4-7 illustrate the dependency of this function on E, τ_o, P_o, and B.

Another useful relation can be derived which utilizes the dependence of T_m on B. To obtain an expression for the condition at T_m first take the derivative of equation 2-6 with respect to temperature

$$\frac{di(T)}{dT} = P_o s_o \{[\exp(\frac{-s_o}{B}\int \exp(\frac{-E}{kT})dT)(\frac{E}{kT^2})\exp(\frac{-E}{kT}]$$

$$+ \exp(\frac{-E}{kT})[\frac{-s_o}{B}\exp(\frac{-E}{kT})\exp(\frac{-s_o}{B}\int \exp(\frac{-E}{kT})dT)]\}$$

Simplifying and setting equal to 0 for the condition at T_m

$$\frac{di(T)}{dT} = \frac{E}{kT_m^2} - \frac{s_o}{B}\exp(\frac{-E}{kT_m}) = 0$$

then

$$T_m = \{\frac{EB\tau(T_m)}{k}\}^{1/2}$$

From this result, with E given by the initial rise approximation, the pre-exponential factor s_o can be calculated.

$$s_o = \frac{BE\exp(\frac{E}{kT_m})}{kT_m^2} \qquad (2\text{-}7a)$$

Once s_o is known P_o may be calculated from the intercept of the initial rise graph using equation 2-5b.

Additional formulation for the relaxation time can be derived in the following way. From equation 2-6

$$\tau(T) = \frac{-P(t)}{i(t)} = \frac{-P_o \exp\left(\frac{-s_o}{B}\int_0^T \exp\left(\frac{-E}{kT}\right)dT\right)}{-P_o s(T) \exp\left(\frac{-s_o}{B}\int_0^T \exp\left(\frac{-E}{kT}\right)dT\right)}$$

Then

$$\ln[\tau(T)] = \ln[P(t)] - \ln[i(t)] \quad . \qquad (2\text{-}8)$$

Since

$$P(t) = \frac{Q(t)}{A}$$

$$Q(t) = \int_o^t i(t)dt$$

$$P_o = \frac{\int_o^\infty i(t)dt}{A} \qquad (2\text{-}8a)$$

where

Q(t) = instantaneous charge held on the capacitor plates by induction

and

$$j(t) = \frac{i(t)}{A}$$

$$\ln[\tau(T)] = \ln[\int_{t}^{\infty} i(t)dt] - \ln[i(t)] \qquad (2\text{-}9)$$

Again, the relation

$$\tau(T) = \tau_o \exp(\frac{E}{kT})$$

when applied to equation 2-9 will yield a straight line of slope E. This relation provides a useful means of verifying results obtained from initial rise and heating rate methods. Equation 2-9 also produces a continuous set of values for τ (T) over the entire temperature range covered by the discharge curve.

For purposes of calculating theoretical discharge curves the approximation formulated by Hastings(1955) and applied by van Turnhout(1975) was used where

$$j(t) = j(T) = \frac{P_o}{\tau_o} \exp(\frac{-E}{kT}) \exp(\frac{-\eta(T)}{\tau_o}) \qquad (2\text{-}10)$$

where

$$\eta(T) = \frac{kT^2}{BE} \exp(\frac{E}{kT}) H(\frac{E}{kT})$$

where

$$H(\frac{E}{kT}) = \{b_1 - a_1 + (b_2 - a_2)kT/E\}(1 + b_1 kT/E + b_2 k^2 T^2/E^2)^{-1}$$

$$a_1 = 2.334733$$

a_2= .250621

b_1= 3.330657

b_2= 1.681534

3-APPARATUS

3-1 Sample Preparation

Samples used in this research were disks of pure ice approximately 1/2 " in thickness and 1 1/2 " in diameter grown and cut using methods described by Gross et. al. (1975),and Gross et. al. (1978). Sample surfaces were polished carefully to assure that they were smooth and parallel. Sample thickness was measured to the nearest .001 ", most showing less than .005 " deviation in thickness over the entire surface. Of course all sample preparation was performed at temperatures well below freezing and care was taken to avoid contamination.The samples discussed in the main body of this work were all taken from from one nearly single crystal ice column grown from pure (distilled and subsequently de-ionized) water.

3-2 Sample Cell-Heating Circuit

The ice sample is placed between two copper electrodes in the aluminum sample holder shown in Figure 8. The sample holder

is then placed into a larger aluminum block (Figure 8) and this entire apparatus enclosed in a stainless steel cryogenic chamber where it is cooled with liquid nitrogen.

Heating of the sample during TSD is accomplished by three feedback-controlled heating elements. It was discovered that, in order to maintain control of sample temperature without oscillation of the temperature about the controller setpoint, the sample must be enclosed in sufficient mass to provide inertia to the heating process. Given this large mass, a heating element distribution was chosen that gave the most uniform radial heat distribution and the highest degree of sensitivity to the control system. Two of these elements are cartridge heaters located in the sample holder on either side of the sample. The third is a heater coil wrapped around the larger aluminum block. These heating elements are all connected in parallel. Control is maintained by a Love Model 52 proportional controller. Heating rates may be programmed .044 Deg/sec and lower. Early problems of a severe temperature gradient across the sample were solved through minor modification of the electrodes. Pre-existing plastic electrode holders were replaced with nearly identical ones made of aluminum. The result was an increased, and more balanced flow of heat from the sample cell walls to the electrodes. The maximum temperature measured across the sample using this new design is about 4^{o} during a 0.044^{o}/sec heating rate test. This gradient decreases with lower heating rates.

In addition to uniform heating, it is often also necessary to be able to cool the sample very rapidly. This is made very difficult by the large mass of the system as required for temperature control. Cooling of the massive aluminum block externally with liquid nitrogen could only provide maximum cooling rates of a few degrees per hour. This problem was remedied by aiming at the wall of the sample cell a direct flow of liquid nitrogen under pressure . Cooling rates of 10-15^{o}/sec have been made possible through addition of this flow. TSD test procedures using this modified apparatus are outlined in Appendix I.

Charging-Discharging System

The charging system consists of a high voltage D.C. power supply providing voltages from 500 to 2000 volts. Blocking electrodes are used even though the conductivity of pure ice is negligible. For this study all tests were run using blocking electrodes made from Teflon coated with copper on one side. The sample is sandwiched between two such discs and placed in the sample cell between the copper electrodes. High voltage coaxial cables connect to electrodes on top of the sample cell and extend out of the cooling vessel to the charging system.

For measuring discharge, the electrode circuit is switched over to a Keithly Model 173 picoammeter capable of measuring currents as low as 1.0×10^{-13} A. Peak currents measured in this study are on the order of 5.0×10^{-9} A. Minimum currents meas-

ured of about 1.0×10^{-12} A lie very close to the noise level of the system. Coaxial leads connecting the electrodes to the electrometer must be grounded carefully and secured from movement so that spurious currents will not be induced in the measuring circuit due to capacitive coupling between leads.

3-4 Data Acquisition

Sample temperature is measured for recording by two type T (copper- constantan) thermocouples located in small holes in the electrodes. The controller uses a type E (cromel-constantan) thermocouple. Both electrode temperatures and discharge current are digitized and recorded by means of a Burr Brown SDM-853 analog to digital converter, a Gulton ANP-9 thermal printer and a Honeywell strip chart recorder. As a safety precaution, for both equipment and personnel, electrode thermocouples are isolated from the recording equipment through buffer amplifiers.With this apparatus digital current vs. temperature data may be recorded at a rate of 6 readings per minute simultaneously with continuous graphical output.

4-INVERSION

In this chapter the theory of the generlized least squares inversion will be developed. The stastical parameters used to evaluate the uniqueness and closeness of the final model to the data will be discussed. Programs used in this study, and procedures for their use are outlined in Appendix II.

4-1 Classical Least Squares Method

The basic approach of the least squares method is to 1) guess at an initial model ,and 2) minimize differences between this model and data by calculating appropriate adjustments to the initial model parameters. Given a function of one independent variable, T, also containing m model parameters, x_i , such that

$$j(T) = f(T, x_1, x_2, x_3, \ldots . x_m)$$

The function may be expanded in a Taylor series about some point

$$j(T_i) = j_o(T_i) + \sum_{k=1}^{m} \frac{\partial j_o}{\partial x_k}(x_k - x_k^o) + \frac{1}{2} \sum_{j=1}^{m} \sum_{k=1}^{m} \frac{\partial j}{\partial x_k} \frac{\partial j}{\partial x_j}(x_k - x_k^o)(x_j - x_j^o) + \ldots .$$

If the function is assumed to be linear with respect to the parameters ,higher order terms may be neglected and

$$j(T_i) = j_o(T_i) + \sum_{k=1}^{m} \frac{\partial j_o(T_i)}{\partial x_k}(x_k - x_k^o)$$

where

x_k^o = intial estimation of the k th parameter

x_k = true k th parameter

Rearranging

$$\Delta J = A\Delta x + \epsilon \qquad (4\text{-}1)$$

where

ΔJ = an n component vector containing all Δj_i.

where $\Delta j_i = j(T_i)^{obs} - j_o(T_i)$.

A = an m x n matrix containing the derivatives.

Δx = an m component vector containing all $(x_k - x_k^o)$.

ϵ = vector containing higher order terms and errors.

In this case

$$A = \begin{bmatrix} \frac{\partial j_\circ(T_1)}{\partial E_A} & \frac{\partial j_\circ(T_1)}{\partial \tau_p} & \frac{\partial j_\circ(T_1)}{\partial P_o} \\ \frac{\partial j_\circ(T_2)}{\partial E_A} & \frac{\partial j_\circ(T_2)}{\partial \tau_o} & \frac{\partial j_\circ(T_2)}{\partial P_o} \\ \vdots & \vdots & \vdots \\ \frac{\partial j_\circ(T_n)}{\partial E_A} & \frac{\partial j_\circ(T_n)}{\partial \tau_0} & \frac{\partial j_\circ(T_n)}{\partial P_o} \end{bmatrix} \qquad (4\text{-}1a)$$

If m=n (i.e., there are as many data points as model parameters) the new parameters may be found from direct inversion of equation 4-1.

v.ce $\Delta x = A^{-1}\Delta J$

if A^{-1} exists

and

$$x_{new} = A^{-1}\Delta J + x_o$$

However, if $m \neq n$, the problem must first be "squared up". In other words, an operator must be found such that

$$\Delta x = H\Delta J$$

This is accomplished by applying the classical least squares

approach to equation 4-1. The set of error residuals is given by

$$\epsilon = \Delta J - A\Delta x$$

The square of the residuals is

$$R^2 = \epsilon^t\epsilon = (\Delta J - A\Delta x)^t(\Delta J - A\Delta x).$$

Expanding this expression and simplifying in matrix form

$$\Delta x = (A^tA)^{-1}A^t\Delta J \qquad (4\text{-}1b)$$

if $(A^TA)^{-1}$ exists.

It is easily shown that for the case where n=m

$$(A^tA)^{-1} = A^{-1}(A^t)^{-1}$$

and thus

$$\Delta x = A^{-1}\Delta J$$

as before.

Parameters derived to evaluate the inversion are the R matrix and the scalar R_f. The R matrix

$$R = HA = (A^tA)^{-1}A^tA \qquad (4\text{-}2)$$

is used to examine the uniqueness of the solution [Jackson(1972)]. The mth row of the n x m matrix contains information concerning the uniqueness of the mth parameter. Inspection of

equation 4-2 shows that the R matrix is the identity matrix, which shows that the least squares solution is a unique solution. The rows of the R matrix are called resolving kernels.

The scalar R_f (fitting parameter) is defined by

$$R_f = \left[\frac{1}{n}\sum_{i=1}^{n}\left(\frac{\Delta j_i}{\sigma_i}\right)^2\right]^{\frac{1}{2}} \qquad (4\text{-}3)$$

and is a statistical measure of the resulting fit

where

σ_i = data point uncertainty.

It is desirable to have $R_f \approx 1$ which implies that the average deviation of the new model from the data is approximately equal to the uncertainty in the data.

Problems arise in the least squares process in the event that the matrix A^tA cannot be inverted. Singularity of the A^tA matrix may occur for two reasons;

1) The matrix is analytically singular.

2) The matrix is numerically singular with respect to the computing algorithm.

Matrices which are nearly singular cause instability in the

inversion process in that calculated adjustments applied to the initial parameters may become disproportionately large. For problems of this nature the generalized eigenvalue-eigenvector decomposition is a useful method of stabilizing the inversion.

4-2 Generalized Eigenvalue-Eigenvector Decomposition

In cases where the matrix A^tA cannot be inverted, the eigenvalue-eigenvector decomposition method allows one to remedy problems of ill conditioning by using a-priori information. Components of the problem may be deleted from consideration resulting in more reasonable adjustments to the initial parameters.

A natural inverse is formed and the problem is reformulated in terms of the eigenvalues and eigenvectors of A^tA

$$\Delta x = V\Lambda^{-1}U^t\Delta J = B\Delta J \qquad (4\text{-}4)$$

where

V = m x m matrix containing the eigenvectors of A^tA

Λ = an m x m diagonal matrix containing the eigenvalues of A^tA

$U = AV\Lambda^{-1}$

B is therefore analogous to the H matrix in the least squares method. Instability in the inversion may be studied and corrected through proper use of the eigen-components. It can be seen in equation 4-4 that the magnitude of the correction of x_i will be inversely proportional to the magnitude of the m th eigenvalue. If the eigenvalues vary by several orders of magnitude the corrections applied by the smaller eigenvalues will be very large and the inversion therefore unstable. Small eigenvalues and their associated vectors may be dropped from consideration and equation 4-4 becomes

$$\Delta x = V_p \Lambda_p^{-1} U_p^t \Delta J = B \Delta J \qquad (4-4a)$$

where

p = number of eigen-components used

It is often convenient to determine stability of the problem in terms of the maximum acceptable ratio of eigenvalues used. In many cases $\frac{\lambda_{max}}{\lambda_{min}} \leq 100$ is a reasonable estimate for initial modeling attempts. However, this exact criterion may also be dependent on both the machine, and the algorithm used to perform the matrix decomposition.

In terms of the eigen-components, the resolving matrix

$$R = BA = V\Lambda^{-1}U^{t}A.$$

Resulting parameter standard deviations are computed from the relation

$$\sigma(x_k) = \sum_{j=1}^{p} \left(\frac{v_{kj}}{\lambda_j}\right)^2.$$

The effect of dropping eigencomponents from consideration can be seen through inspection of the eigenvalues. The jth column contains the m components of the vector associated with the jth eigenvalue. The ith component of each vector corresponds to the ith model parameter. The relative magnitudes of these components reveal the relative contribution of the eigenvalue to the determination of the new model parameters. If an eigenvalue-vector is omitted from consideration a certain amount of information about all parameters provided by the data is lost. It can be easily shown that if p=m (all eigencomponents kept) the solution to equation 4-4 is the same as the least squares solution. If p=0 (no eigen-components used) the initial parameters are unaffected. It must be stressed that in dropping eigen-components, added confidence is given to the initial model. When eigen-components are deleted, a trade-off is made between the relative contributions of the data and initial model to the final parameters. Parameters derived to evaluate this trade-off are formulated

$$r_k^p = \sum_{i=1}^{m} \left(\sum_{j=1}^{p} v_{kj} v_{ij} - \delta_{ki} \right)^2 . \qquad (4\text{-}5)$$

An r_k of 1 indicates total data dependence in the final value of the kth parameter. Inversely, r_k=0 indicates that the resulting parameter is totally dependent on the initial model and the inversion has no effect on that parameter. Equation 4-5 shows that as data dependence is lost (i.e eigen-components deleted) new parameter standard deviation is lowered.

RESULTS

5-1 Explanation of Results

The typical TSD of pure ice consists of 3 to 4 overlapping peaks, of the form of equation 2-10, with apparent maxima at approximately 125° K, 140° K, 155° K, and 190° K. These maxima are each shifted to some degree from their true position by the superposition. Of these 4 peaks the 3 largest, occuring in the temperature range from 100° K to 170° K, were focused on for analysis. For convenience these peaks will be referred to as A, B, and C from coldest to warmest, respectively. The strong overlapping of these peaks has made it very difficult to apply any of the routine methods of analysis such as the initial rise approximation (equation 2-7), or equation 2-9. An attempt was made to conduct a series of partial heating tests as discussed by Perlman(1970). However, these tests failed due to inability to change the sample temperature rapidly enough.

For this study two types of tests were used to 1) determine the relative magnitudes and approximate positions of all peaks, and 2) selectively charge individual peaks. The first of these objectives is accomplished by applying the charging potential during slow cooling from 200° K to 100° K. This is called a full charge test and results in charging all polarization mechanisms to saturation at the temperature at which the charging field

is removed (equations 2-5a).

The sample may also be charged at a fixed temperature and rapidly cooled to freeze in the polarization. This is called a partial charging test and can be used as a means of isolating overlapping peaks if $\tau_1(T_{ch}) \ll t_{ch} \ll \tau_2(T_{ch})$. However, attempts to isolate the overlapping peaks in the spectrum of pure ice failed, again, due to the slow response of sample temperature and the proximity of the peak maxima.

All data analyzed in this study are contained in Appendix IV.

5-2 Partial Charging Tests

The partial charging tests listed in Table I were all performed on a single sample (# 308/7-3) showing an anomalous spectrum in which peak B is absent or shifted. This sample was used for extensive study because the two existing peaks are consistent in position with the corresponding peaks A and C of the normal discharge spectrum. In addition, these peaks are almost totally separate, showing only minor overlapping in full charge tests (Figures 29-31). A series of partial charging tests was performed on this sample to determine the activation energies and relaxation times, as well as the temperature dependence of ϵ_s for the polarization mechanisms.

Figures 9 and 10 illustrate the data used for initial rise

approximation of E for these tests. τ_o and P_o were determined using equations 2-7a and 2-8a. These parameters were then used as initial estimates for modeling with the generalized eigenvalue-vector method. These modeling results are listed in Tables II and III. Figures 11-19 illustrate these results. The temperature dependence of ϵ_s for these mechanisms is shown in figure 32.

It must be pointed out that , due to the use of blocking electrodes (Teflon-on-copper disk), the actual forming field is only a small fraction of the applied field (V_{ch}/l_s). See Appendix III for a discussion of the effects of blocking electrodes and TSD curves obtained without blocking layers.

5-3 Full Charging Tests

Having, for the first time, reasonable estimates of trapping parameters for two of the three overlapping peaks, an attempt was made to apply these parameters to a typical full charge test. The function used to model the usual fully charged TSD spectrum was simply the summation of three functions of the form of equation 2-10 such that

$$j(T)_{TOT} = j_1(T)+j_2(T)+j_3(T)$$

where

$j(T)_{TOT}$= Total current

$j_1(T) = j(T,E_1,\tau_{o1},P_{o1})$

$$j_2(T) = j(T, E_2, \tau_{o2}, P_{o2})$$

$$j_3(T) = j(T, E_3, \tau_{o3}, P_{o3})$$

These results are listed in Table IV and illustrated in figures 20-28. All full charge data were modeled using a three peak model. Tests F18-F21 are full charging tests on the sample showing the anomalous discharge spectrum. The results of this modeling are listed in Table IV and illustrated in Figures 29-31.Total static dielectric constant for these peaks are plotted in Figure 32 along with total static dielectric constant from partial charge tests.

Table V contains a summary of average results from full charge tests on normal fully charged samples at B=0.044^{o}/sec , and 0.010^{o}/sec. Table VI contains a summary of results of 3 peak modeling of the fully charged spectrum of sample #308/7-3 at B=0.044^{o}/sec.

5-4 Interpretation of Results - Peak Separation

Activation energy (E)

The normal TSD spectrum from fully charged samples using B=0.044^{o}/sec shows three peaks with activation energies of 7.21 kcal/mole, 8.24 kcal/mole , and 9.89 kcal/mole for peaks A,B, and C respectively. Tests on similarly prepared samples using B=0.010^{o}/sec (see Figures 27 and 28) yield activation energies 7.23 kcal/mole, 8.21 kcal/mole, and 9.99 kcal/mole . Results from

the anomalous spectra indicate two peaks corresponding in position with peaks A and C of the normal spectrum with activation energies of 7.03 kcal/mole and 10.4 kcal/mole. The first of these values is somewhat lower than that obtained for the A peak of the normal fully charged spectra, and the second, significantly higher than that of the normal C peak.This effect could be the result of the shifting of the B peak to warmer temperatures in the anomalous spectrum .However such an assumption would require further support since the anomalous spectra could actually be the result of only two isolated responses.

Pre-exponential factor (τ_o)

Comparison of τ_o from normal and anomalous spectra shows that τ_o differs very little for the A peaks, being only slightly higher in the anomalous spectrum. Unfortunately, in order to achieve stability of the inversion of normal spectra, τ_o for peak C was strongly constrained to the initial model value. It is for this reason that τ_o for normal and anomalous C peaks are nearly equal. τ_o for peak B in normal spectra was also strongly constrained to the initial model "guesstimate" of 5.0×10^{-12}.

Static dielectric constant (ϵ_s)

Total ϵ_s determined from 0.044^o/sec and 0.010^o/sec tests yield approximately equal values of ϵ_s(78.0, 73.8). This result is in agreement with the principle of charge invariance of Gross (1968).Full charge tests on the anomalous spectra yield a

slightly higher value (83.5). If peak A is subtracted from the normal spectrum the resulting ϵ_s is approximately equal to that of peak C of the anomalous spectrum (≈ 40). This further supports the assumption that peak B is present in the anomalous spectra and shifted strongly to higher temperatures.

Comments

In light of the apparent shifting of the B peak in the anomalous spectrum it may be assumed that the A peak of the anomalous spectrum represents an isolated response . It is also believed that this A peak results from the same polarization mechanism and is consistent with that of the normal spectrum. However trapping parameters from peak C of the anomalous spectrum should not be accepted as representing a single isolated mechanism. Results suggest that this peak is caused by total overlapping of peaks B and C which appear consistently in the normal spectrum but are usually separate. Therefore, fitting results for peaks B and C from normal spectra should be accepted.

Table 1

Summary of Tests

Partial Charge Tests

Test #	Sample	T_{ch}	t_{ch}	Fig.
D62A	308/7 #3	123.2	2 hr.	14
D68A	"	128.2	5 hr. 15 min.	15
D69A	"	133.2	2 hr. 10 min.	16
D71A	"	118.2	6 hr. 45 min.	13
D72A	"	113.2	17 hr.	12
D73A	"	108.2	24 hr.	11
D75B	"	153.0	35 min.	17
D76B	"	148.0	1 hr. 20 min.	18
D77B	"	144.0	2 hr.	19

Full Charge Tests

Test #	Sample	Fig.
F3	308/7 #1	20
F5	"	21
F6	"	22
F7	"	23
F9	"	24
F10	"	25
F11	"	26
F16	308/7 #2	27
F17	"	28
F18	308/7 #3	29
F19	"	30
F21	"	31

Table II

Results of Inversion - Peak A

Sample 308/7-3
Peak A

V_{ch} = 1500V, β = 0.044 Deg/Sec

Test	T_{ch} (^{o}k)	E (cal/mole)	τ_o ($\times 10^{-11}$ Sec)	P_o ($\times 10^{-8}$ C/cm^2)	ε_s
D73A	108.2	7050. ± 8.4	3.58 ± .012	7.14 ± .173	61.0
D72A	113.2	7061. ± 8.34	3.56 ± .012	6.87 ± .171	58.8
D71A	118.2	7014. ± 8.42	3.57 ± .012	6.94 ± .172	59.4
D62A	123.2	7010. ± 11.2	3.56 ± .008	5.1 ± .173	41.4
D68A	128.2	6997. ± 13.3	3.56 ± .008	4.28 ± .171	37.8
D69A	133.2	7059 ± 27.5	3.57 ± .004	2.05 ± .172	19.6

Table III
Sample 308/7-3
Results of Inversion - Peak C

Peak C

V_{ch} = 1500V, β = 0.044 Deg/Sec

Test	T_{ch} (^{o}k)	E (cal/mole)	τ_o ($\times 10^{-13}$ Sec)	P_o ($\times 10^{-8}$ C/cm^2)	ε_s
D77B	144.0	10420. ± 90	.957 ± .38	2.75 ± .099	25.3
D76B	148.0	10350. ± 118.0	1.42 ± .48	2.27 ± .11	21.4
D75B	153.0	10420. ± 87.4	1.01 ± .37	1.78 ± .10	17.5

Table IV

Summary of Inversion Results of Full Charge Tests

Tests F3 - F11 sample 308/7-1

Test	β $\left(\frac{\text{Deg}}{\text{Sec}}\right)$	Peak	E $\left(\frac{\text{cal}}{\text{mode}}\right)$	τ_o $(\times 10^{-12}\ \text{Sec})$	P_o $\left(\times 10^{-8}\frac{\epsilon}{\text{cm}^2}\right)$	ϵ_s
F3	0.043	A	7260 ± 5.78	34.5 ± .31	3.99 ± .08	34
		B	8240 ± 13.3	4.97 ± .05	2.71 ± .08	24
		C	9860 ± 14.6	.113 ± 4.6×10^{-18}	1.78 ± .07	16
F5	0.043	A	7130 ± 4.5	35.2 ± .15	4.55 ± .06	38
		B	8190 ± 12.4	4.9 ± .03	2.4 ± .06	21
		C	9900 ± 19.9	.113 ± $4.\times10^{-18}$	1.76 ± .06	16
F6	0.043	A	7160 ± 4.1	35.5 ± .13	4.85 ± .057	40
		B	8290 ± 10.4	5.05 ± .03	2.62 ± .06	23
		C	10000 ± 14.8	.113 ± $1.\times10^{-18}$	1.46 ± .057	11
F7	0.042	A	7230 ± 3.92	36.1 ± .22	5.02 ± .063	42
		B	8300 ± 11.3	4.9 ± .022	2.38 ± .062	21
		C	10100 ± 12.9	.113 ± 1.2×10^{-18}	1.61 ± .051	15
F9	0.043	A	7280 ± 5.75	34.2 ± .22	4.0 ± .073	34
		B	8310 ± 11.35	4.84 ± .035	2.63 ± .69	23
		C	10100 ± 10.9	.113 ± 5×10^{-18}	2.0 ± .053	18
F10	0.043	A	7320 ± 6.14	31.6 ± .17	4.03 ± .065	34
		B	8280 ± 7.1	5.04 ± .05	3.82 ± .063	32
		C	9930 ± 9.5	.113 ± 6.2×10^{-18}	2.34 ± .06	21
F11	0.043	A	7190 ± 8.9	35.0 ± .38	4.43 ± .189	37
		B	8070 ± 22.7	5.0 ± .017	2.55 ± .022	22
		C	9360 ± 87.2	.113 ± 5.5×10^{-18}	1.5 ± .013	14

(continued)

Table IV (continued)

Summary of Inversion Results of Full Charge Tests

Tests F16 - F17 sample 308/7-2

continuation

Tests F18 - F21 sample 308/7-3

Test	Deg/Sec	Peak	E (cal/mode)	τ_o ($\times 10^{-12}$ Sec)	P_o ($\times 10^{-8}$ €/cm^2)	ε_s
F16	0.010	A	7240 ± 17.4	37.7 ± .48	5.24 ± .26	49.7
		B	8160 ± 42.8	5.0 ± .084	1.81 ± .026	19.1
		C	9880 ± 75.4	.113 ± 4.x10^{-18}	.542 ± .214	7.8
F17	0.011	A	7220 ± 14.8	39.9 ± .97	5.6 ± .28	49.9
		B	8290 ± 92.3	4.95 ± .05	1.2 ± .27	13.7
		C	10100 ± 182.	.113 ± 1.7x10^{-17}	.478 ± .228	7.3
F18	0.044	A	7120 ± 3.7	32.8 ± .99	4.7 ± .12	41.2
		B	7870 ± 30.4	4.83 ± .034	1.58 ± .115	15.8
		C	10400 ± 7.95	.113 ± 3.7x10^{-18}	3.04 ± .054	27.7
F19	0.044	A	7110 ± 2.88	34.3 ± .85	5.23 ± .093	45.5
		B	7870 ± 31.4	4.69 ± .02	1.28 ± .09	13.4
		C	10400 ± 6.52	.113 ± 2.5x10^{-17}	3.04 ± .045	27.7
F21	0.044	A	7090 ± 11.6	29.7 ± .19	5.76 ± .09	49.8
		B	7800 ± 26.3	5. ± .046	1.19 ± .085	12.7
		C	10400 ± 11.7	.113 ± 3.16x10^{-18}	1.68 ± .043	16.6

Table V

Average Parameter Summary

Full charge tests

$-\beta = 0.044\ ^{o}/Sec -$

Peak	E $\left(cal/mole\right)$	τ_o $(x10^{-12} Sec)$	ε_s
A	7211 ± 49	34.58 ± .51	37.4 ± 1.15
B	8240 ± 30	4.96 ± .03	24.2 ± 1.35
C	9892 ± 88	.113 ± *	16.4 ± 1.08
			ε_s (Total) = 78.0

$-\beta = 0.010\ ^{o}/Sec -$

A	7230 ± 5	38.8 ± .08	49.8 ± .1
B	8225 ± 46	4.97 ± .02	16.4 ± 1.9
C	9990 ± 78	1.13 ± *	7.6 ± .17
			ε_s (Total) = 73.8

* Standard deviation very small due to strong model dependence in inversion

Table VI

Average Parameter Summary

Full charge tests

Sample # 308/7-3

$-\beta = 0.044\ ^{o}/Sec -$

Peak	E $\left(cal/mole\right)$	τ_o $(x10^{-12} Sec)$	ε_s
A	7107 ± 7.2	32.27 ± .11	45.5 ± 2.02
B	7846 ± 19.0	4.84 ± .05	13.97 ± .77
C	10400 ± *	.113 ± *	24.0 ± 2.9
			ε_s (Total) = 83.5

* Standard deviation very small due to strong model dependence in inversion

6-DISCUSSION

6-1 Possible Polarization Mechanisms

Space Charge

Space charge polarization can ocurr in ice of very high purity when impurity ions build up at sample-electrode surfaces [Gross (1977) p. 4)]. Small fractures within the ice sample may also serve as regions for possible space charge accumulation, significantly increasing its effects in pure ice.

Peaks resulting from space charge drift have at least two characteristics which enable them to be distinguished from dipolar orientation peaks. The first of these characteristics is a strong dependence on sample-electrode surface conditions [Gross (1977)]. This characteristic may be noted in the consistency of peaks in position and magnitude between samples tested. Regardless of the care taken in preparation of samples there will undoubtedly be variations in smoothness and parallelism of sample surfaces. Of the 3 peaks presented in this study, the intermediate peak (B) shows the greatest variation. However, no systematic trend may be seen in this variation between samples.

The second distinguishing feature of space charge peaks is the non-linearity of ϵ_s with respect to V_{ch} contrary to dipolar polarization (equation 2-1).This effect was investigated in a

series of partial charging tests using charging potentials of 1000 V, 1250 V, 1500 V, 1750 V, and 2000 V. Results of these tests were inconclusive due to the strong superposition of peaks. Total polarization did increase with increasing field strength in a highly non-linear manner. However, discussion of the linearity of any one of the three overlapping peaks would require decomposition of these curves into the appropriate 2 or 3 peak spectra and possible modification of modeling proceedures (see SUGGESTIONS).

As stated previously, a fourth peak does appear at approximately 190^{o}K. This peak is variable in position and magnitude. The discharge current of this peak is often weak, appearing to die out erratically after reaching its maximum. Unfortunately the dependence of this peak on V_{ch} was not investigated.

Dipole Orientation

Dipolar orientation may occur in ice with more than a single relaxation time [Gross (1977)]. Mechanisms with shorter relaxation times may be caused by lattice defects introduced by impurities. Chamberlain and Fletcher (1971) report a shift of the dipolar orientation peak to higher temperatures with decreasing HF concentration. This result illustrates the interdependence of free charge and dipolar relaxation mechanisms through lattice defects caused by such impurities. Lattice defects may also result from rapid growth of the ice crystal [Gross (1977)].

Another possible mechanism for dipolar relaxation in pure ice is suggested by Grossweiner and Matheson (1954) in which an impurity ion influences the orientation of surrounding dipoles. Their work on thermoluminescence in ice indicates that impurity ions may be surrounded by a dipole sheath and that the response of the dipolar mechanism may be influenced by this relationship.

6-2 Summary of Other Works in TSD of Ice

Previous works conducted in this laboratory [Huppunen (1978)], focused on the coldest peak, yielded a range of activation energies for this peak of 6.75 kcal/mole to 8.5 kcal/mole determined by the initial rise method, and maximum total ϵ_s of 58. This activation energy is consistent with the value of 7.0 kcal/mole obtained in current studies using the same apparatus. However, the activation energy determined for peak B in current work (8.2 kcal/mole) also lies within these limits. The discrepancy in ϵ_s may be due to the different methods used to determine P_o. Huppunen determined ϵ_s by graphical integration of TSD curves. In current work P_o has been obtained from curve fitting results. The discrepancy noted above is small compared to the discrepancy between these results and the expected value of >200.

Johari and Jones(1975) report activation energy of 11.4 kcal/mole for the coldest peak and total ϵ_s of >250 at 100^o K. It can be seen from TSD curves presented by the above that severe

overlapping exists. No comment is offered regarding the effect of this overlapping on calculation of activation energy. Further, Figure 2 of Johari and Jones (1975) shows that the current discharge does not drop to zero at the end of the heating cycle. No mention is made regarding the effect of this current offset in determination of ϵ_s.

Chamberlain and Fletcher (1971) report two peaks in pure ice, one occuring at 100° K, and the other, randomly occuring between 125° K and 135° K. The first of these peaks is believed to be associated with the release of L defects and dipole relaxation.

Grossweiner and Matheson (1954), in a study of luminescence in ice,report a principal trap depth of approximately 7.4 kcal/mole with pre-exponential factor of 5.0×10^{-9}. It is interesting to note that this activation energy corresponds fairly well with the value 7.0 kcal/mole determined for the principal relaxation peak (A) in this study.It is also interesting to note that their principal luminescent peak coincides in position with peak C of the TSD spectrum obtained in this study. These findings may be significant in light of Grossweiner and Matheson's postulation of a complex relationship between an impurity center and surrounding sheath of oriented dipoles. Future investigation into the proposed interaction between dipole and luminescent processes may yield interesting results.

7-CONCLUSIONS

Peaks A and C of the TSD spectrum of pure ice appear to be due to first order relaxation mechanisms. Peak A may be the result of the dipole orientation reported by Chamberlain and Fletcher (1971), being consistently stronger than all other peaks. Peak C , a smaller peak appearing with great consistency, may be the result of small impurity concentration on the dipolar relaxation process. This peak coincides with an impurity center related luminescent peak of Grossweiner and Matheson (1954) with much higher energy of activation than reported by these authors.

Peak B of this study, as well as the peak at 190^{o} K, are generally felt to be the results of extrinsic effects. Both of these peaks show significant irregularity. Of these two, peak B appears with greater consistency and may be the result of space charge effects at surfaces of small fractures in the sample. A possible explanation for the shift of this peak in the anomalous curves is the existence of a large fracture in the sample. Unfortunately this sample was accidentally melted before it could be inspected following TSD testing . The peak at 190^{o} K, being highly erratic and often masked by noise at the end of the heating cycle, is believed to be due to space charge effects at sample-electrode surfaces.

8- Suggestions for Further Work

There are many avenues open for further work in the TSD laboratory at New Mexico Tech.. Modifications to existing experimental apparatus as well as extension of currently used modeling proceedures will greatly improve powers of data resolution and interpretation.

8-1 Cooling System

The major shortcoming of the TSD apparatus, at this time, is the degree of difficulty involved in cooling the sample rapidly. This problem may be solved by extending the circulation of liquid nitrogen throughout the aluminum block, possibly in coils around the cavity containing the sample holder.

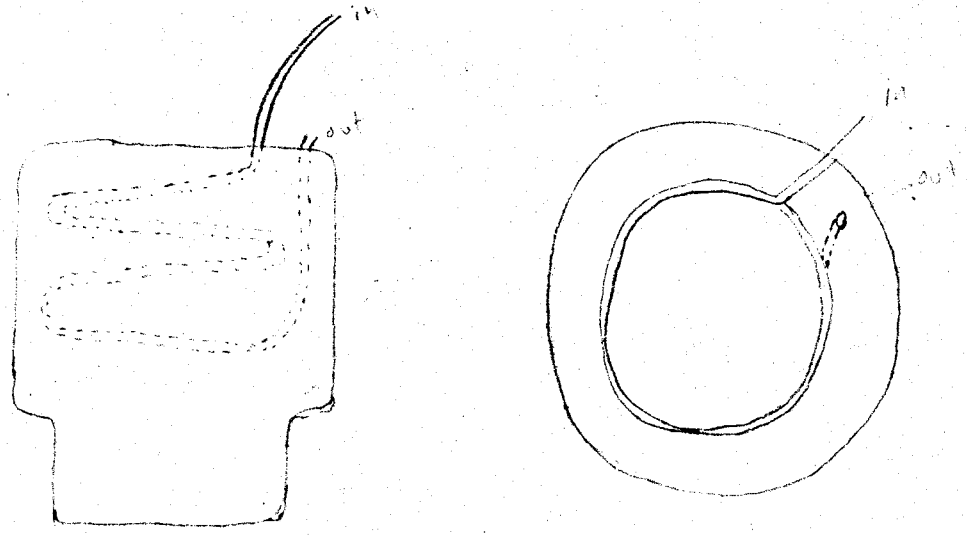

Modifications To Aluminum Block

This modification may be made without changing the sample holder. If this does not give adequate results a similar coil may be introduced somewhere closer to the sample (within the sample holder itself). This, of course, would require complete replacement of the currently used sample holder and containing block.

8-2 Guard Electrodes

Guard electrodes may be used to reduce edge effects of the sample and electrodes on the forming field (see diagram below). Deviation of the forming electric field vectors from the uniform, parallel distribution will lower the effective forming field perpendicular to the interfacies.

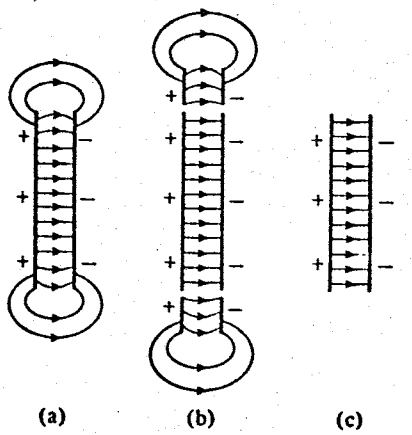

Fig. 63. The electric field of a charged parallel-plate capacitor with and without guard rings; also, an idealized map of this field.

from Rojansky (1971), p. 96

Addition of this type of assembly to the currently used apparatus would require total change in the set-up. However, I feel that this change should be made.

8-3 Programming Modifications

Currently used modeling programs may easily be modified to facilitate more thorough investigations of possible solutions. At this time, two programs are used to model TSD data with one OR three peak spectra. A single program should be developed which fits up to four peak spectra. Each TSD curve should be modeled using all feasible numbers of peaks.

Parameter, and data uncertainties need much further consideration than was given in this study. More reliable estimates of trapping parameter uncertainties may be obtained through further experimentation and application of other methods of analytical determination of trapping parameters from TSD data (some "whole curve" and "half width" methods are discussed by Chen (1969)).

Acknowledgments

I would like to gratefully acknowledge the continued support and patience of Dr. Gerardo Wolfgang Gross while conducting this study in a manner which truly allowed me to work independently and to apply concurrent areas of study to great advantage.

I would also like to thank Dr. John Schlue for assistance and suggestions regarding the theory of least squares curve fitting and its application.

Further thanks to Jessie Chisholm, Moe Peteet, Barbara Fazio-Kendall, and many others at the TCC for their patience and indispensible assistance in programming and editing of the material presented in this study.

LIST OF REFERENCES

Chamberlain, J.S.,and N. H. Fletcher (1971): Low temperature polarization effects in ice. Phys. Kondens. Materie 12: 193-209.

Chen, R. (1969): On the calculation of activation energies and frequency factors from glow curves. J. Appl. Phys. 40(2): 570-585.

Gross, B. (1968): Time-temperature superposition theory for electrets. J. Electrochem. Soc. 115: 376-381.

Gross, G.W. (1977):Dielectric dispersion and conductivity of ammonium compounds in ice. Research proposal submitted to the National Science Foundation.

Grossweiner, L.I., and M.S. Matheson (1954): Fluorescence and thermoluminescence of ice. J. Chem. Phys. 22(9):1514-1526.

Hastings, E. (1955): Approximation for Digital Computers. Princeton Univ. Press, Princeton: 188 p.

Haering, R.R., and N. E. Adams (1960):Theory and application of thermally stimulated discharge currents in photoconductors. Phys. Review 117(2): 451-456.

Huppunen, J. L. (1978): Thermally stimulated discharge currents in ice.Unpublished M.S. Research Paper , Dept of Geoscience, New Mexico Institute of Mining and Technology:(37 p.).

Jackson, D.D. (1972):Interpretation of inaccurate, insufficient,

and inconsistent data. Geophys. J. Royal Ast. Soc. 28: 97-109.

Johari, G.P., and S. J. Jones (1975):Study of the low temperature "transition" in ice I_h by thermally stimulated depolarization measurements. J. Chem. Phys. 62: 4213-4223.

National Bureau of Standards (1974): Thermocouple Reference Tables Based on the IPTS-68. NBS Monograph 125, p. 401 (quadratic equation for -200° C to 0° C)

Perlman, M. (1971): Thermal currents and the internal polarization in carnauba wax electrets. J. Appl. Phys. 42(7): 2645-2652.

Rojansky, V. (1971): Electromagnetic Fields and Waves. Prentice-Hall, Englewood Cliffs, N.J.: 464 p.

van Turnhout, J. (1975): Thermally Stimulated Discharge of Polymer Electrets. Elsevier, Amsterdam: 335 p.

List of Commonly Used Symbols

A - Area of one capacitor plate

B - Heating rate ($^{o}K/sec$)

E - Activation energy

E_p - Polarization forming field

ϵ_s - Static dielectric constant

ϵ_∞ - Optical (high frequency) dielectric constant

i - Discharge current

j - Discharge current density

k - Boltzmann's constant

l_s - Sample thickness

N_{dip} - Number of dipoles

P - Polarization ($Coulomb/cm^2$)

p - Dipole moment of ice

Q - Charge on capacitor plate

s_o - Attempt to escape frequency factor (sec^{-1})

σ - Surface charge density

T - Temperature (kelvin)

T_m - Temperature of TSD maximum

t_{ch} - Isothermal charging time

τ - Relaxation time (sec)

τ_o - Pre-exponential factor (sec)

FIGURE LEGENDS

Fig. 1- a) Charge distribution on plates of capacitor in vacuum under potential V.
b) Charge distribution on plates of capacitor under potential V with dielectric medium.

Fig. 2- Space charge drift in dielectric medium

Fig. 3- a) Water molecule
b) Electrical dipole analogy of water molecule

Fig. 4- Change of TSD curve with activation energy

Fig. 5- Change of TSD curve with τ_o

Fig. 6- Change of TSD curve with initial polarization (P_o)

Fig. 7- Change of TSD curve with heating rate

Fig. 8- Apparatus for measuring TSD in ice

Fig. 9- Plot of ln[i(T)] vs. 1000/T for variable temperature partial charging tests on peak A of sample 308/7-3. Activation energy (E) is determined from the initial rise (low temp.) portion (See Table II).

Fig. 10- Plot of ln[i(T)] vs. 1000/T for variable temperature partial charging tests on peak A of sample 308/7-3.

Activation energy (E) is determined from the initial rise (low temp.) portion (See Table III).

Figs. 11-19 Partial heating series on sample 308/7-3.

V_{ch}=1500 V, B=0.044°/sec

x-Observed TSD, — — — -initial estimate,

———— -fitting result

11) D73 A - T_{ch}=108.2° K

12) D72 A - T_{ch}=113.2° K

13) D71 A - T_{ch}=118.2° K

14) D62 A - T_{ch}=123.2° K

15) D68 A - T_{ch}=128.2° K

16) D69 A - T_{ch}=133.2° K

17) D77 B - T_{ch}=144.0° K

18) D76 B - T_{ch}=148.0° K

19) D75 B - T_{ch}=153.0° K

Figs. 20-31 Full charge runs , V_{ch}=1500V , □ -observed TSD,

— — —-fitting result

20) F3 - B=0.043 °/sec (sample 308/7-1)

21) F5 - " "

22) F6 - " "

23) F7 - B=0.042 °/sec "

24) F9 - B=0.043 °/sec "

25) F10 - " "

26) F11 - " "

27) F16 - B=0.010 °/sec (sample 308/7-2)

28) F17 - B=0.011 °/sec "

29) F18 - B=0.044 samp/e 308/7-3)

30) F19 - B=0.044 °/sec (sample 308/7-3)

31) F21 - " "

Fig. 32 - ϵ_s vs. T_{ch}

x - Sample 308/7-3, peak A

◇ - Sample 308/7-3, peak B

⊠ - Average typical full charge, total ϵ_s (B=0.044°/sec)

⊕ - " " " " " (B=0.010°/sec)

□ - Sample 308/7-3 full charge, total ϵ_s (B=0.044°/sec)

Figs. 33-35 Partial charge runs on sample 308/09-2 without foils,

T_{ch}=123. K, V_{ch} = 1500 V, β = 0.044°/sec,

X -observed TSD, — — —-fitting result

33) D80 - t_{ch} = 2 hr.

34) D81 - t_{ch} = 3 hr.

35) D85 - t_{ch} = 6 hr. 30 min.

Figs. 36-38 Partial charge runs on sample 308/7, with foils,

T_{ch} = 123. K, V_{ch} = 1500 V, β = 0.044°/sec,

X - observed TSD, — —— - fitting result

36) D36 - t_{ch} = 4 hr.

37) D39 - t_{ch} = 4 hr.

38) D41 - t_{ch} = 4 hr.

(a) (b)

Figure 1

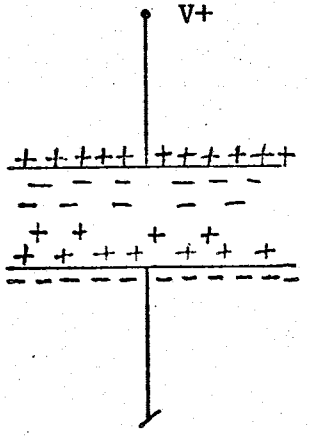

Figure 2

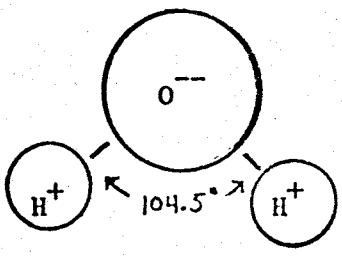

(a)

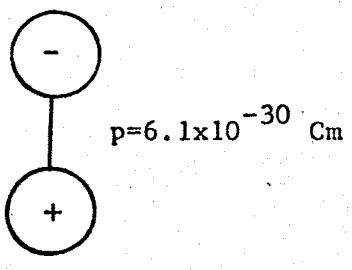

(b)

Figure 3

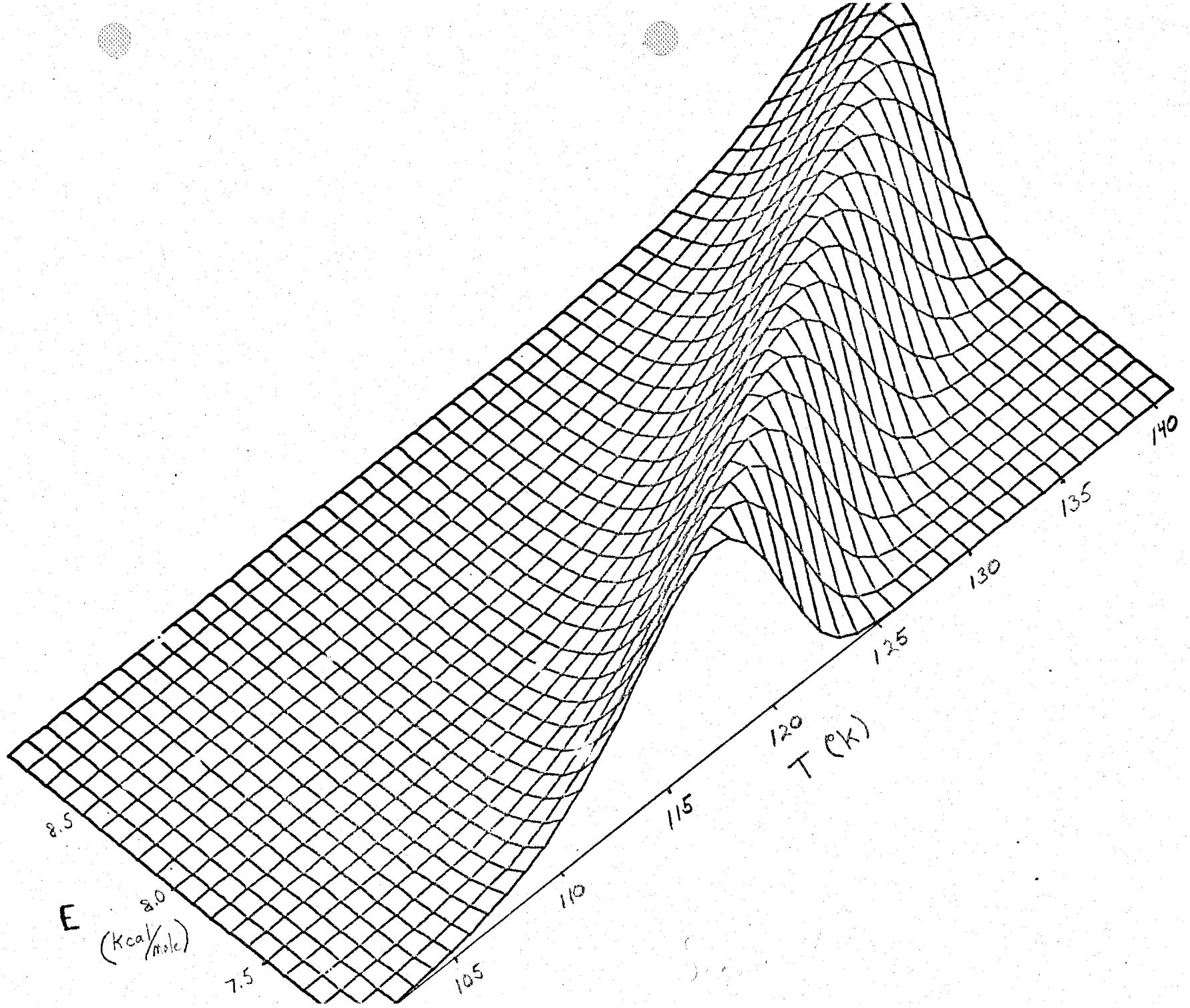
8.5
8.0
7.5
E
(Kcal/mole)
105
110
115
120
125
130
135
140
T (°K)

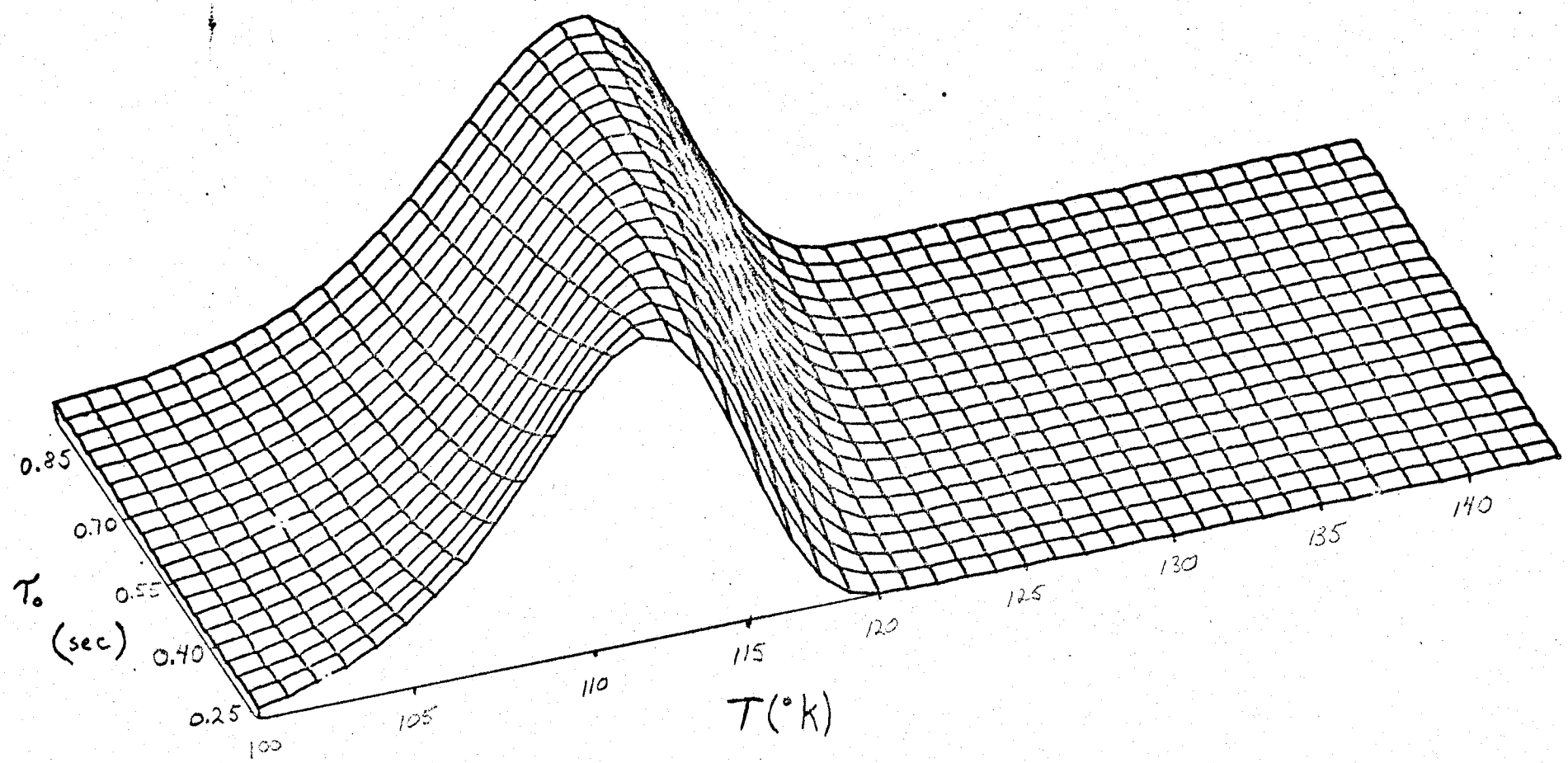
0.85
0.70
0.55
0.40
0.25
τ_o
(sec)
100
105
110
115
120
125
130
135
140
T(°K)

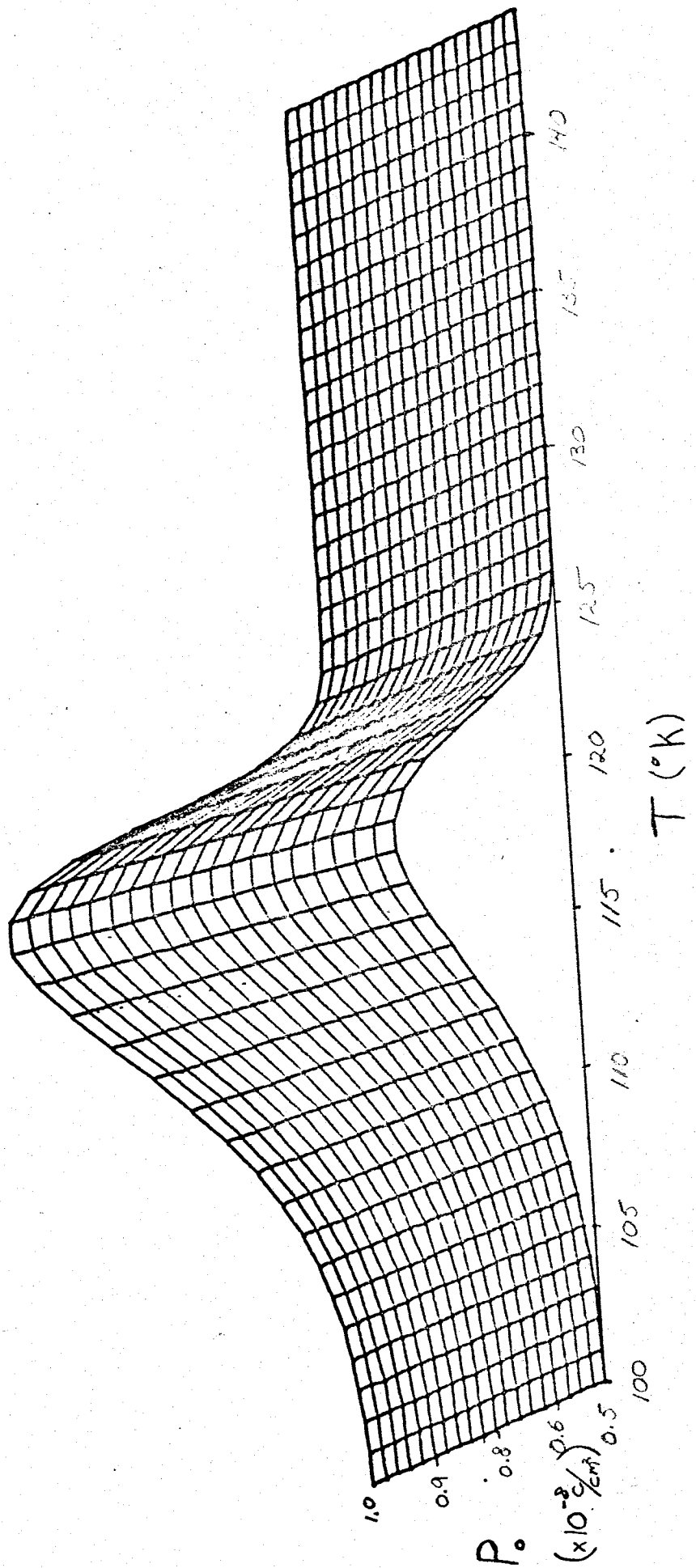
1.0
0.9
0.8
0.6
0.5
P°
(x10⁻³ c/cm²)
100
105
110
115
120
125
130
135
140
T (°K)

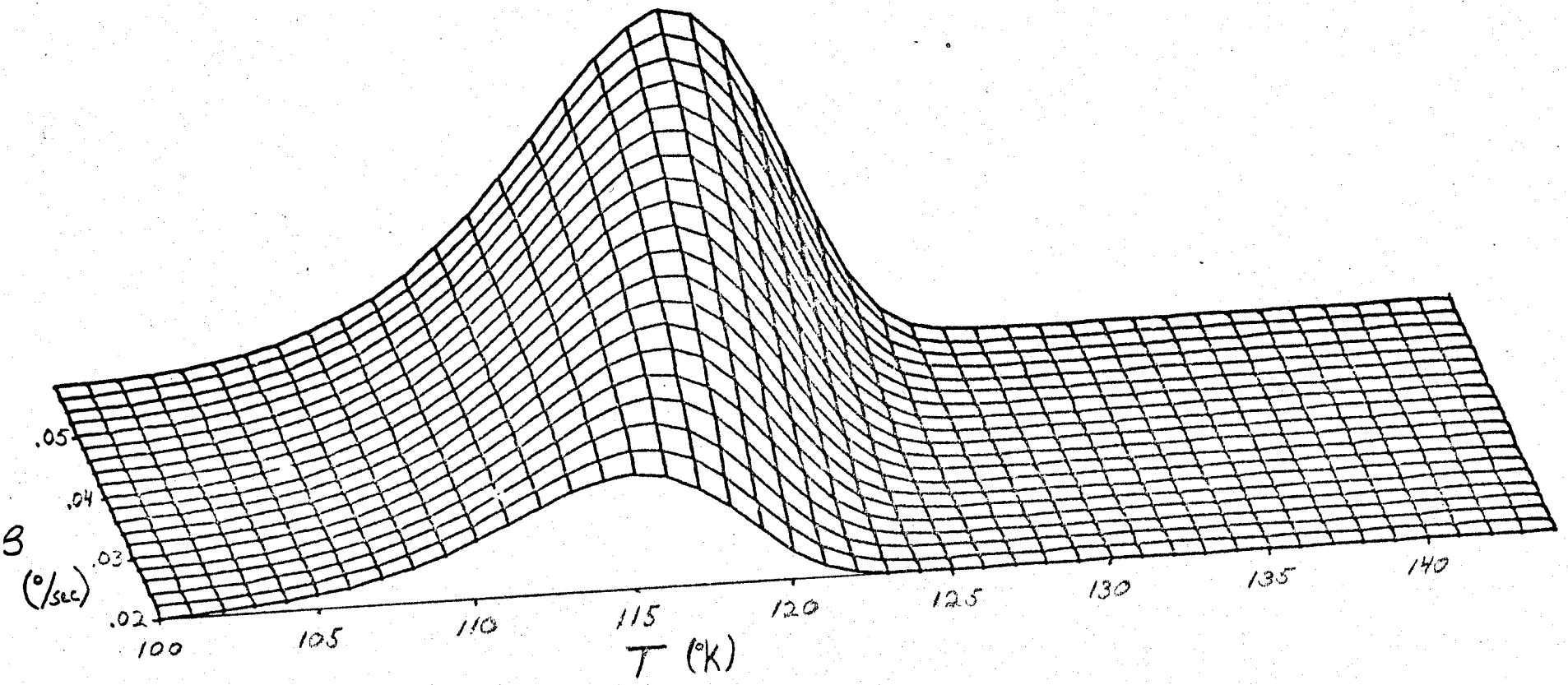
.05
.04
.03
.02
B
(°/sec)
100
105
110
115
120
125
130
135
140
T (°K)

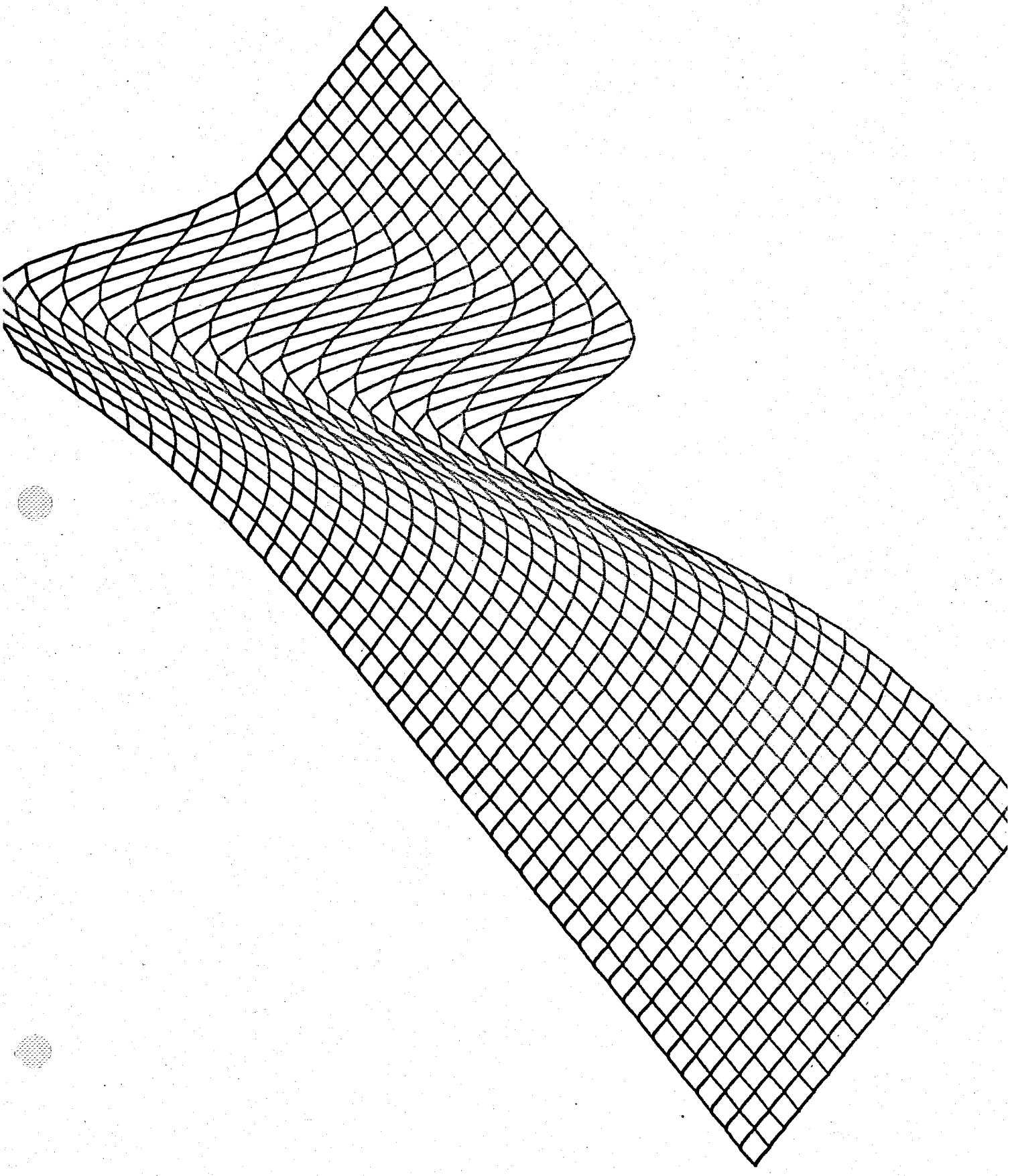

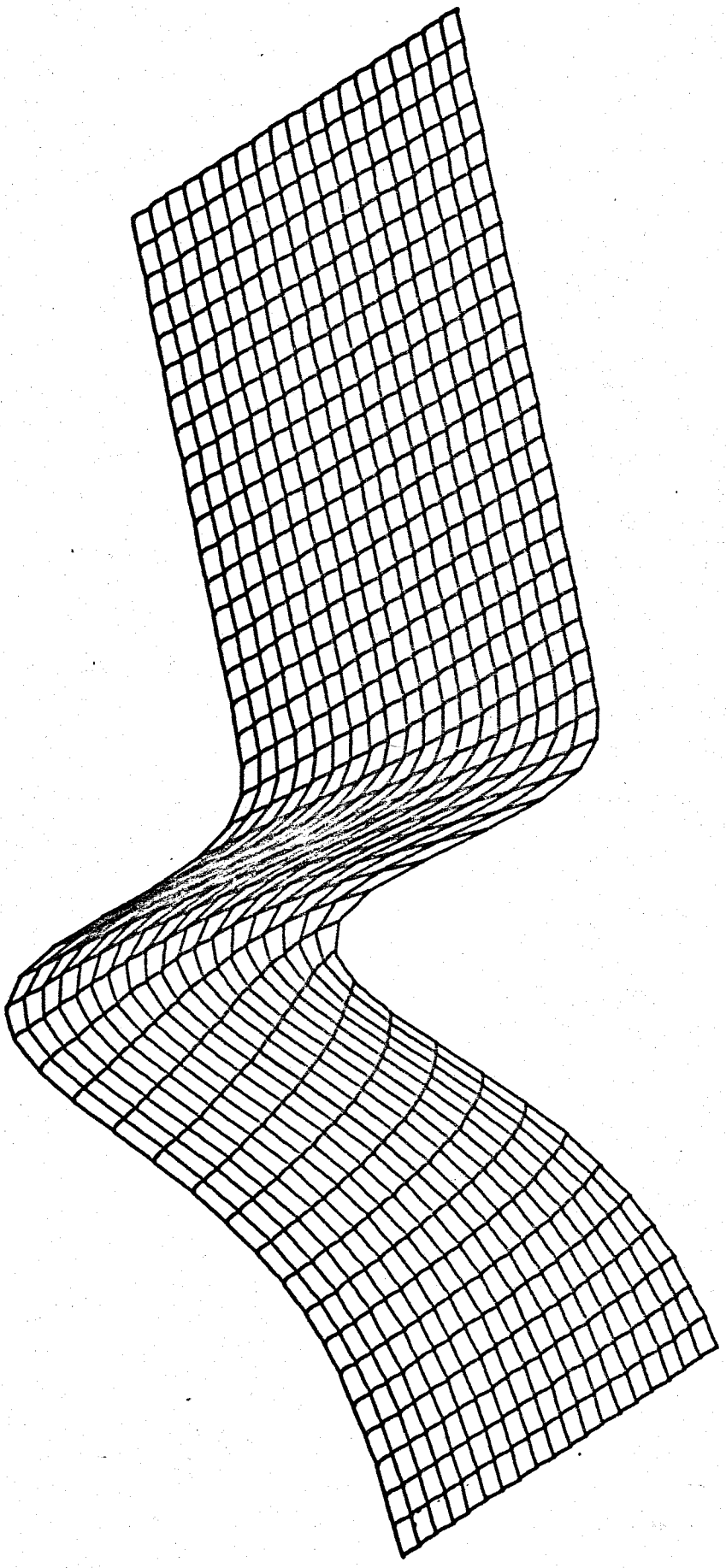

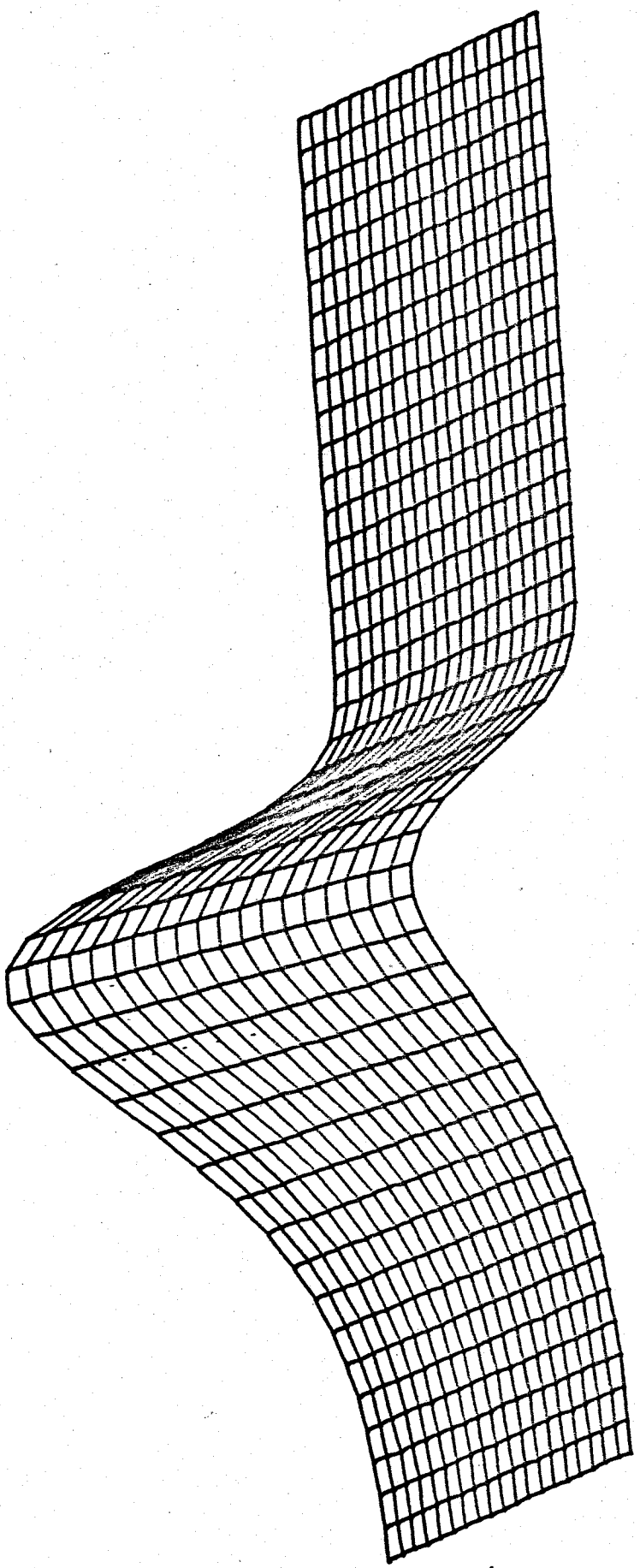

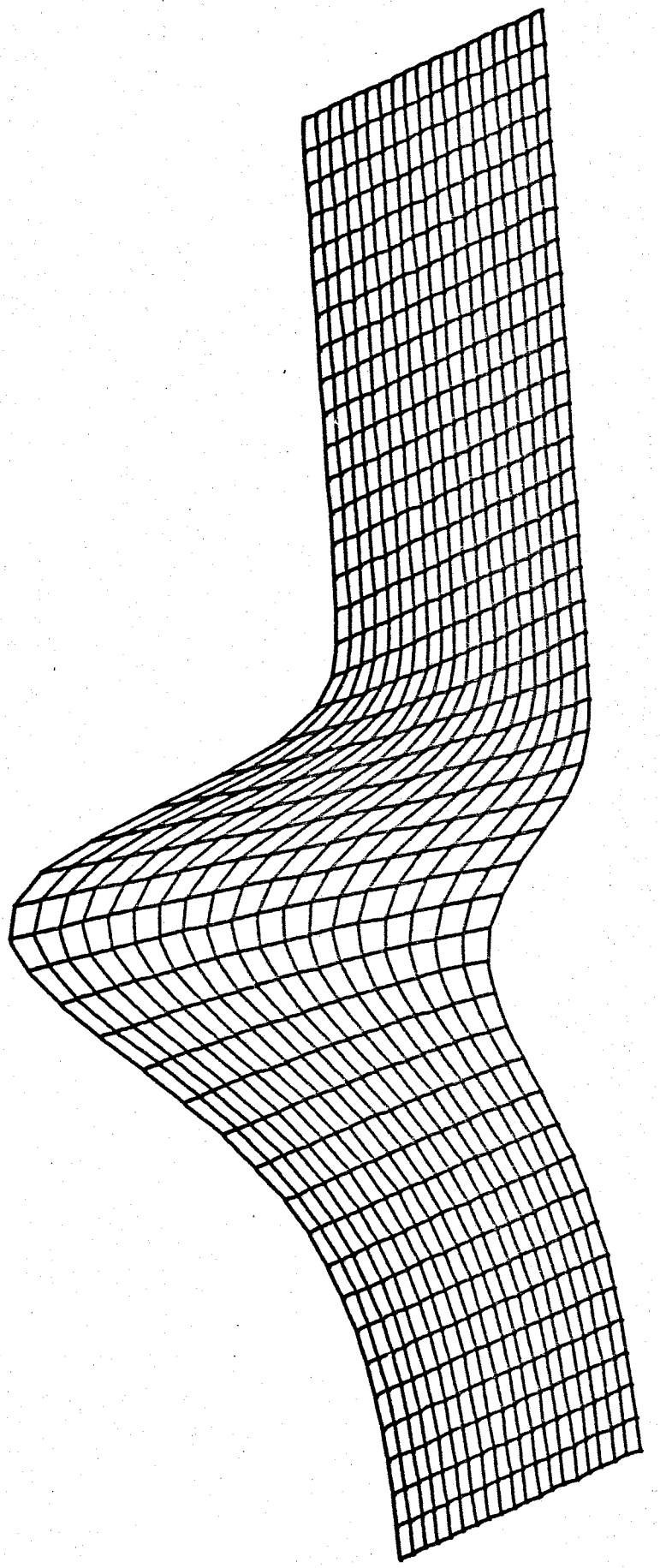

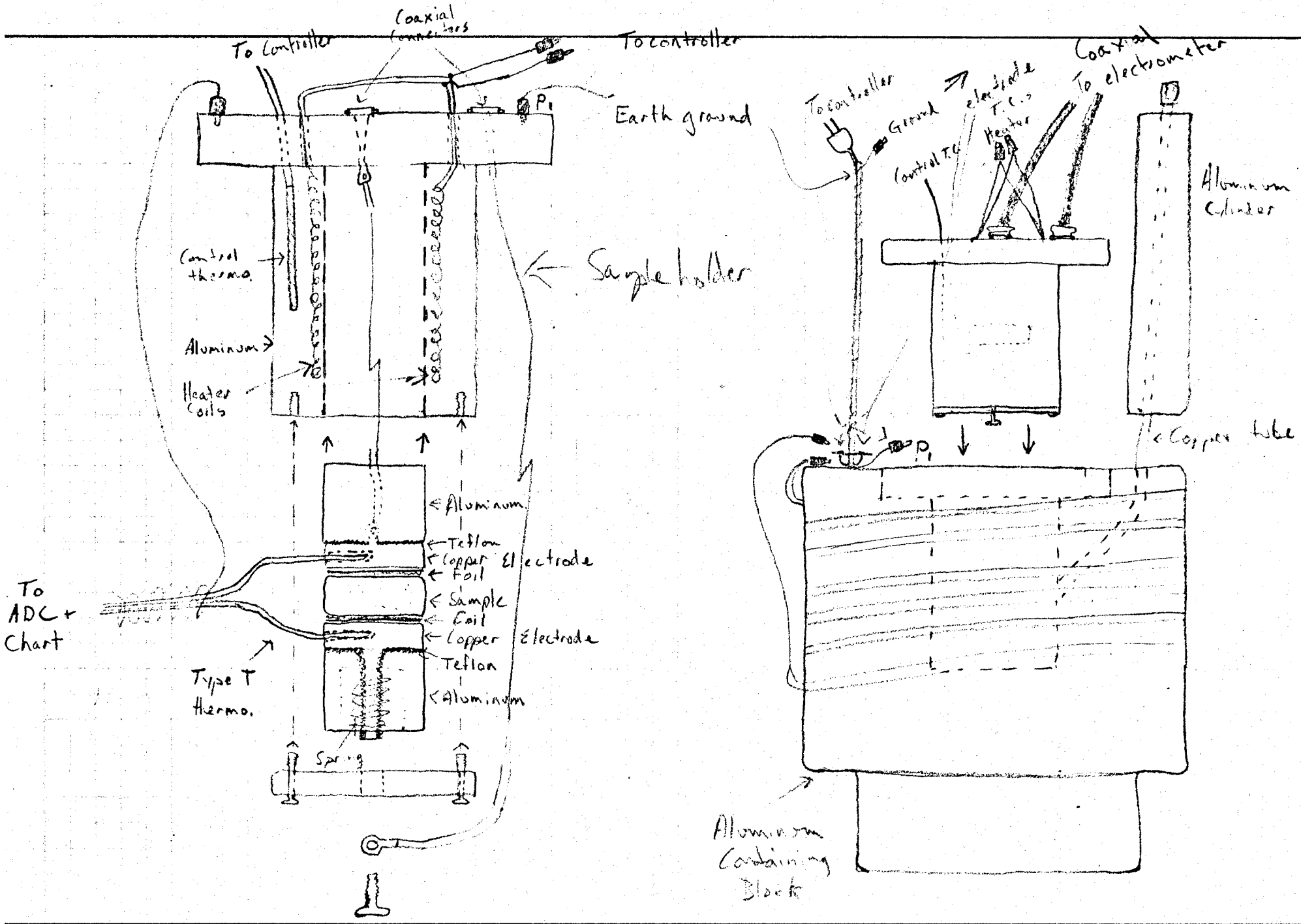
To Controller
Coaxial Connectors
To controller
P1
Earth ground
Control thermo.
Sample holder
Aluminum
Heater Coils
Aluminum
Teflon
Copper Electrode
Copper Foil
Sample Coil
Copper Electrode
Teflon
Aluminum
To ADC + Chart
Type T Thermo.
Spring
To controller
Ground
Control T.C.
Heater
Coaxial To electrometer
Aluminum Cylinder
Copper tube
P1
Aluminum Containing Block

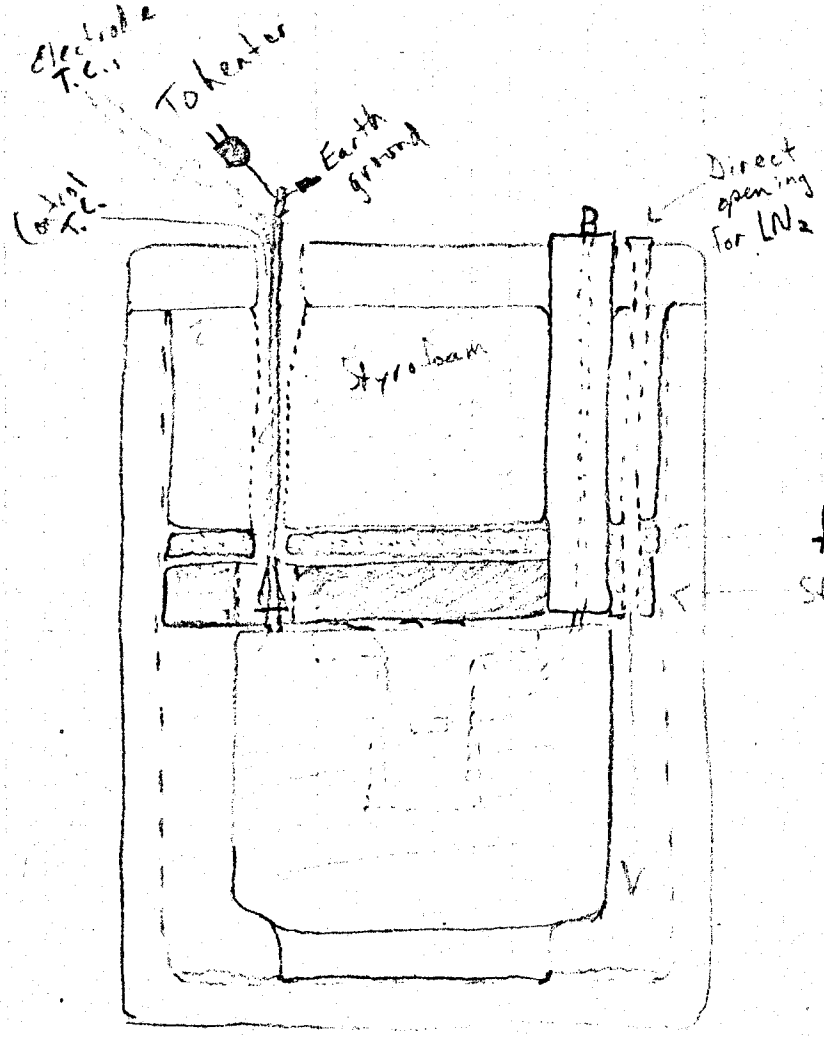

Cryogenic Vessel

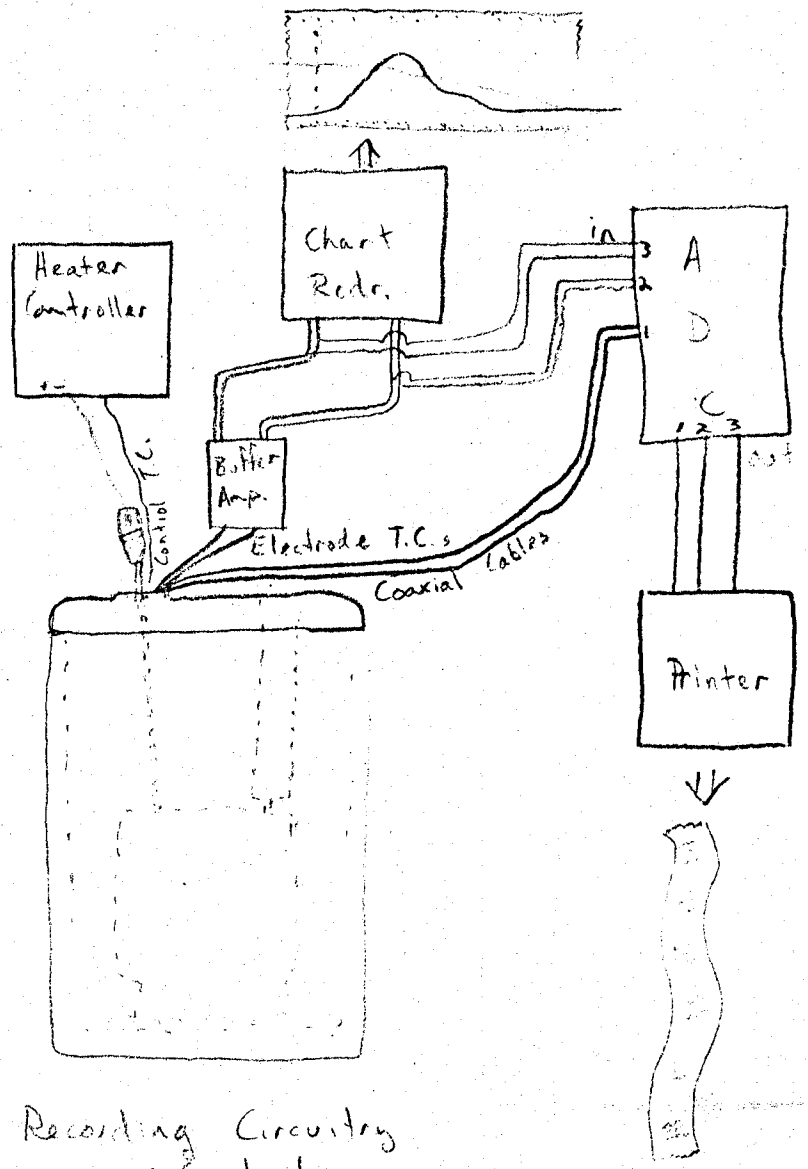

Recording Circuitry + Control

Figure 9

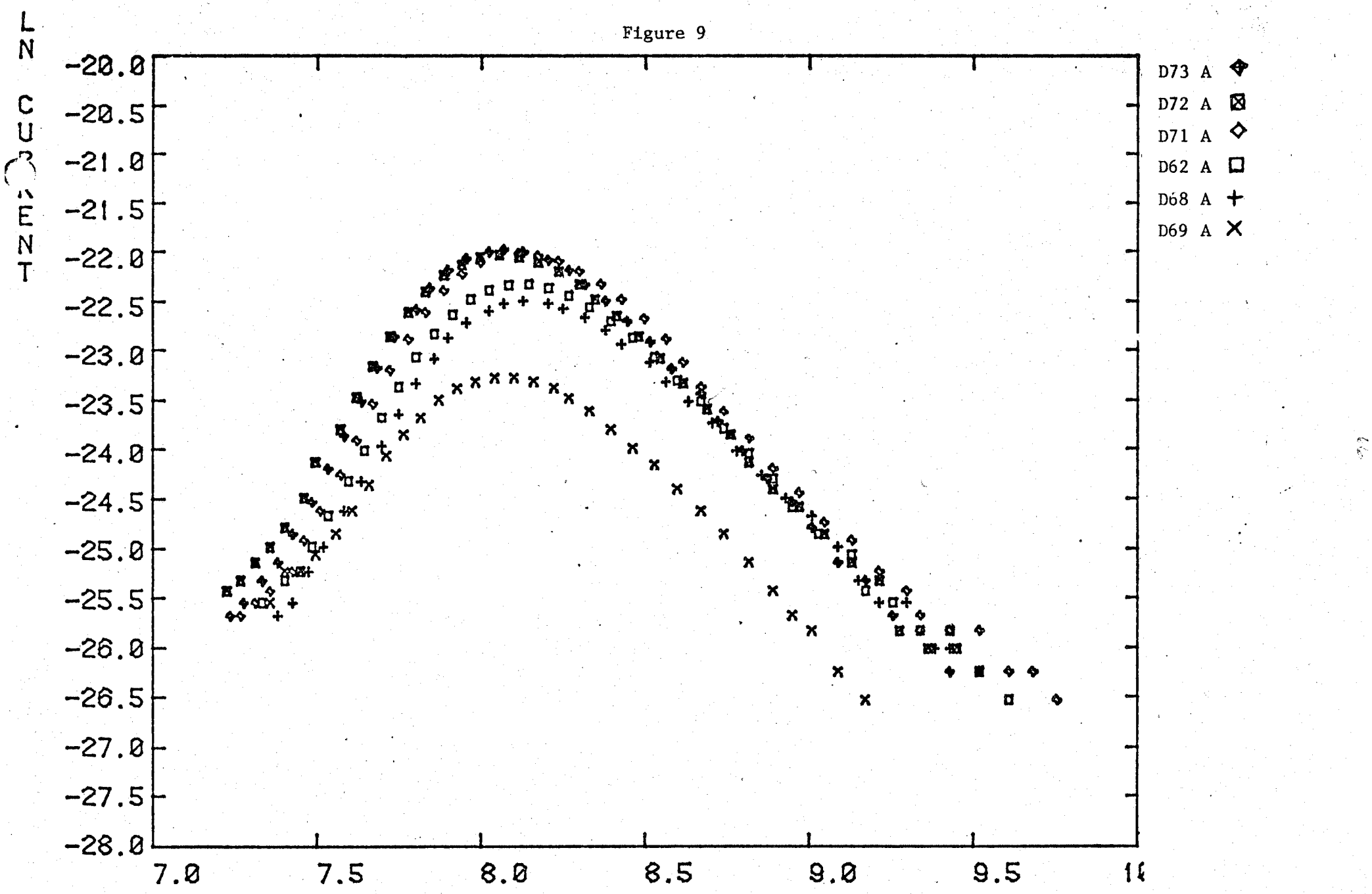
LN CURRENT
-20.0
-20.5
-21.0
-21.5
-22.0
-22.5
-23.0
-23.5
-24.0
-24.5
-25.0
-25.5
-26.0
-26.5
-27.0
-27.5
-28.0
7.0
7.5
8.0
8.5
9.0
9.5
D73 A
D72 A
D71 A
D62 A
D68 A
D69 A

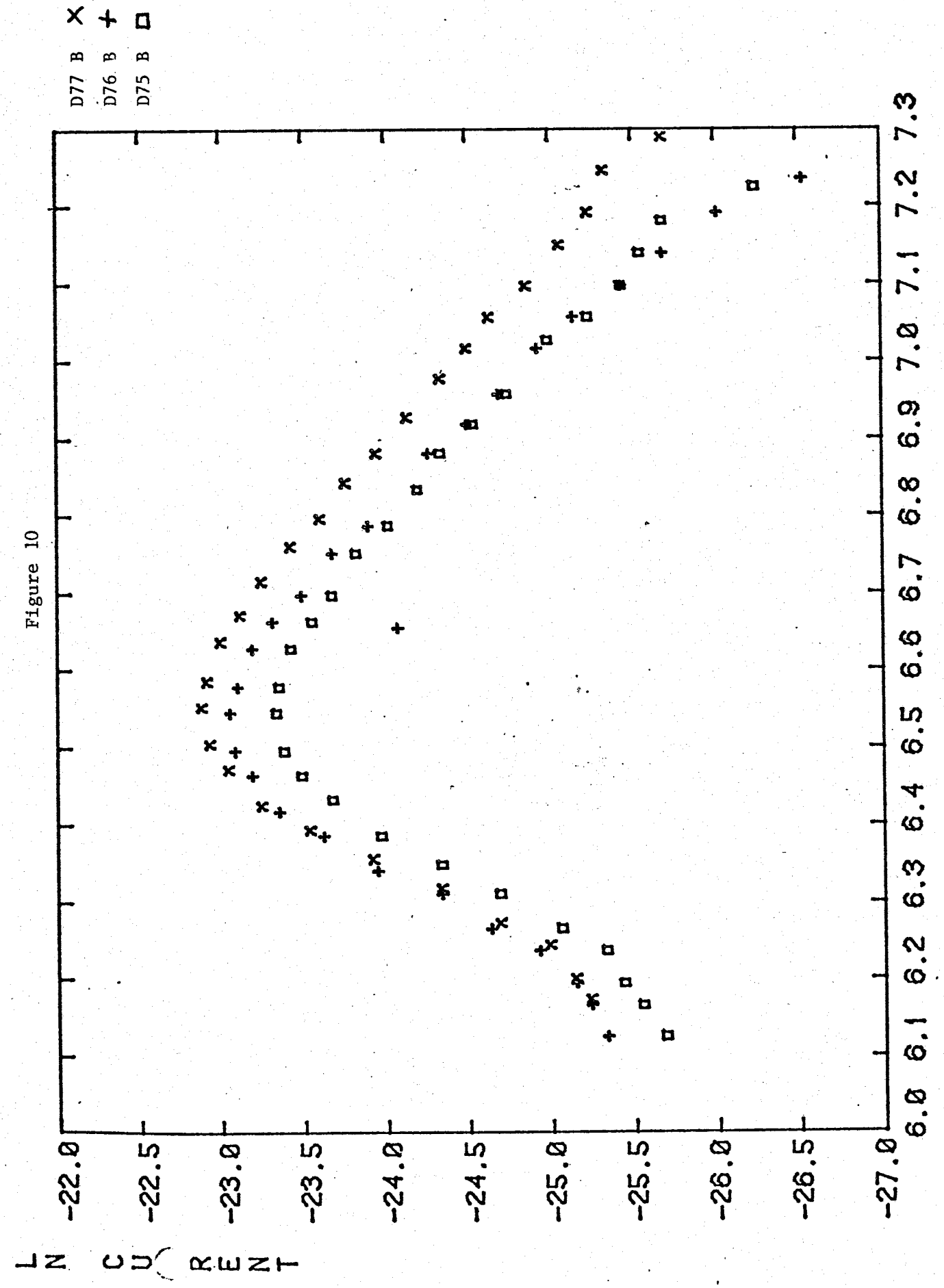
D77 B
D76 B
D75 B
LN CURRENT
-22.0
-22.5
-23.0
-23.5
-24.0
-24.5
-25.0
-25.5
-26.0
-26.5
-27.0
6.0
6.1
6.2
6.3
6.4
6.5
6.6
6.7
6.8
6.9
7.0
7.1
7.2
7.3

Figure 10

× - Observed data

– – – - Initial Estimate

——— - fitting results

Figure 11

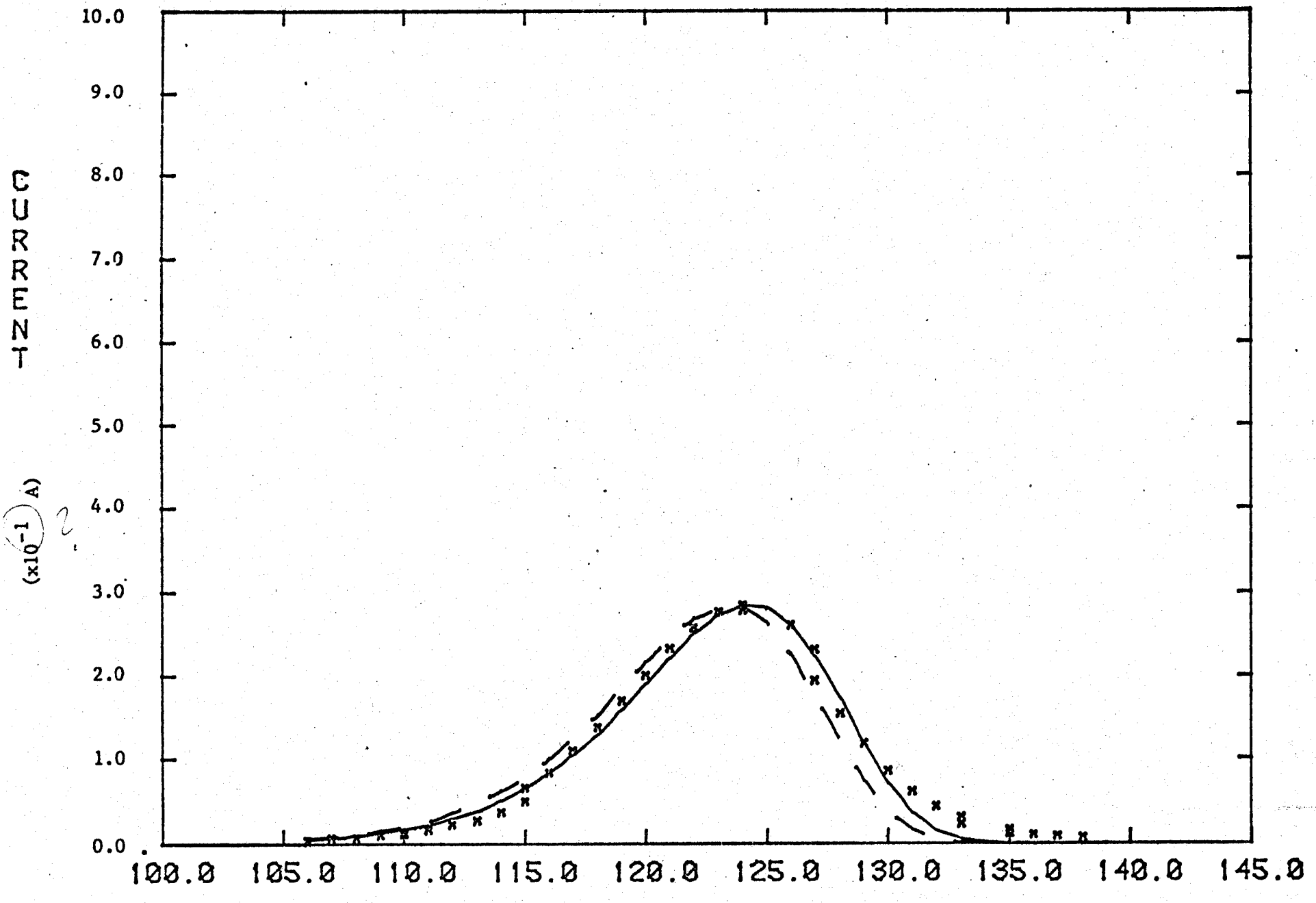

Figure 12

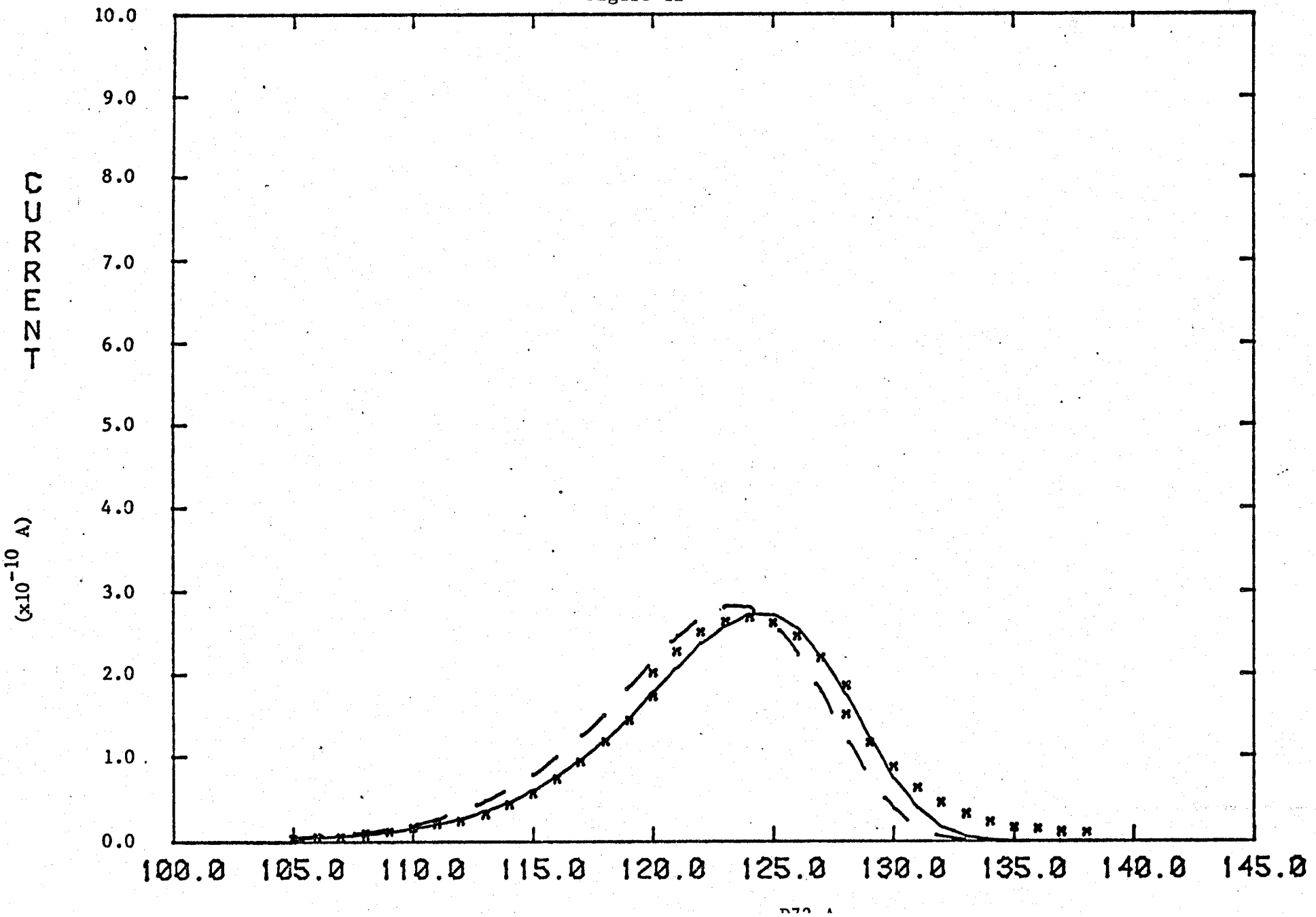
estimate
fitting results
INTENSITY
(x10^-10 A)
10.0
9.0
8.0
7.0
6.0
5.0
4.0
3.0
2.0
1.0
0.0
100.0
105.0
110.0
115.0
120.0
125.0
130.0
135.0
140.0
145.0

Figure 13

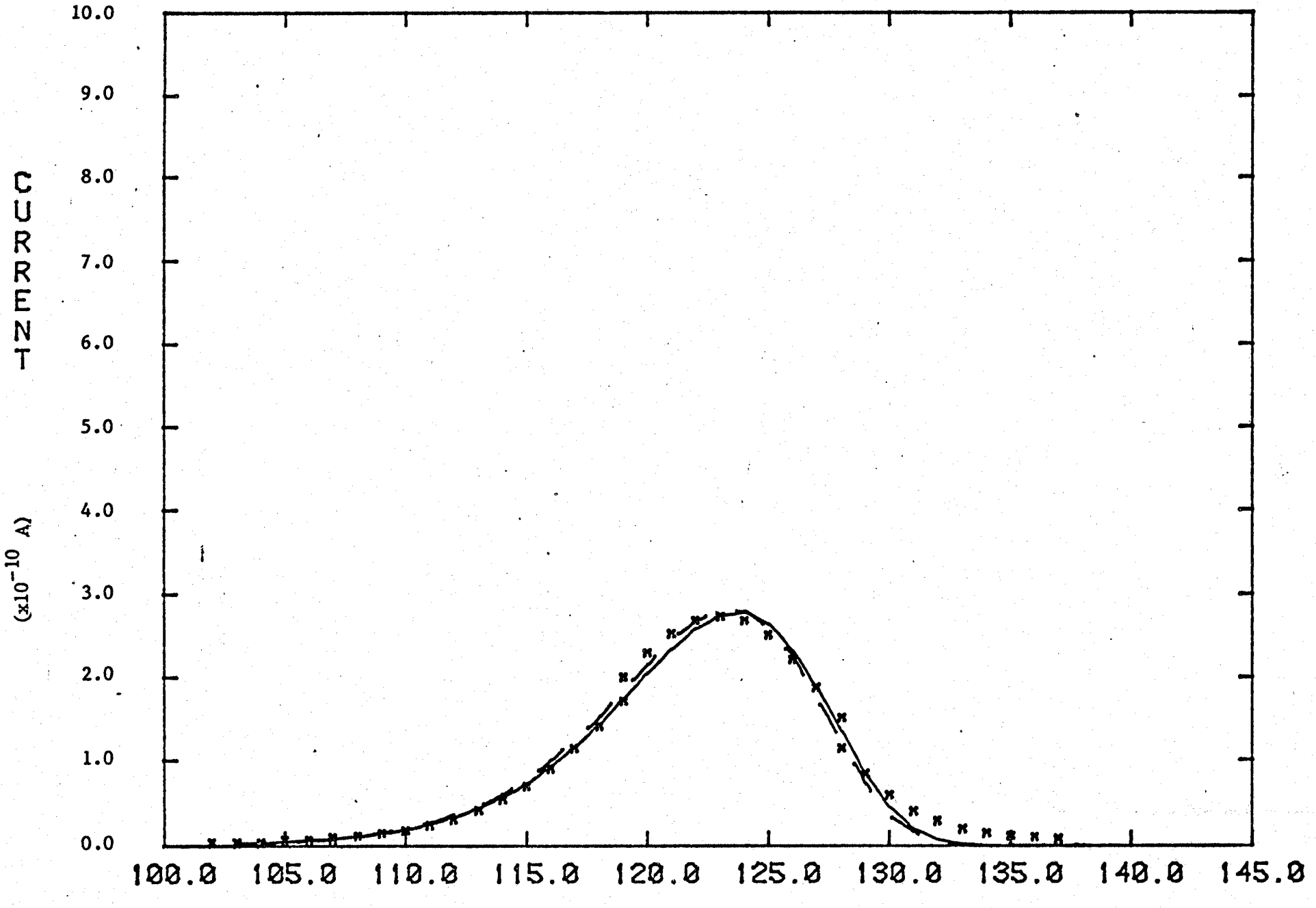
- initial estimate
- fitting results
INTENSITY
(x10^-10 A)
10.0
9.0
8.0
7.0
6.0
5.0
4.0
3.0
2.0
1.0
0.0
100.0
105.0
110.0
115.0
120.0
125.0
130.0
135.0
140.0
145.0

— — — initial estimate
——— fitting results

Figure 14

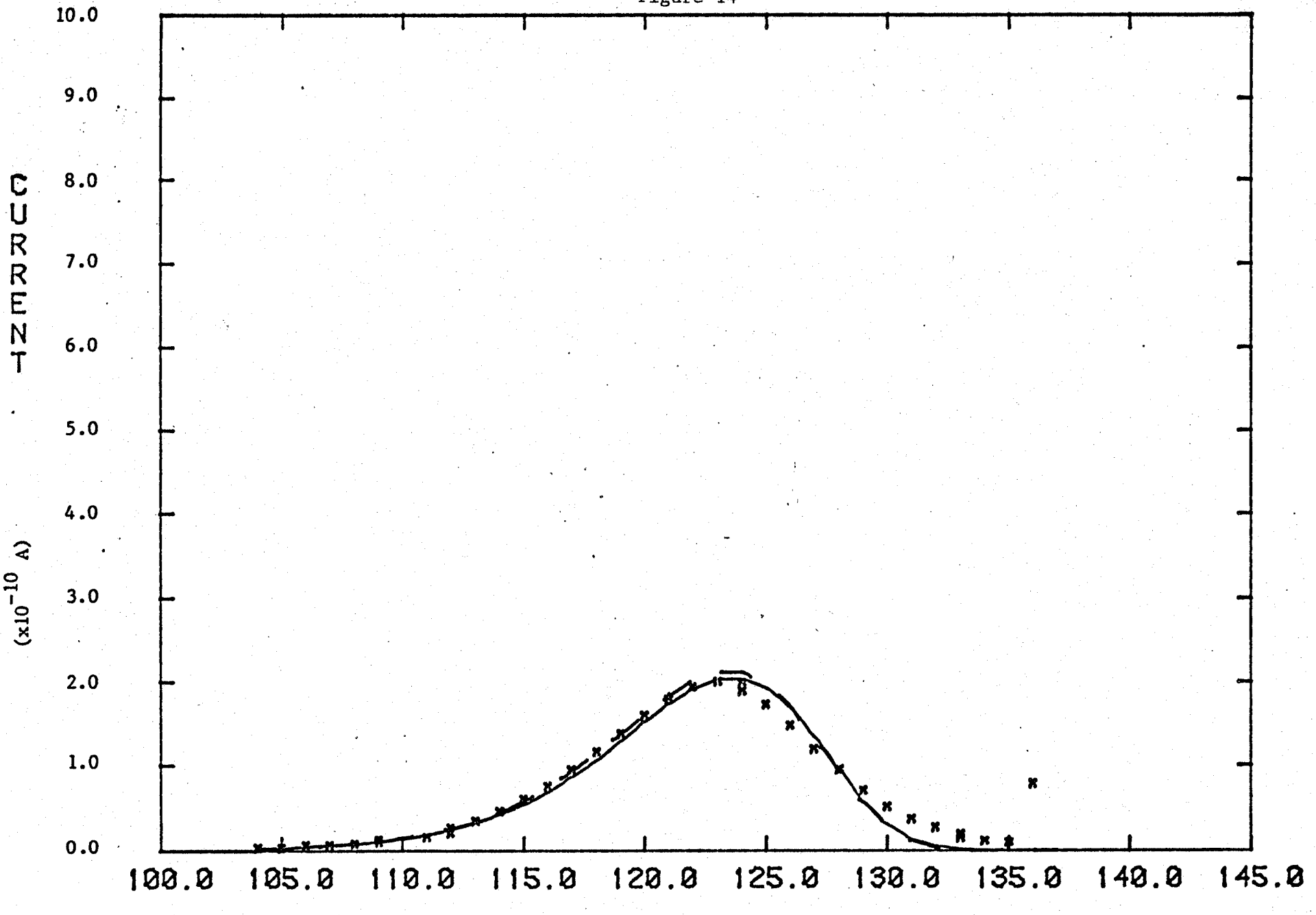

Figure 15

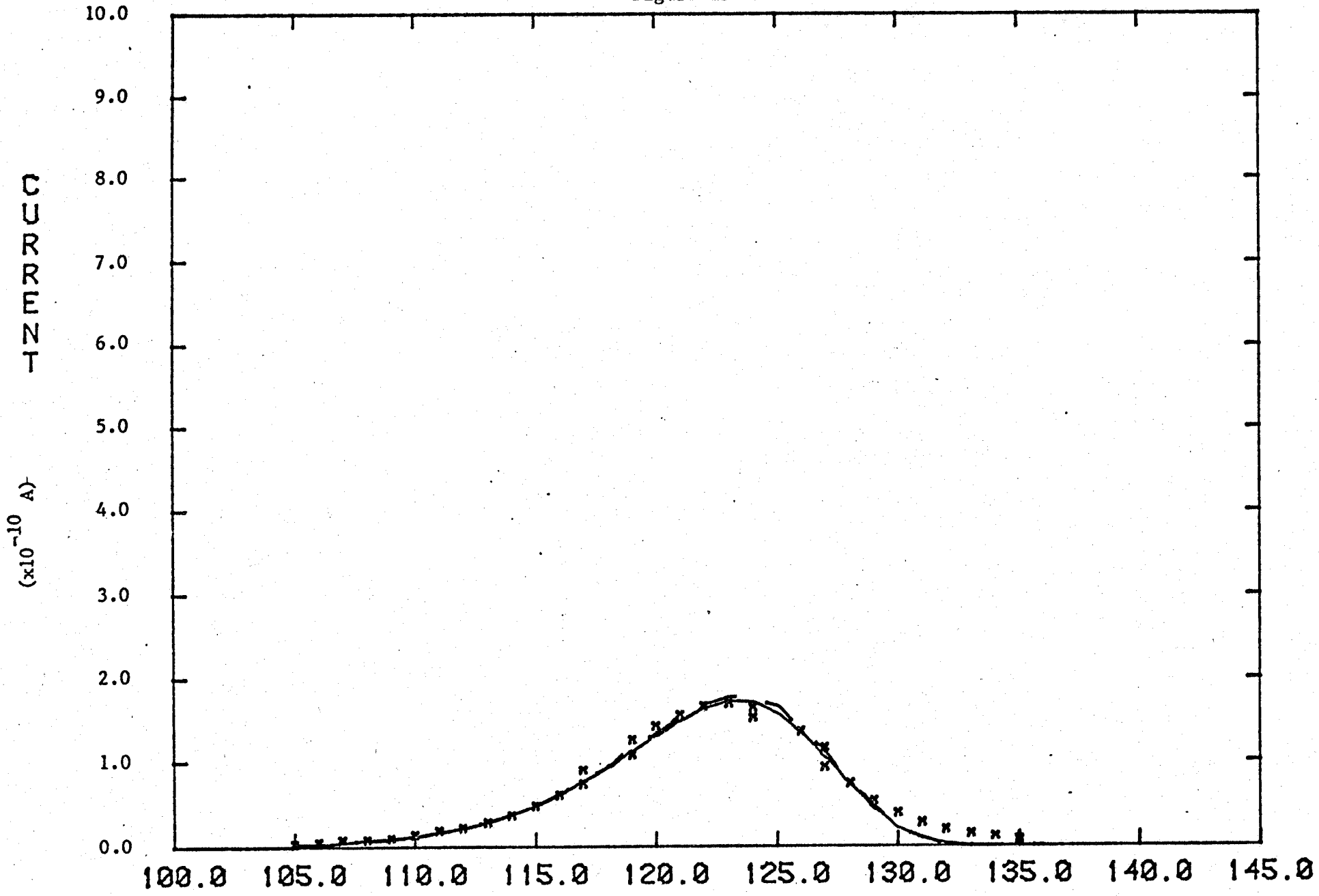
CURRENT
(x10^-10 A)
10.0
9.0
8.0
7.0
6.0
5.0
4.0
3.0
2.0
1.0
0.0
100.0
105.0
110.0
115.0
120.0
125.0
130.0
135.0
140.0
145.0

Figure 16

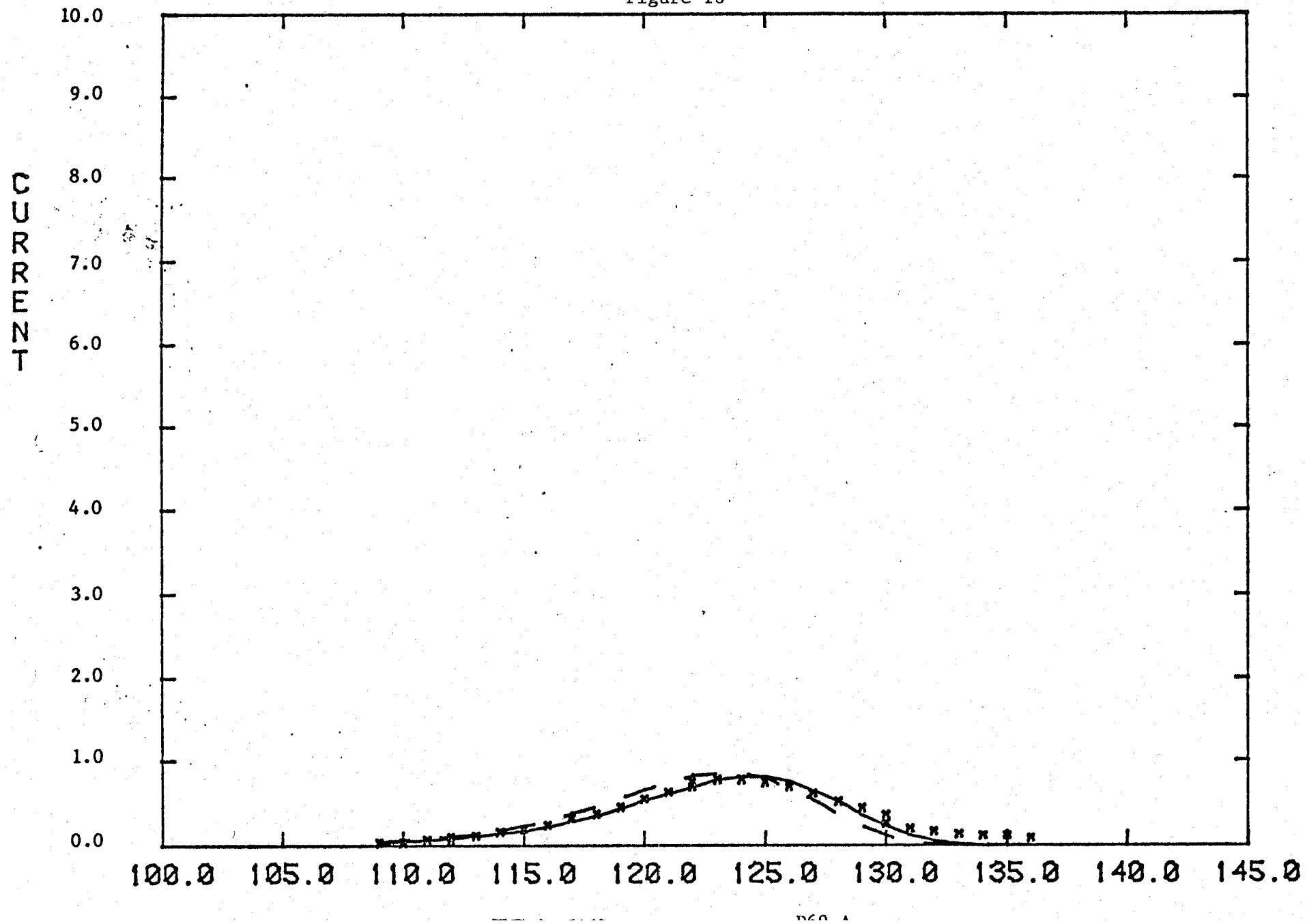
initial estimat
fitting results
CURRENT
10.0
9.0
8.0
7.0
6.0
5.0
4.0
3.0
2.0
1.0
0.0
100.0
105.0
110.0
115.0
120.0
125.0
130.0
135.0
140.0
145.0

Figure 17

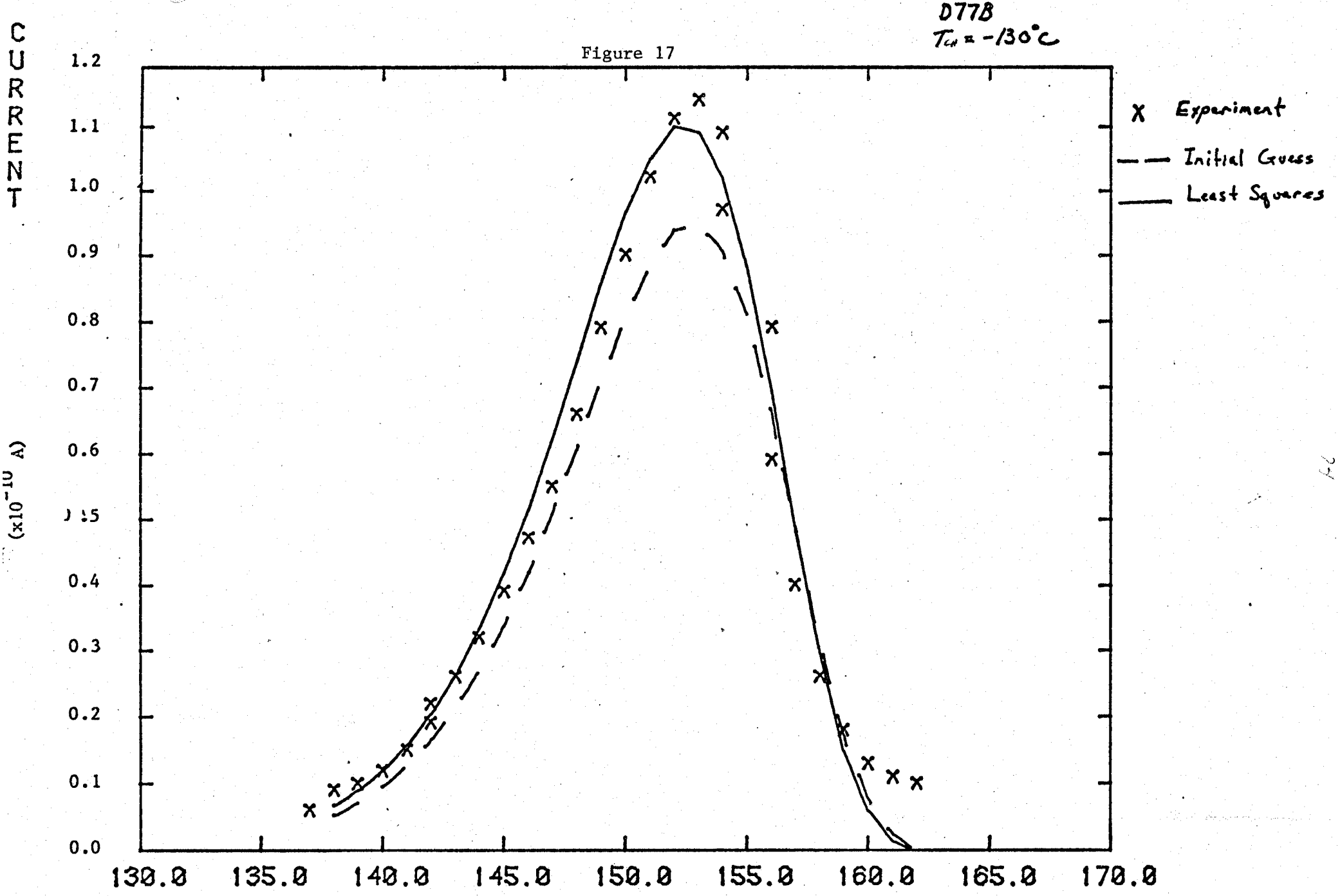
D778
T_{cal} = -130°C
CURRENT
(x10^{-10} A)
1.2
1.1
1.0
0.9
0.8
0.7
0.6
0.5
0.4
0.3
0.2
0.1
0.0
130.0
135.0
140.0
145.0
150.0
155.0
160.0
165.0
170.0
X Experiment
Initial Guess
Least Squares

Figure 18

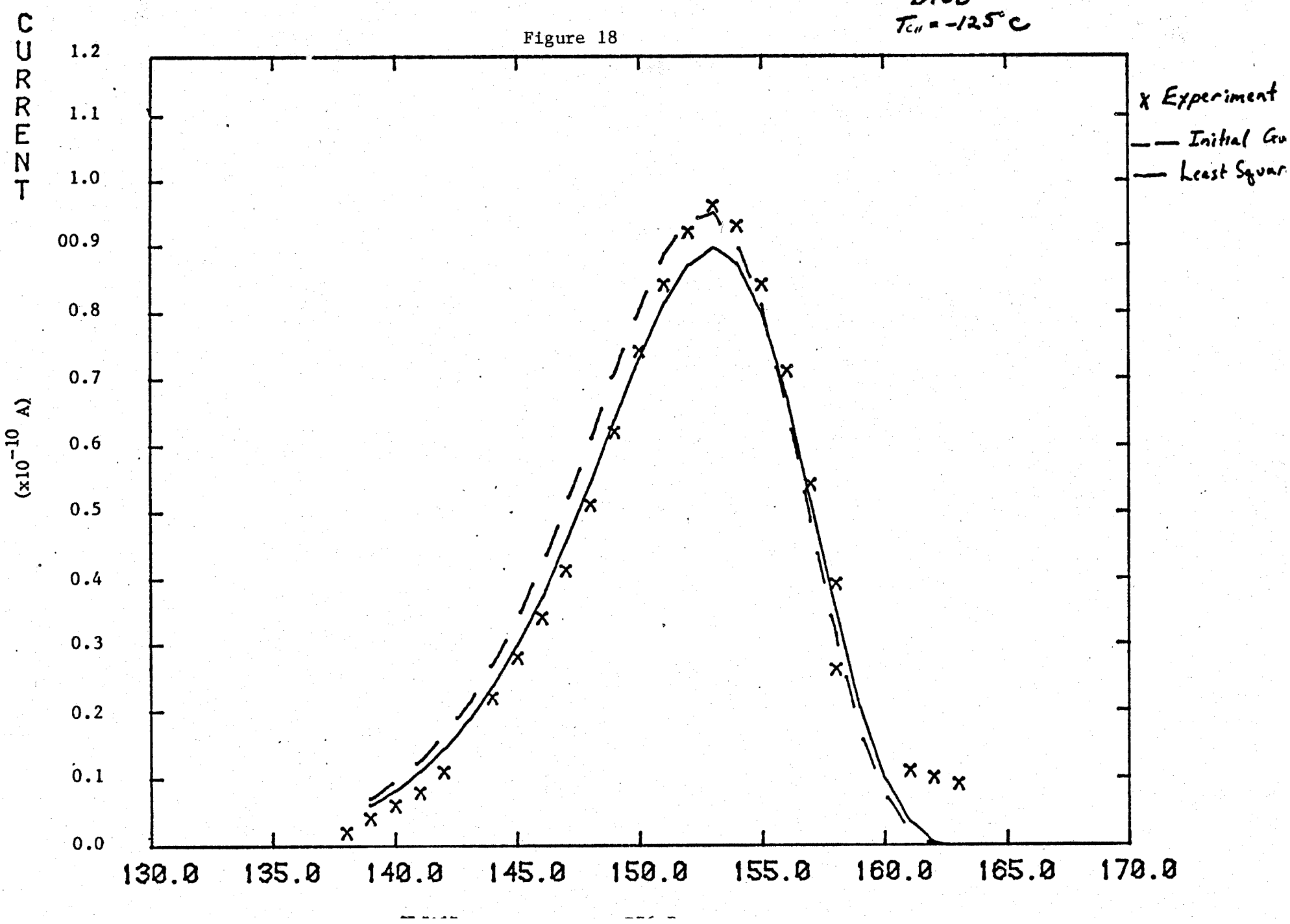
#D76B
$T_{c\parallel} = -125°C$
CURRENT
(x10^{-10} A)
1.2
1.1
1.0
00.9
0.8
0.7
0.6
0.5
0.4
0.3
0.2
0.1
0.0
130.0
135.0
140.0
145.0
150.0
155.0
160.0
165.0
170.0
x Experiment
Initial Gu
Least Squar

Figure 19

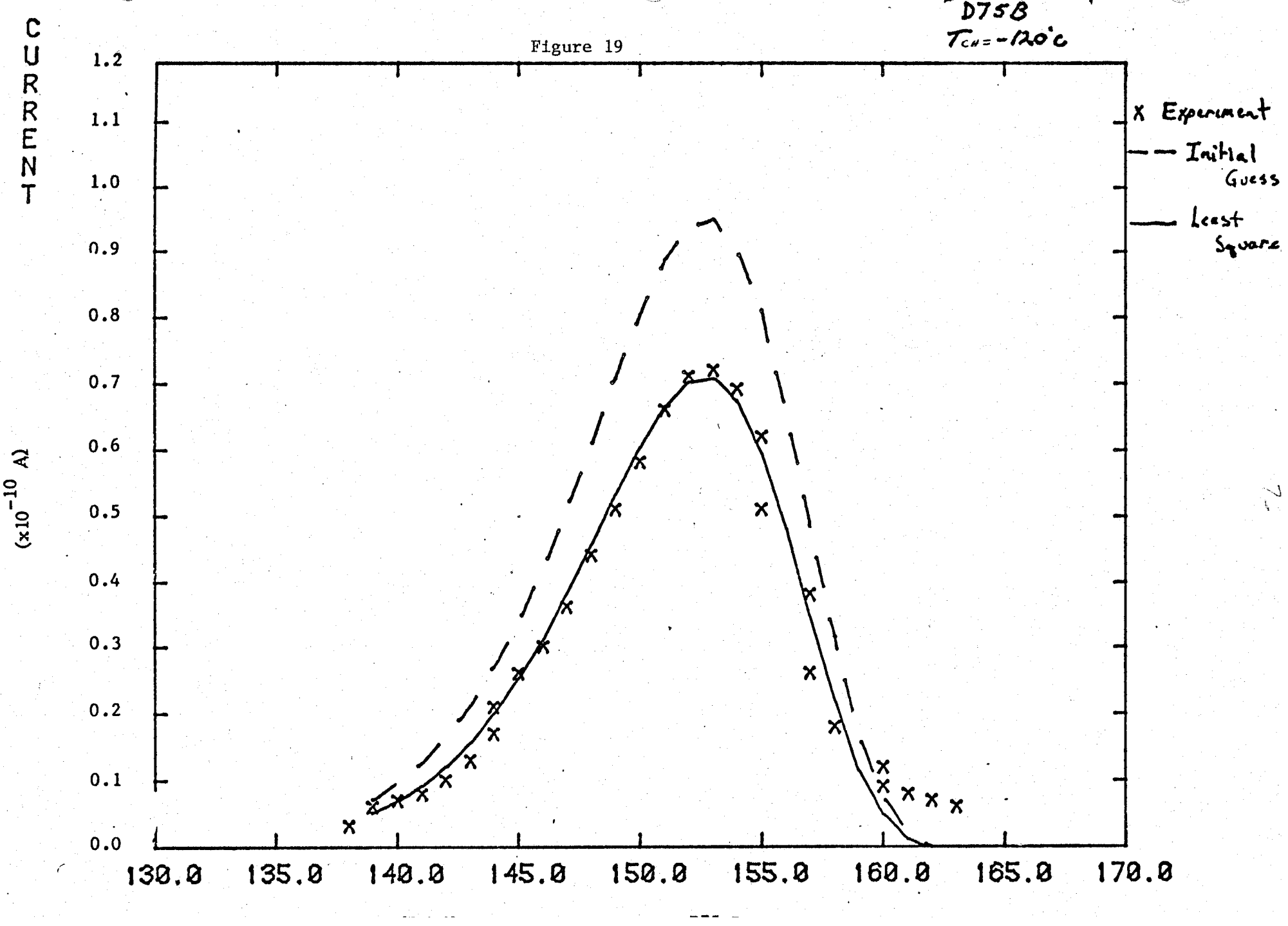
#D75B
$T_{CH} = -120°C$
CURRENT
$(x10^{-10}$ A)
1.2
1.1
1.0
0.9
0.8
0.7
0.6
0.5
0.4
0.3
0.2
0.1
0.0
130.0
135.0
140.0
145.0
150.0
155.0
160.0
165.0
170.0
X Experiment
Initial Guess
Least Square

□ - Observed data

——— - Fitting results

Figure 20

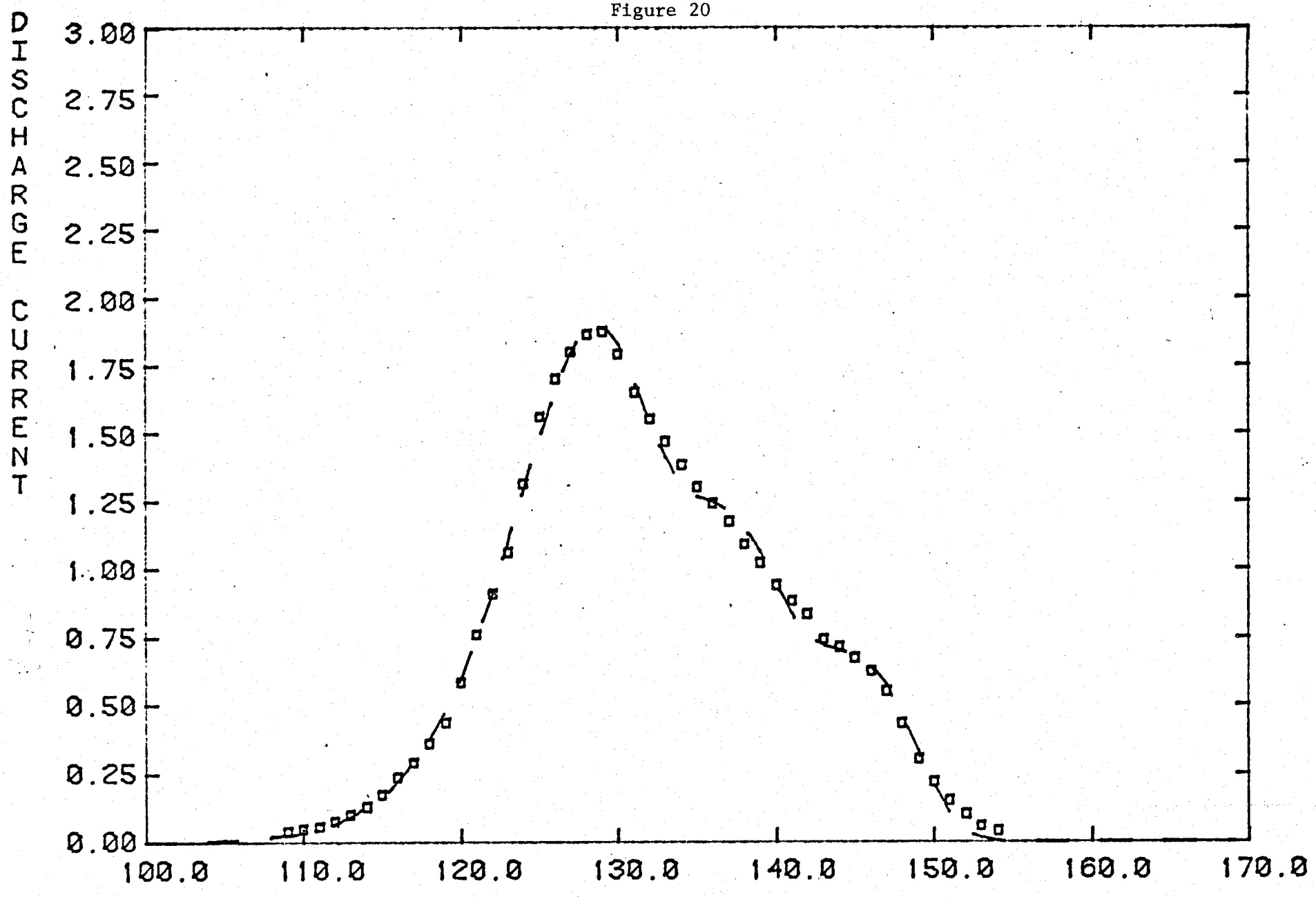

---- fitting results

Figure 21

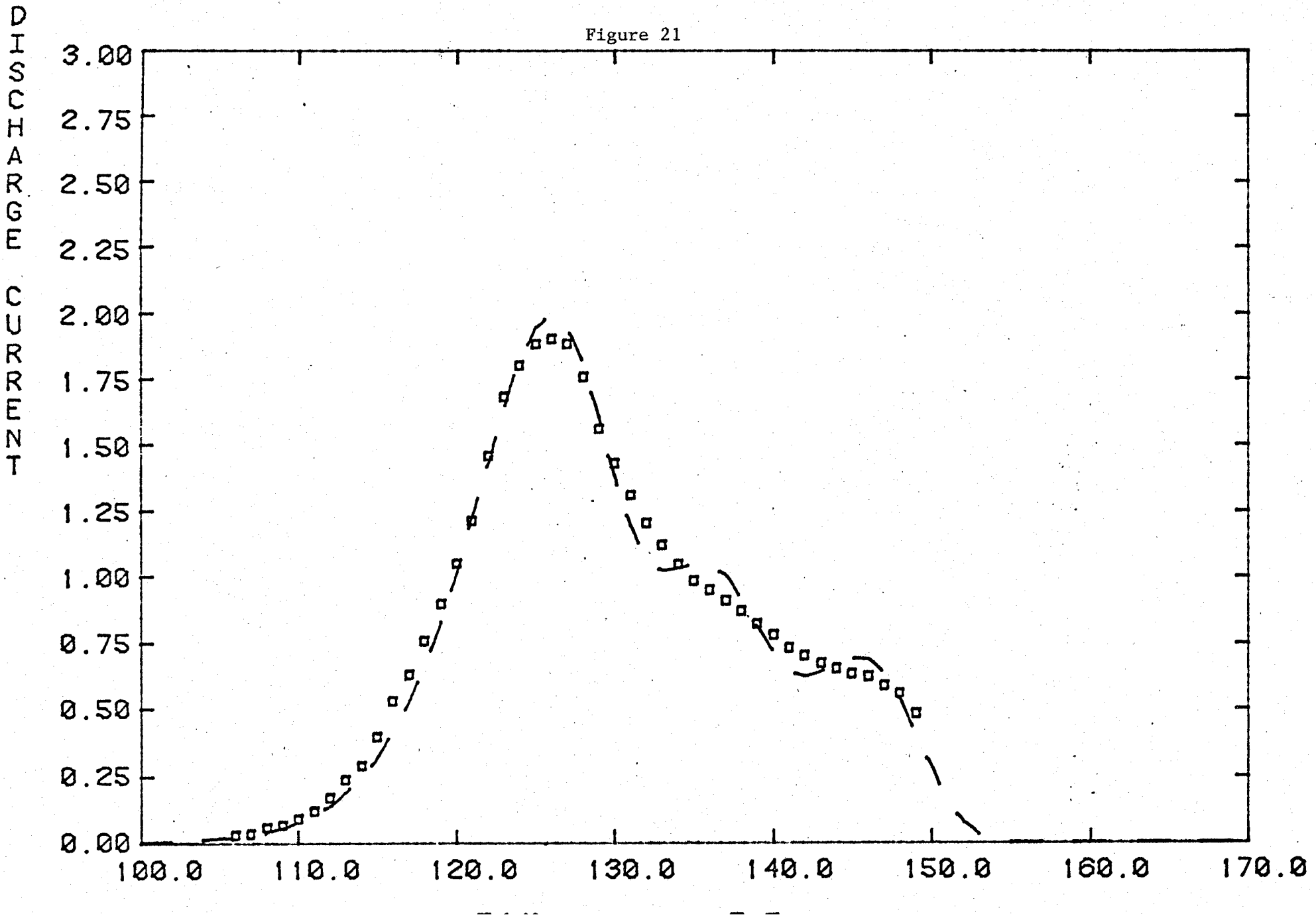

Figure 22

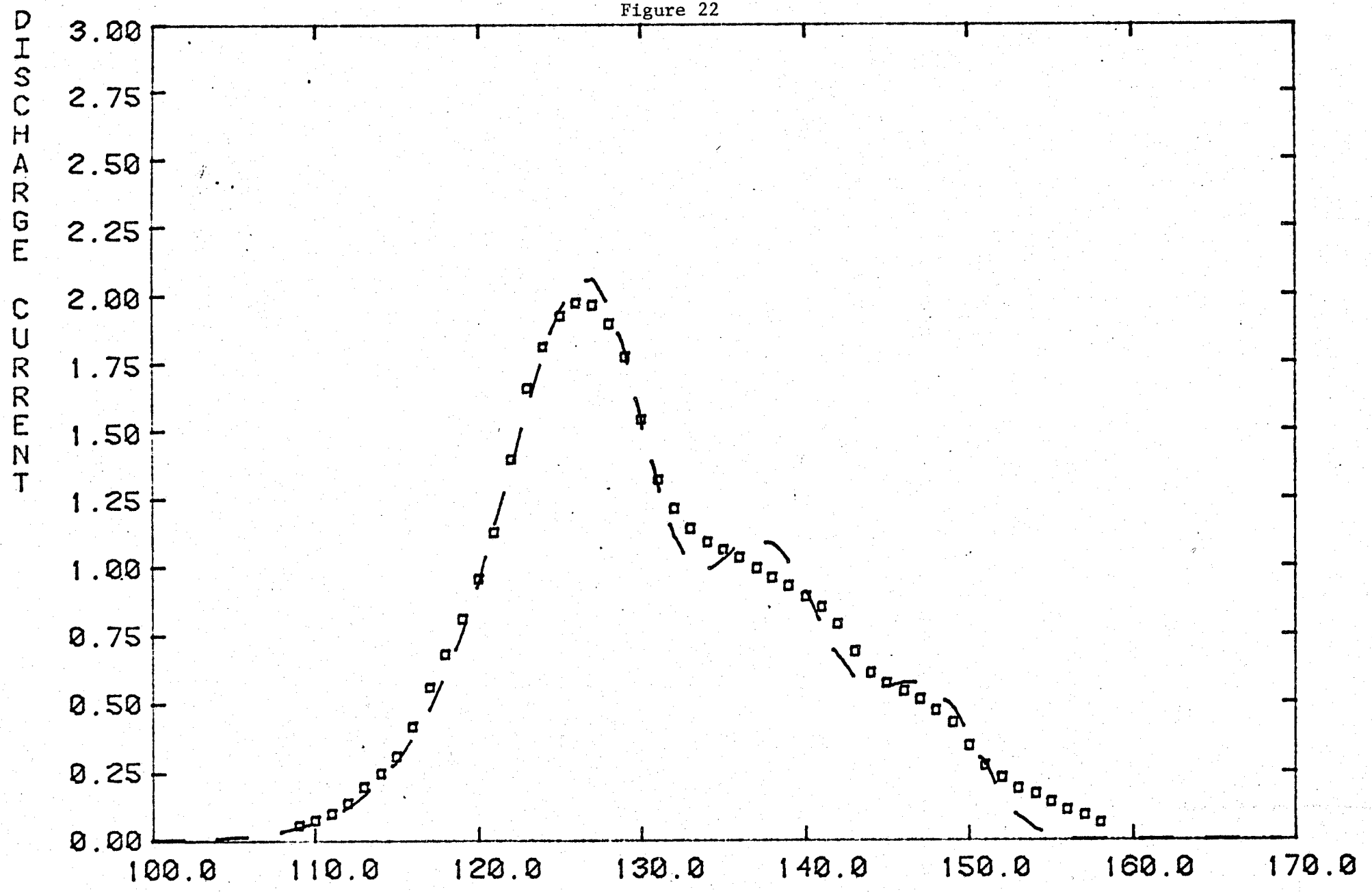
□ Observed T-D
Fitting results
DISCHARGE CURRENT
3.00
2.75
2.50
2.25
2.00
1.75
1.50
1.25
1.00
0.75
0.50
0.25
0.00
100.0
110.0
120.0
130.0
140.0
150.0
160.0
170.0

□- Observed TSD

——— - fitting results

Figure 23

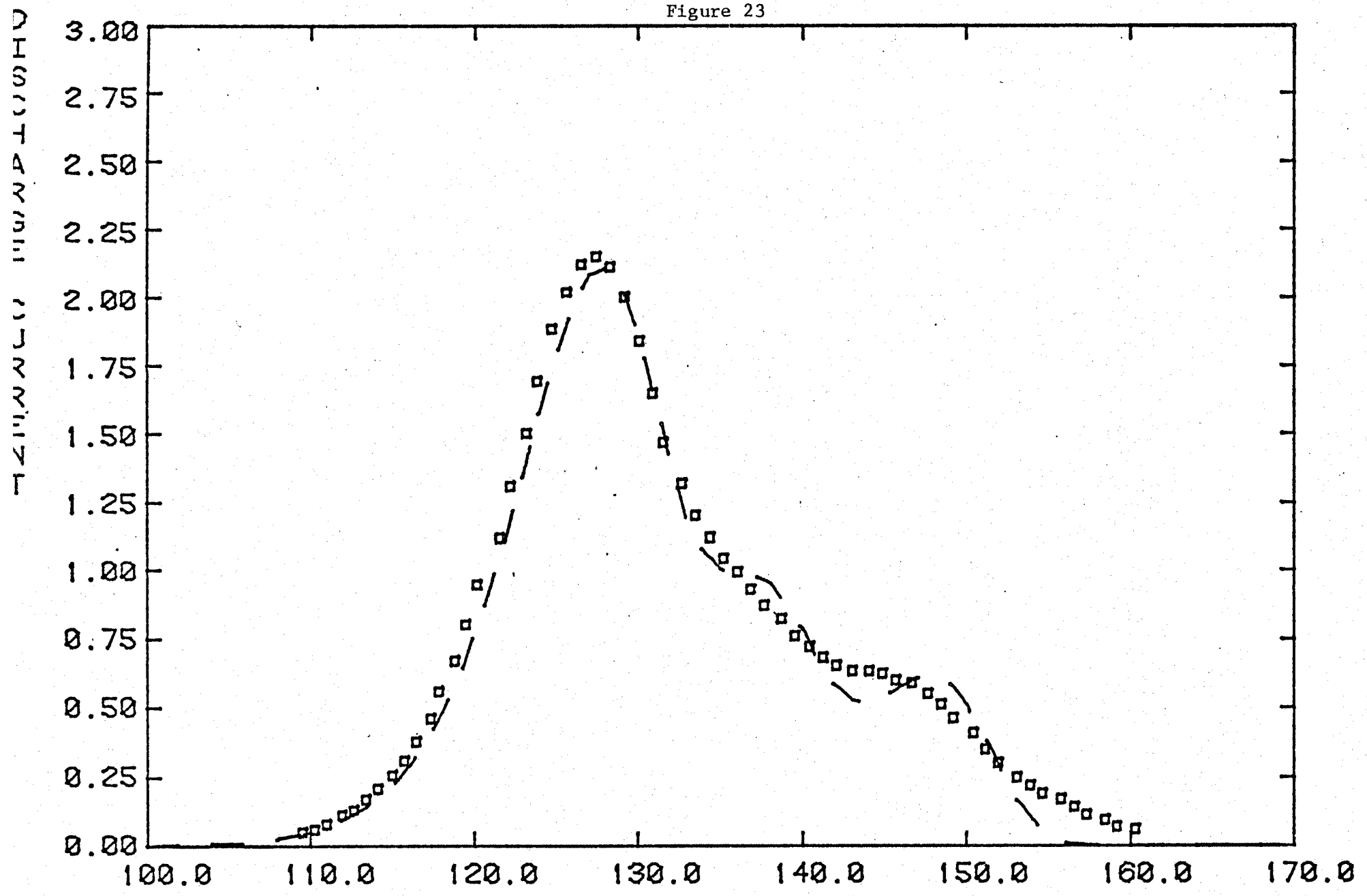

□ Observed I-D

——— Fitting results

Figure 24

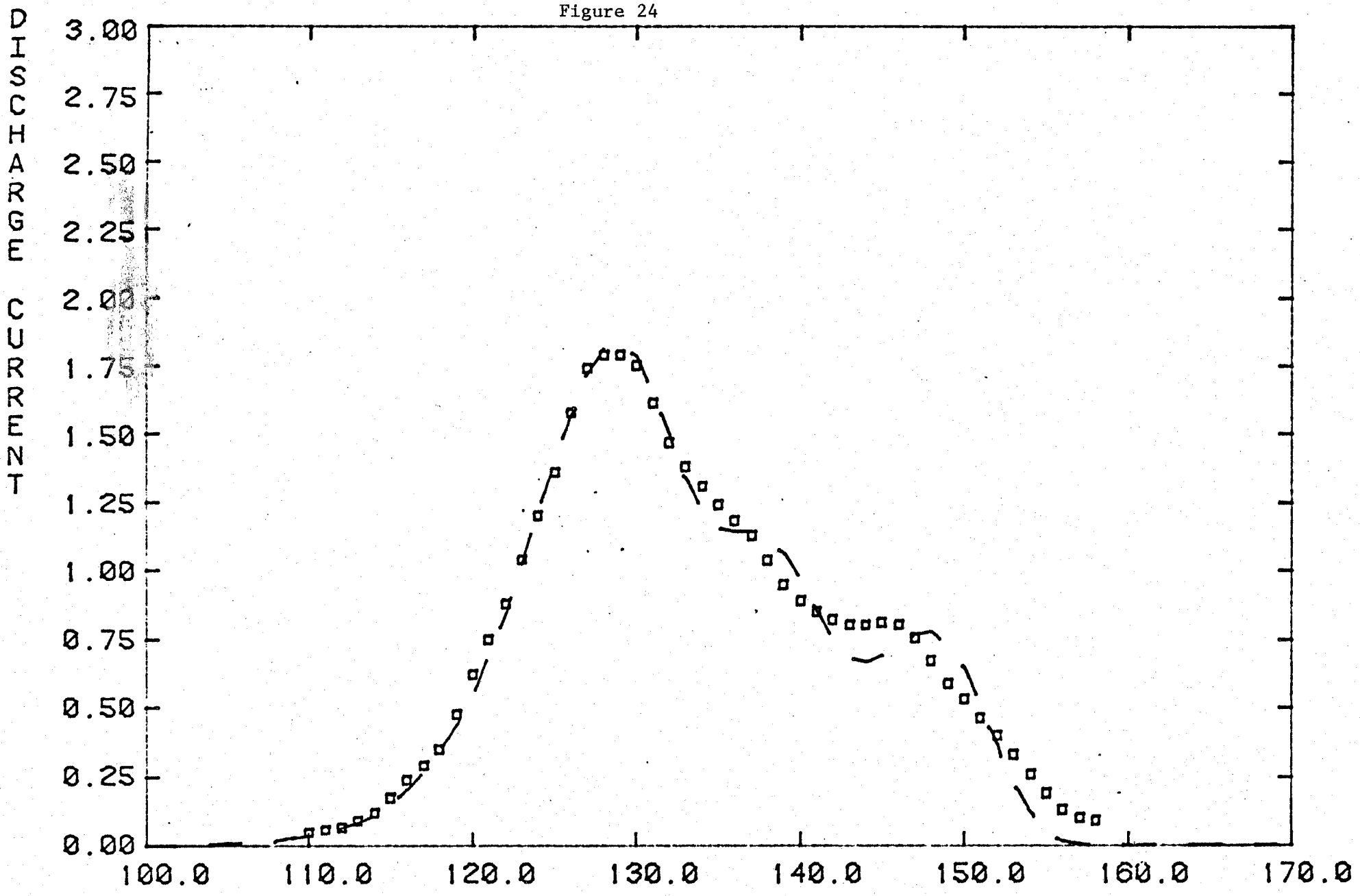

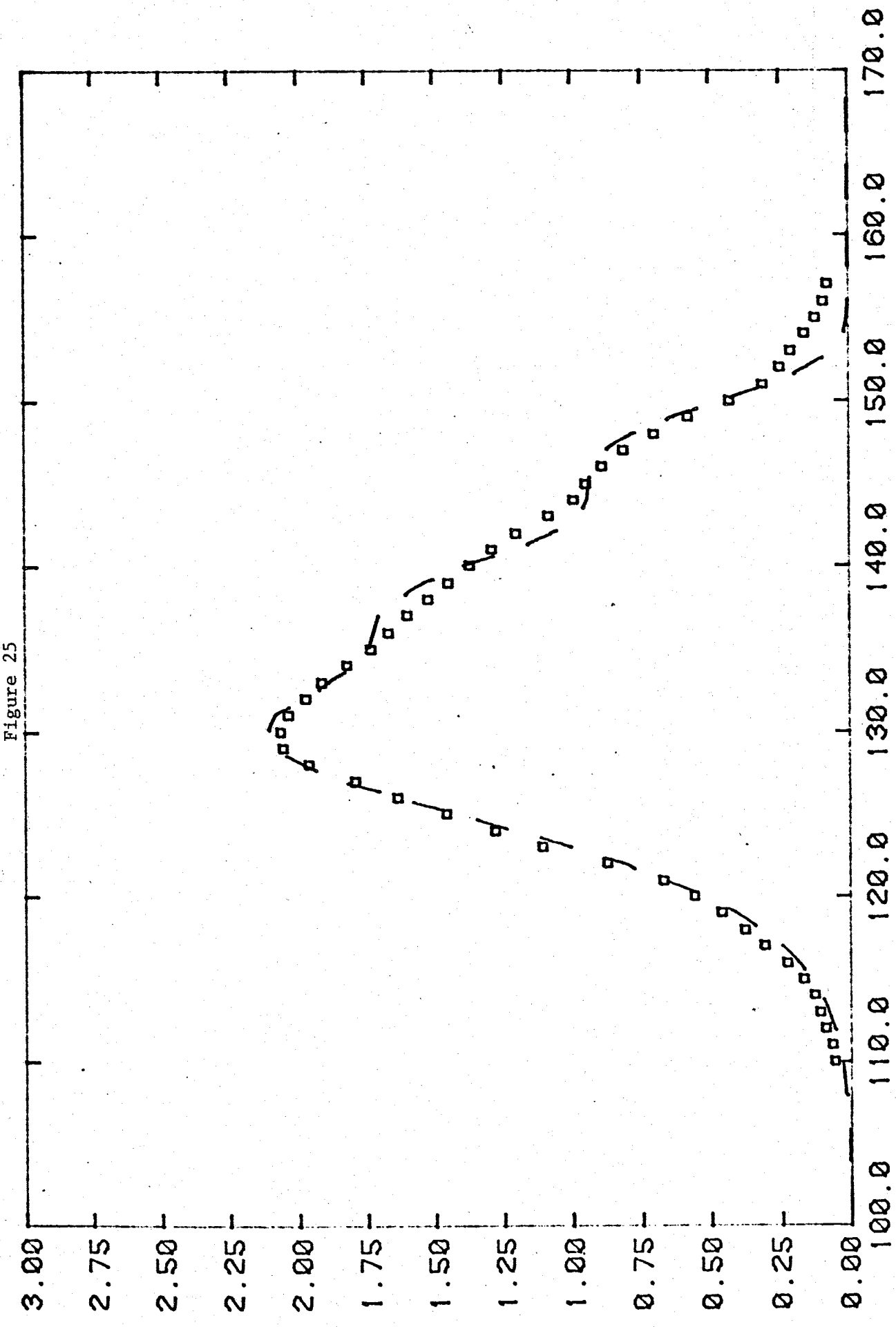
DISCHARGE CURRENT
3.00
2.75
2.50
2.25
2.00
1.75
1.50
1.25
1.00
0.75
0.50
0.25
0.00
100.0
110.0
120.0
130.0
140.0
150.0
160.0
170.0

Figure 25

□ - Observed data

— — — fitting results

Figure 26

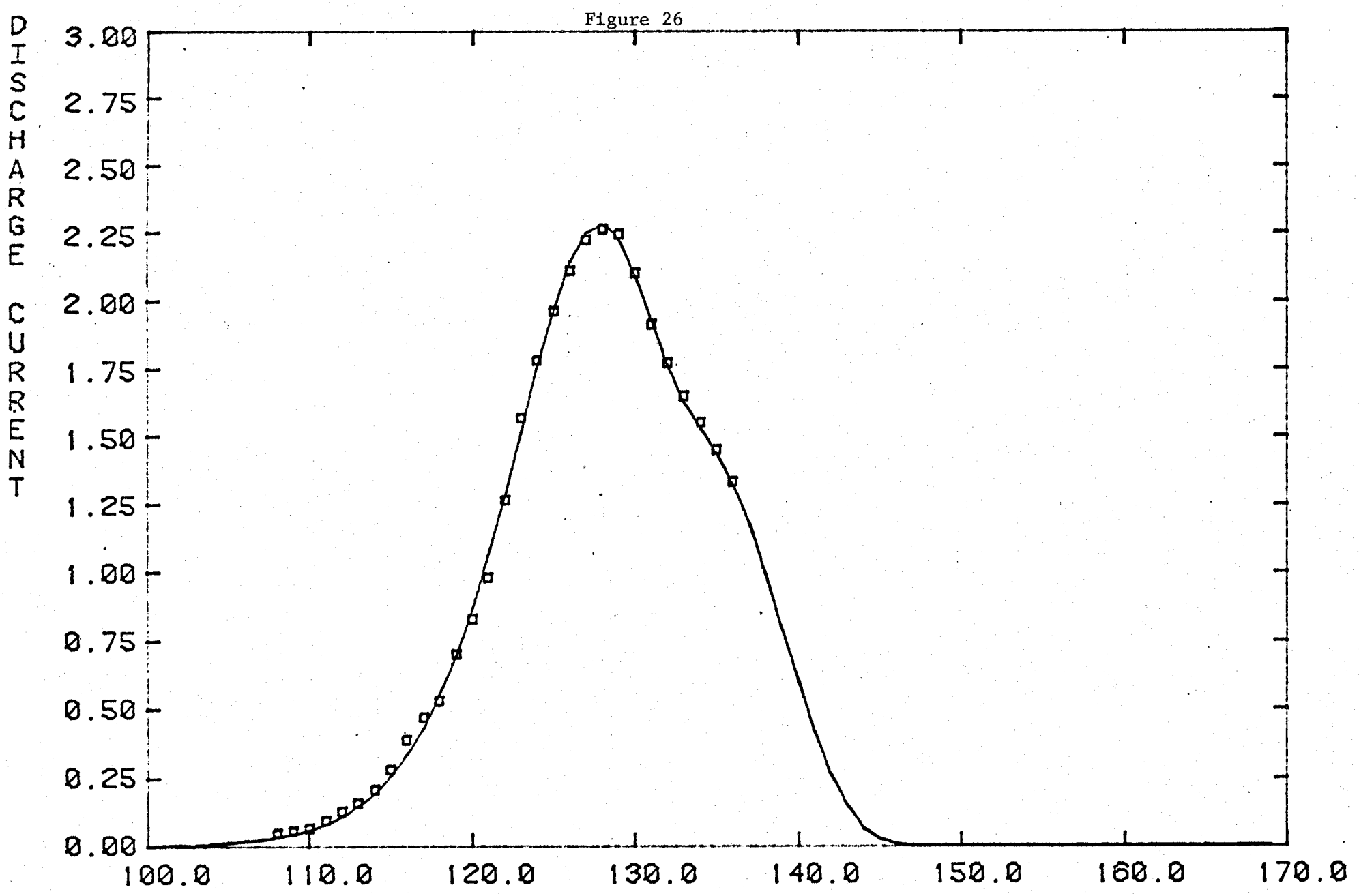

Figure 27

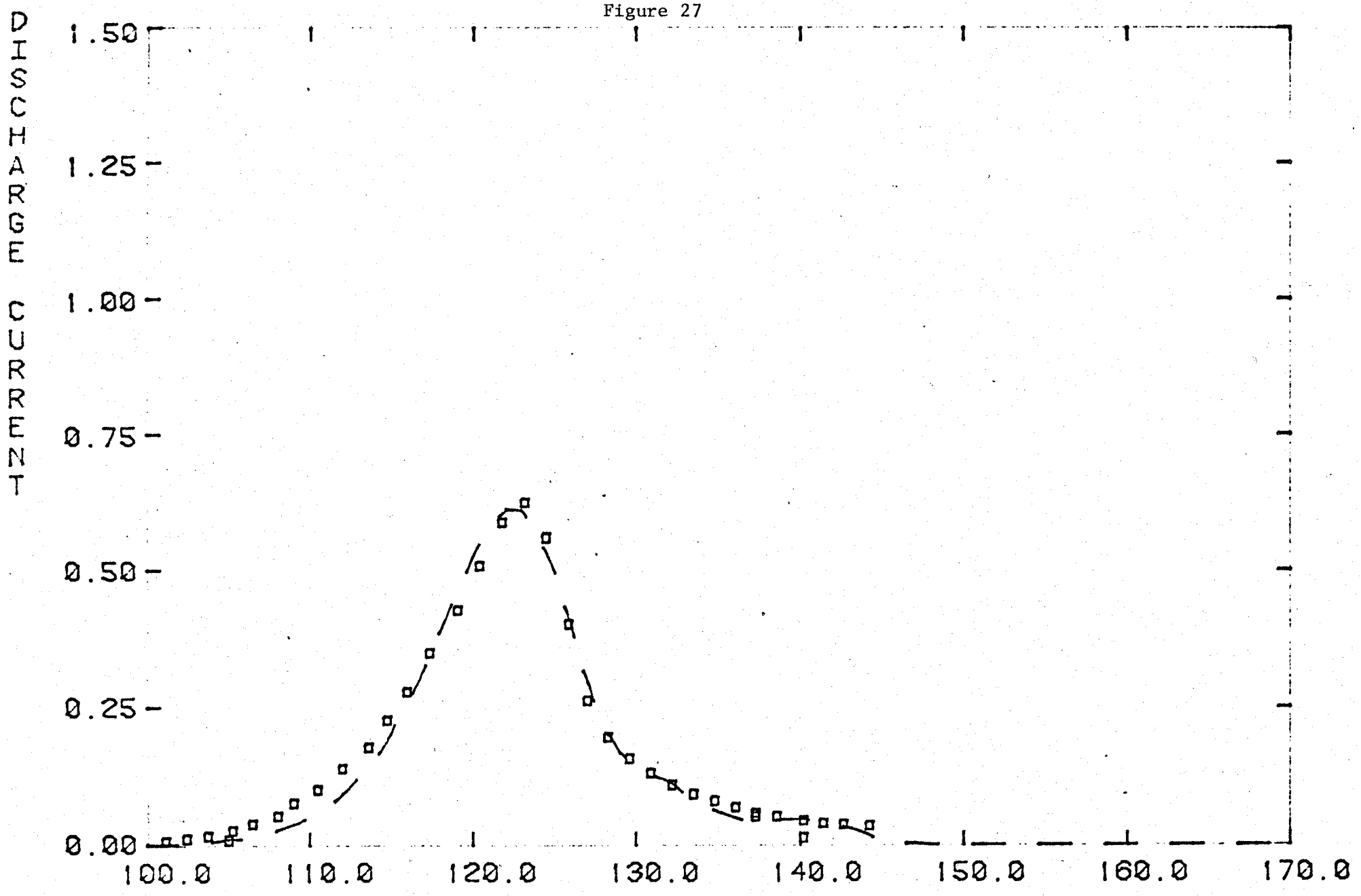
DISCHARGE CURRENT
1.50
1.25
1.00
0.75
0.50
0.25
0.00
100.0
110.0
120.0
130.0
140.0
150.0
160.0
170.0

□ - observed TSD

——— fitting results

Figure 28

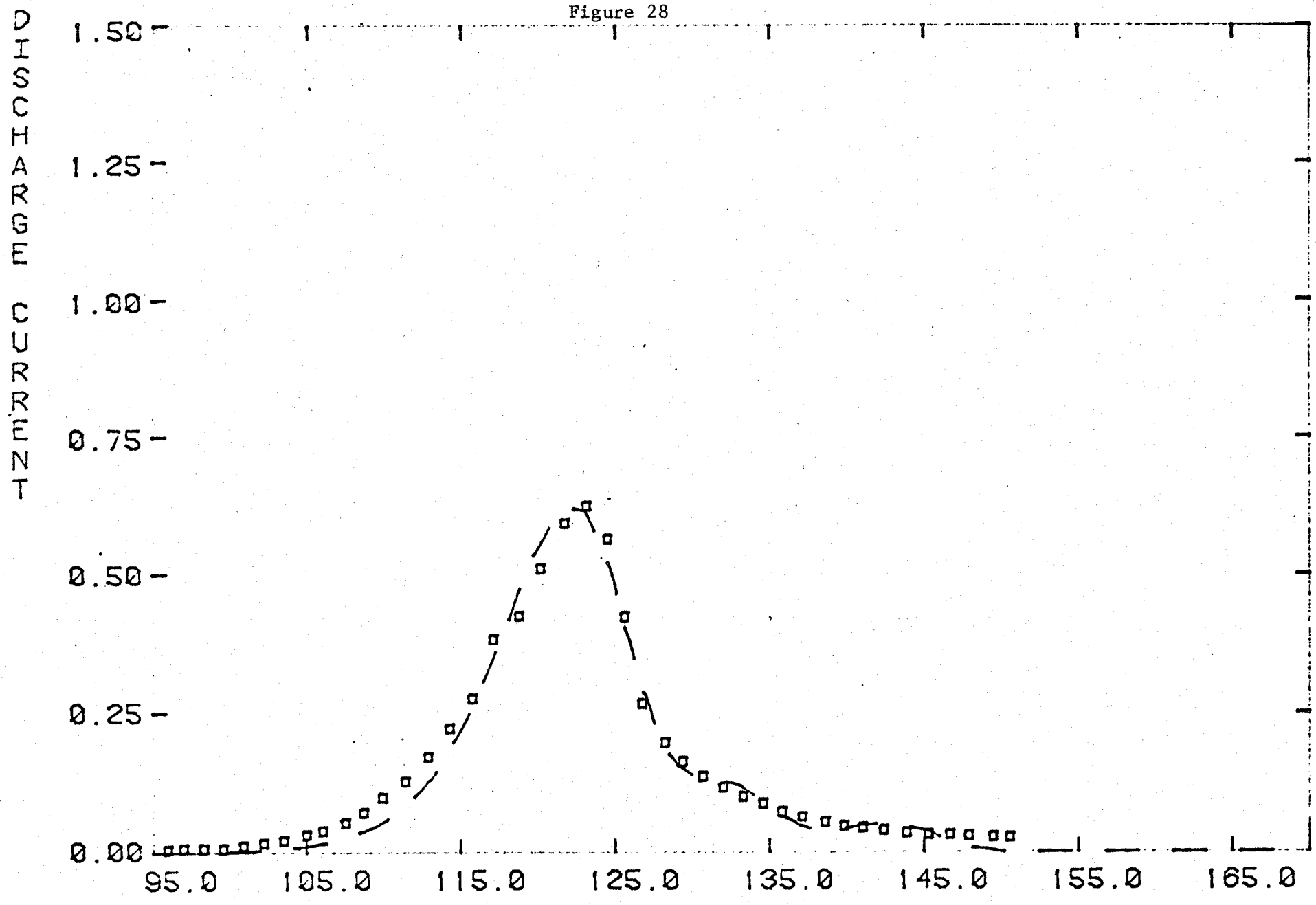

Figure 29

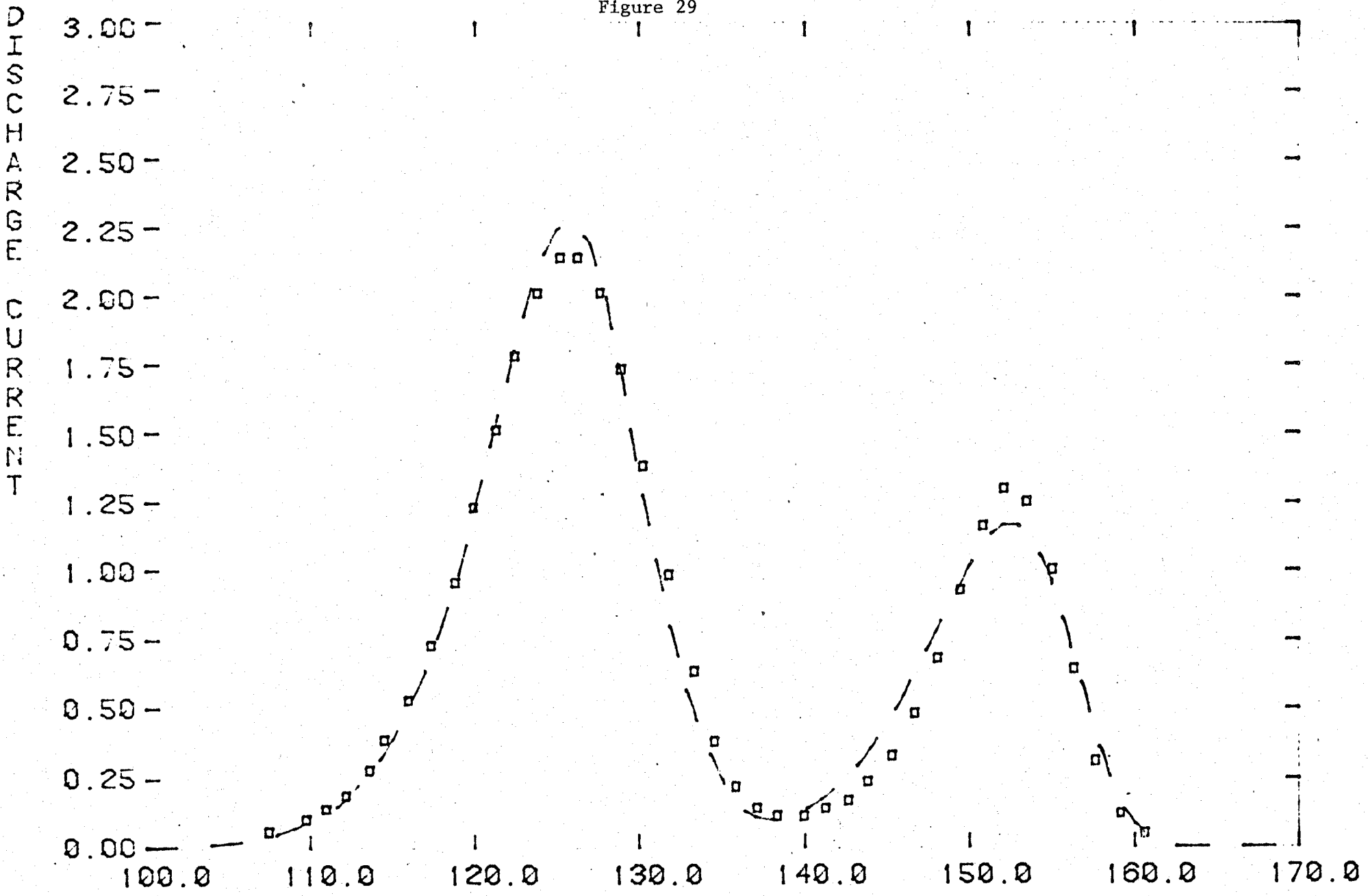
DISCHARGE CURRENT
3.00
2.75
2.50
2.25
2.00
1.75
1.50
1.25
1.00
0.75
0.50
0.25
0.00
100.0
110.0
120.0
130.0
140.0
150.0
160.0
170.0

Fitting results

Figure 30

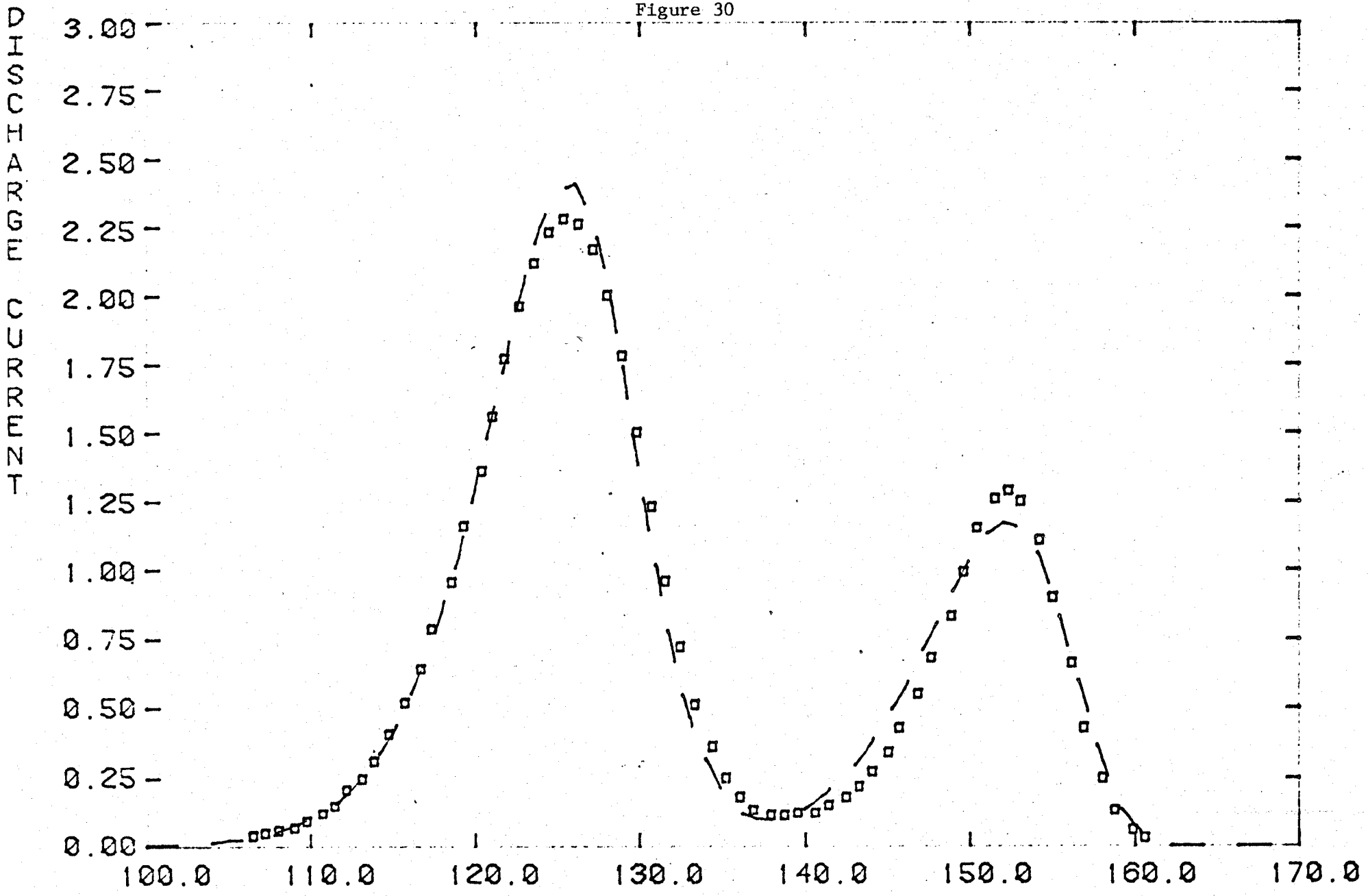

Figure 31

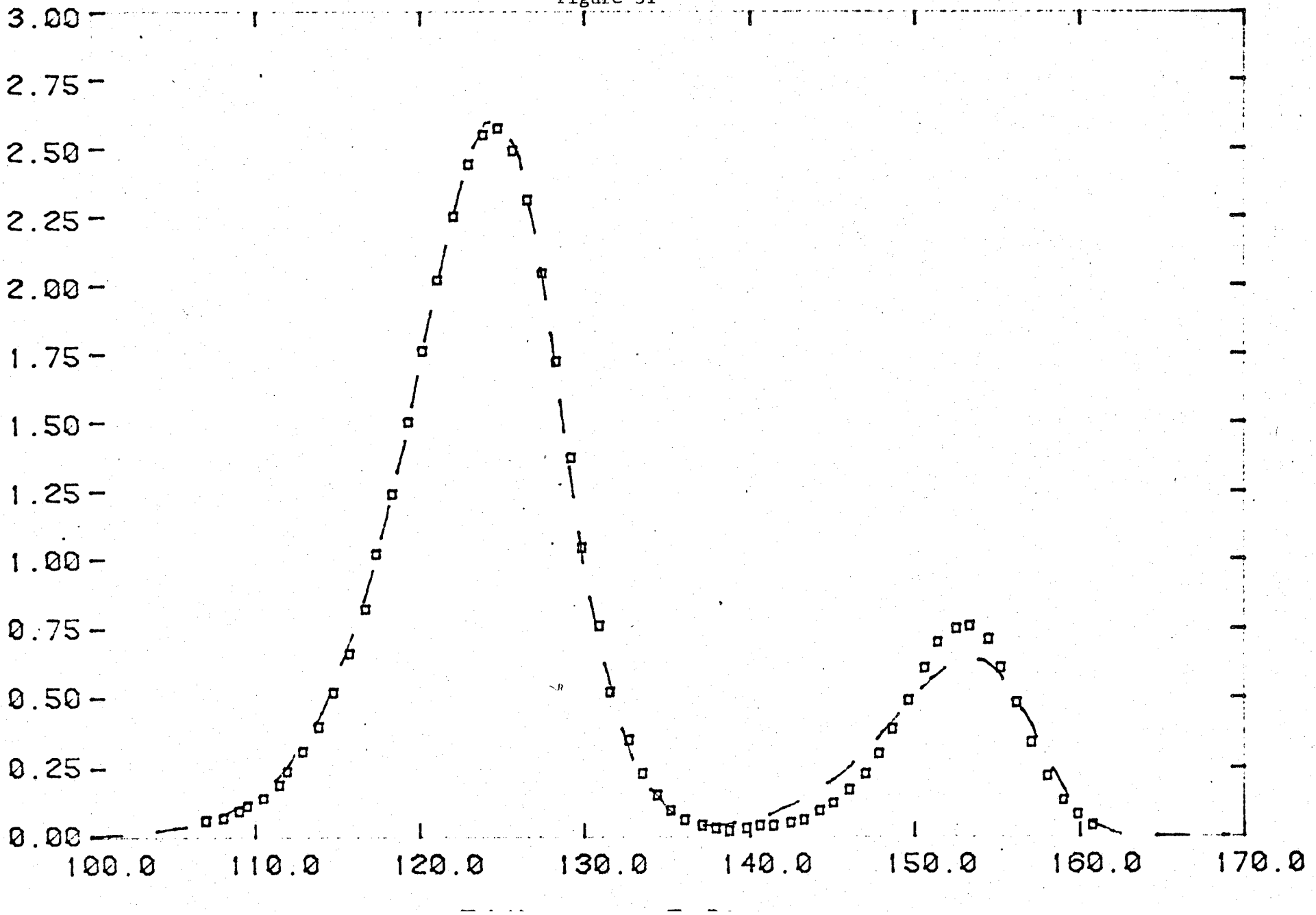
3.00
2.75
2.50
2.25
2.00
1.75
1.50
1.25
1.00
0.75
0.50
0.25
0.00
100.0
110.0
120.0
130.0
140.0
150.0
160.0
170.0

Figure 32

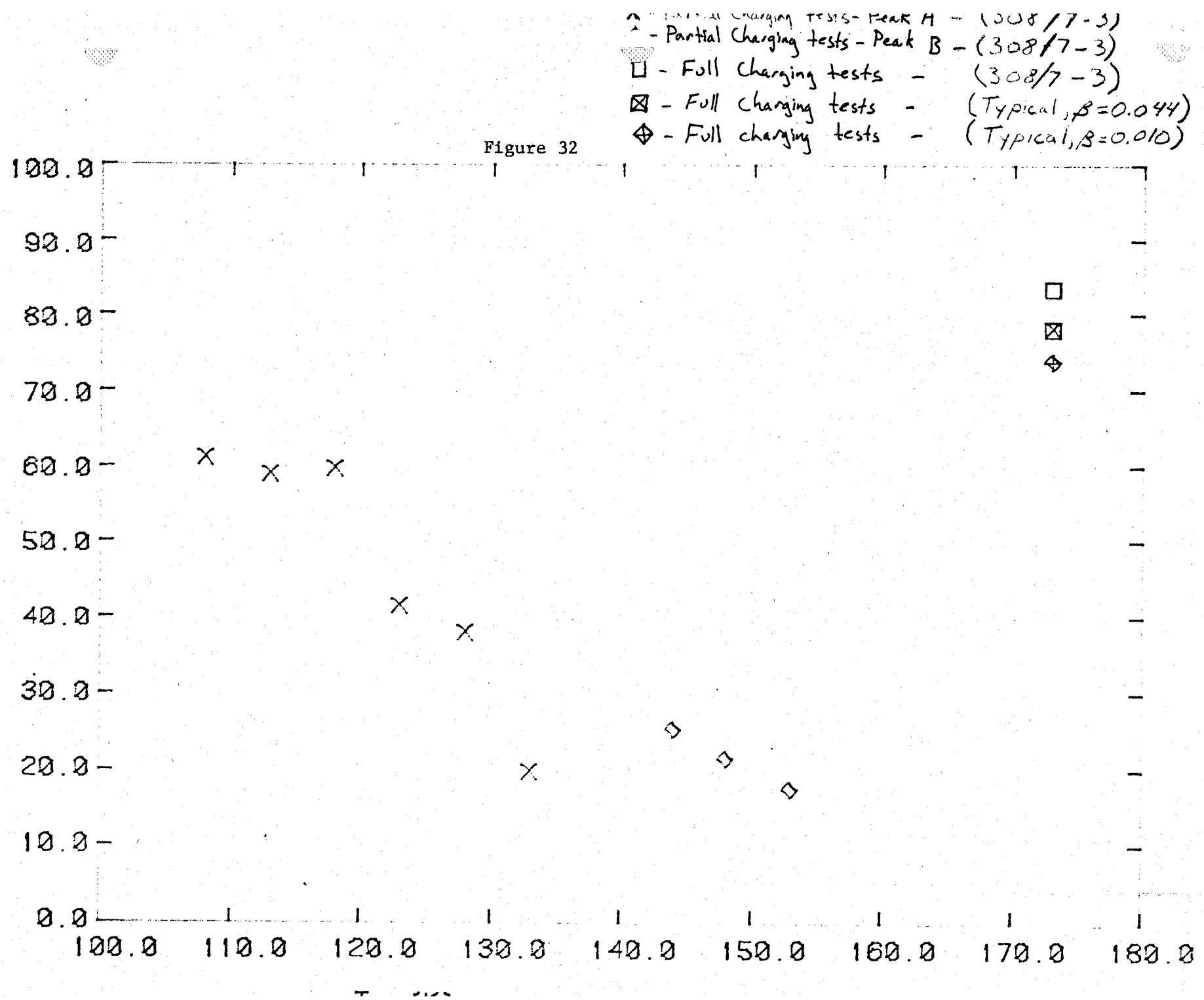
△ - Partial Charging tests - Peak A - (308/7-3)
△ - Partial Charging tests - Peak B - (308/7-3)
□ - Full Charging tests - (308/7-3)
⊠ - Full charging tests - (Typical, β=0.044)
◈ - Full charging tests - (Typical, β=0.010)
STATIC DIELECTRIC CONSTANT
100.0
90.0
80.0
70.0
60.0
50.0
40.0
30.0
20.0
10.0
0.0
100.0
110.0
120.0
130.0
140.0
150.0
160.0
170.0
180.0

Figure 33

x - observed ISV

- - - - fitting results

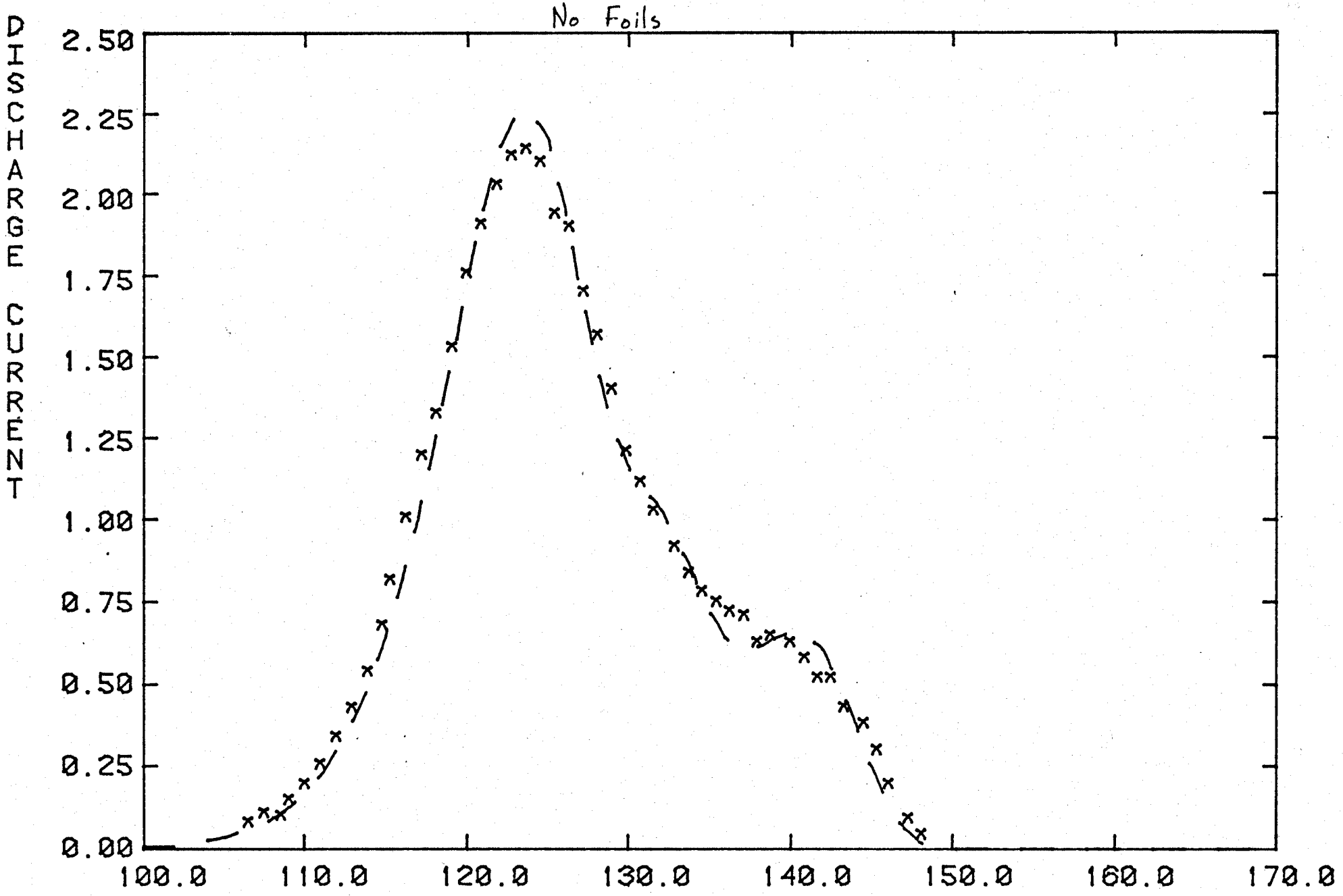

- - - - fitting result

figure 34 NO FOILS

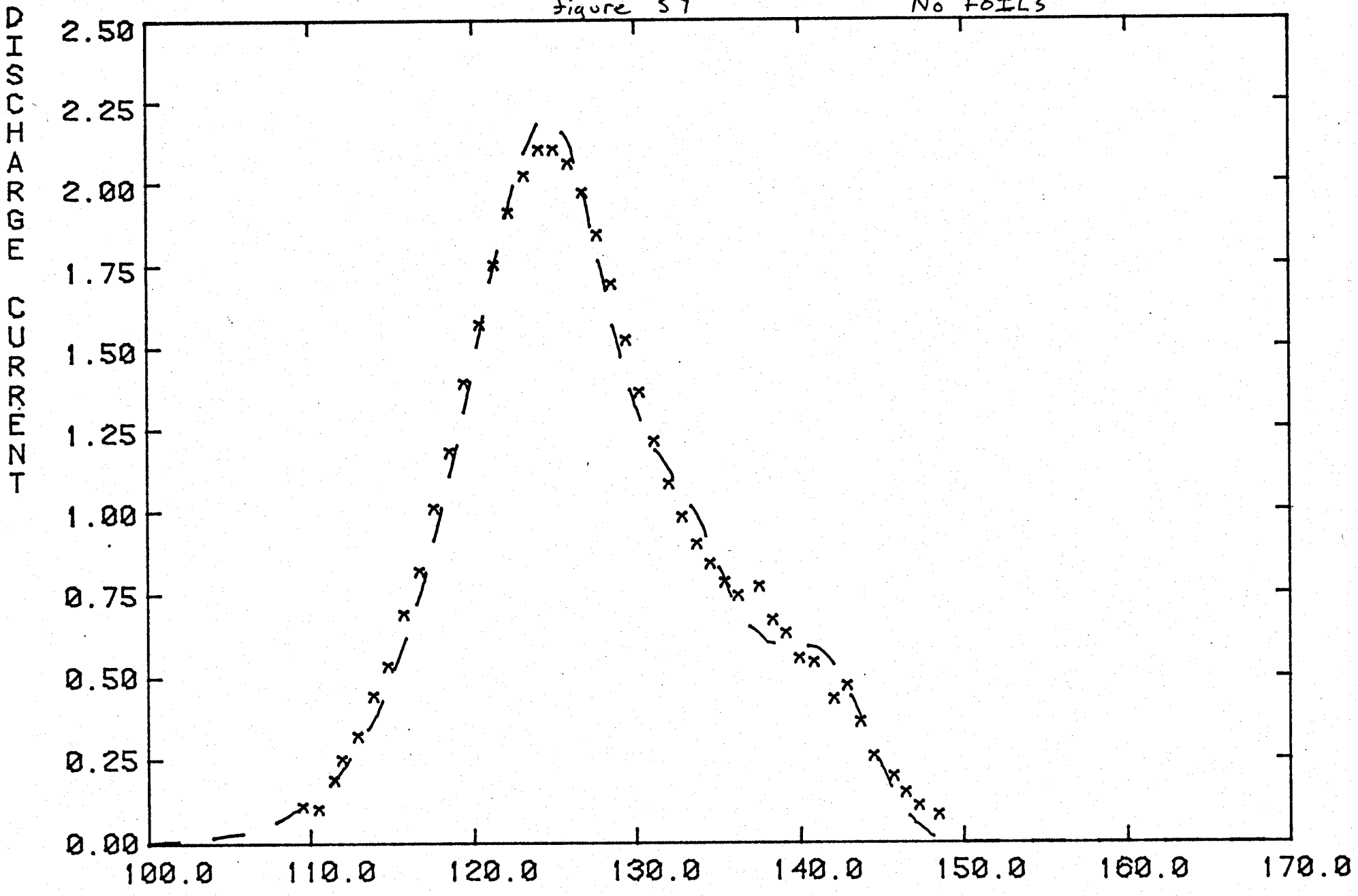

× - Observed ISD

— — — - fitting results

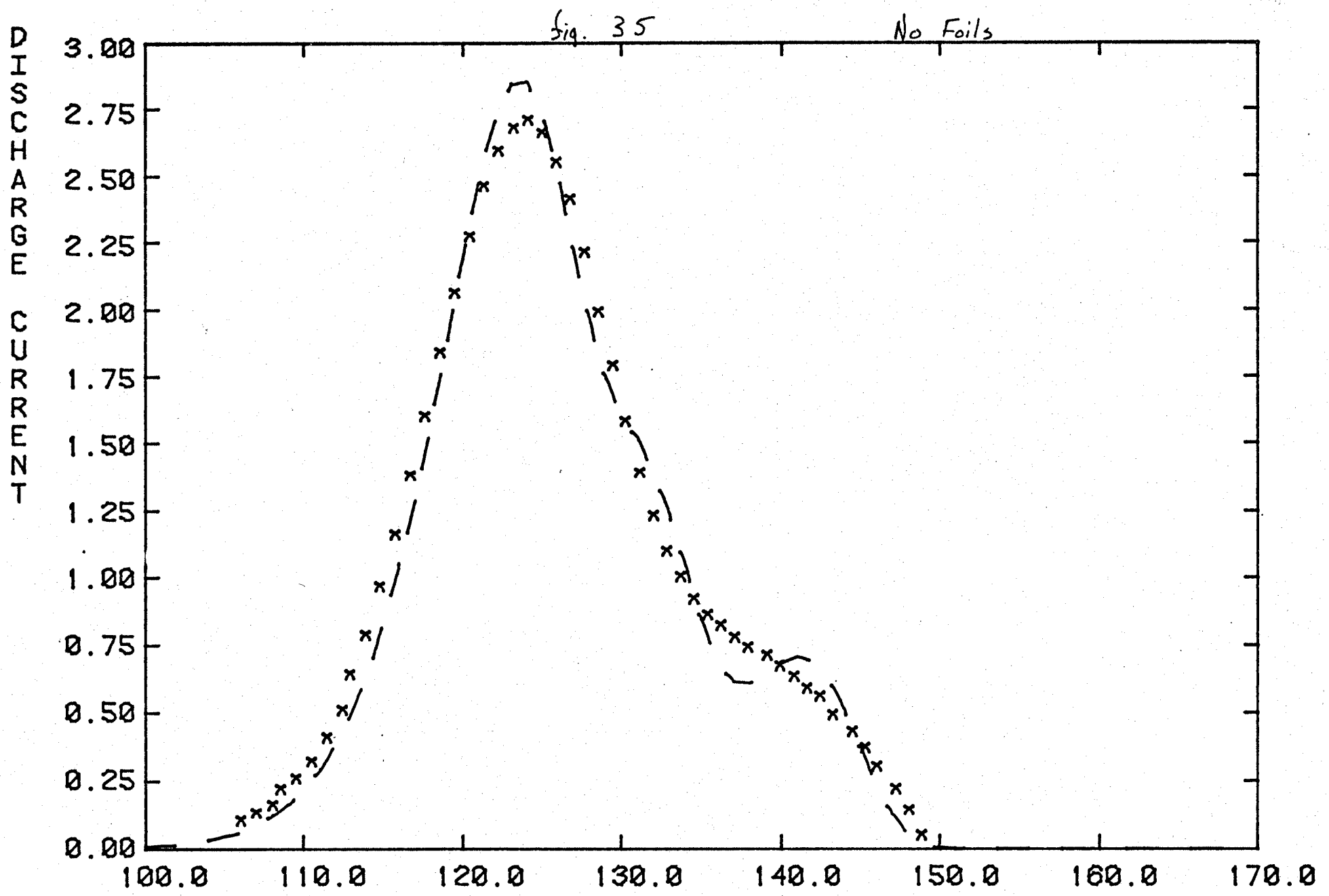

× Observed TSD

— — — - fitting result

Fig. 36

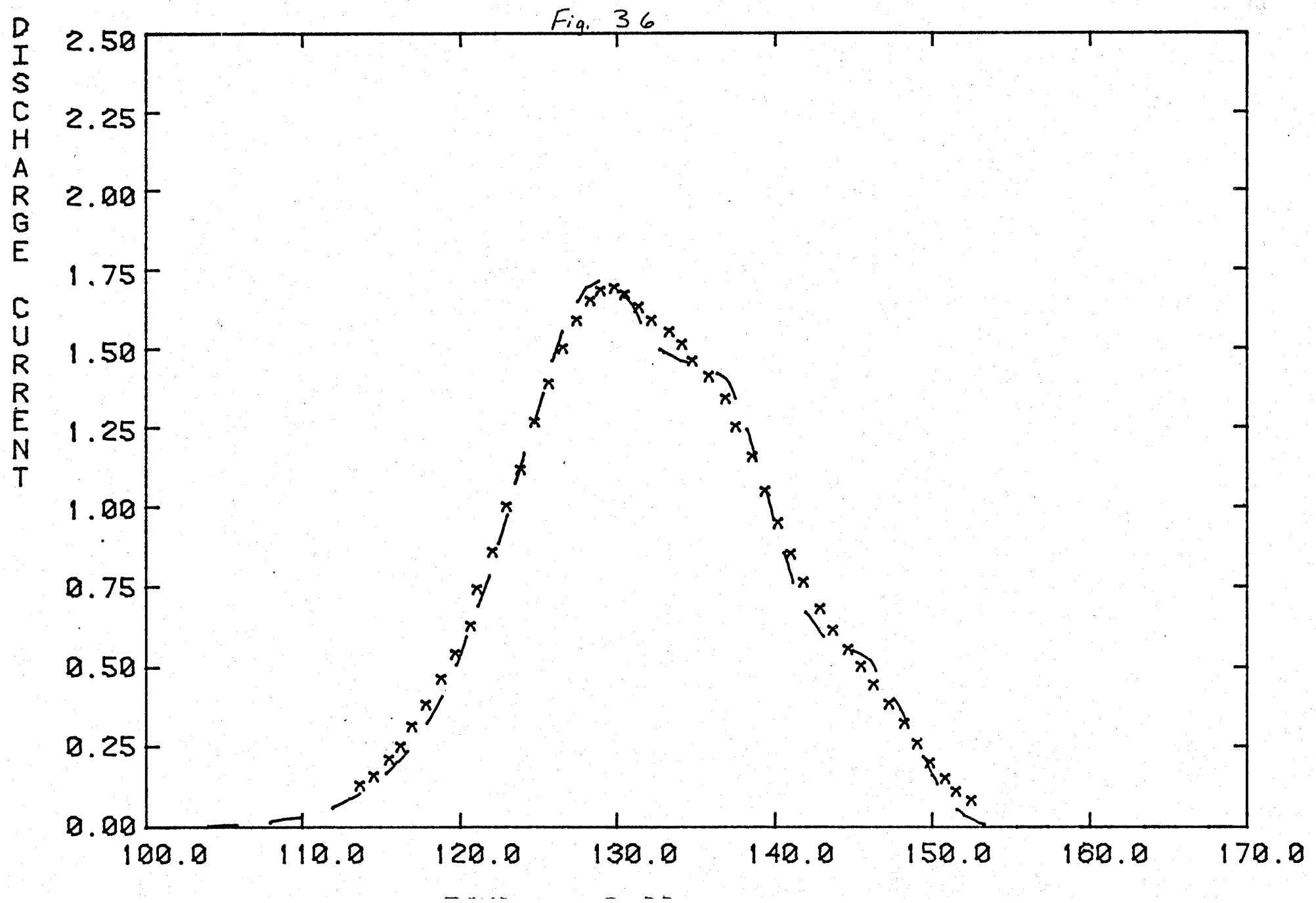

× - observed ISD

— — — - fitting result

Fig 37

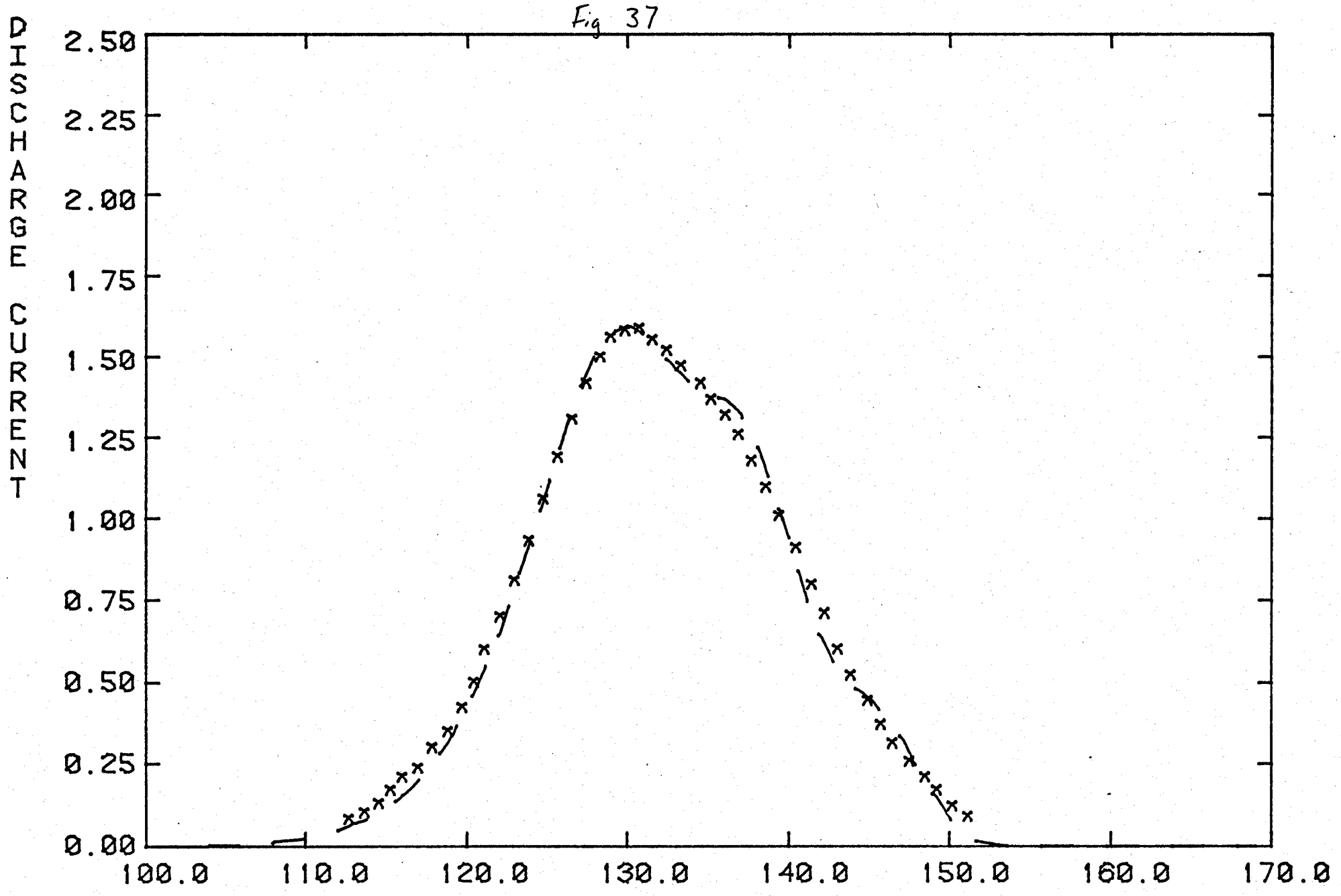

x - Observed ISD

— - — - fitting result

Fig. 38

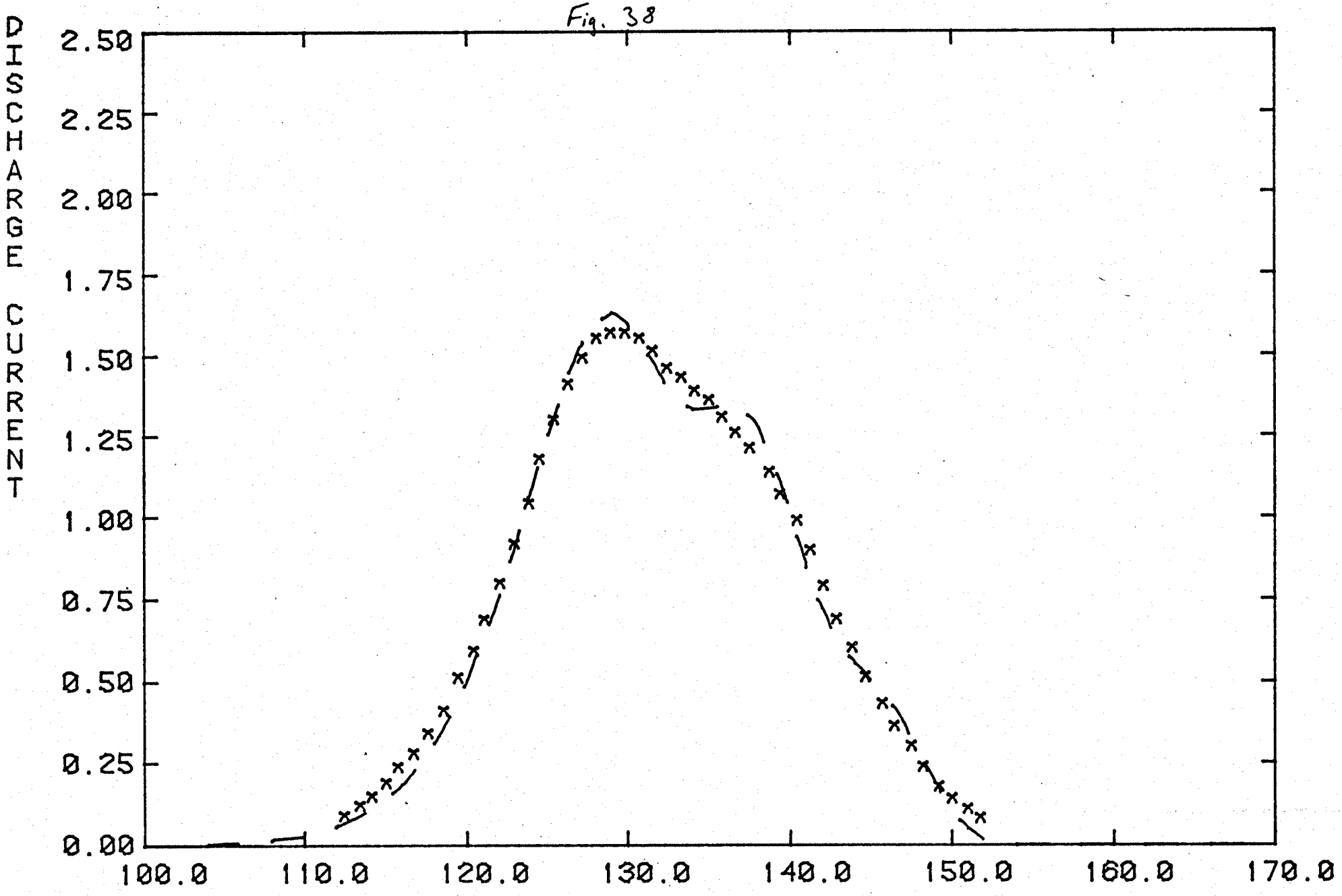

APPENDIX I

I- Modified Experimental Proceedures

Procedures used for partial charging and full charging tests reported in this study are similar to those used by Huppunen (1977) on this apparatus. Revision of proceedures were made upon introduction of a direct line of LN_2 flow to the wall of the sample cell. This flow line consists of two main seqments of 5/16 " copper tubing connecting the sample cell to a tank of LN_2. The first segment runs from the tank to the cryogenic vessel. The second segment continues into the cryogenic vessel to the sample cell and is encased in an 3" diameter aluminum cylinder which is closed at the bottom around the copper tube. In order to achieve maximum cooling rates, this line must be purged and pre-cooled just prior to cooling of the sample.

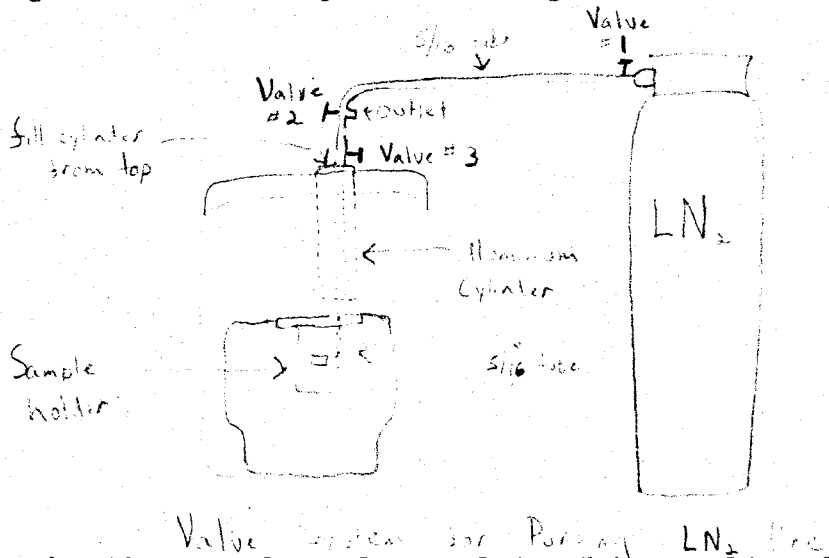

The three valves located in this cooling line and the aluminum cylinder allow nearly the entire length of the line to be

purged in the following way :

i) Close valve #3, open valve #2, open valve #1. When LN_2 comes out of the opening at valve #2 -CLOSE VALVE #2 (cools segment from tank to valve #2).

ii) With a dewar, fill the aluminum cooling cylinder (cools segment from valve #2 to sample cell).

* Test should proceed immediately so system is as cold as possible.

Test Procedures

Partial Charge Tests- Rapid Cooling

1) Warm sample to 250° K.

2) Set controller at desired charging temperature (T_{ch}).

3) Cool sample with LN_2 until the temperature is stable at T_{ch}.

4) TURN ON HIGH VOLTAGE D.C. potential (V_{ch}) for time t_{ch}.

*****(PURGE COOLING SYSTEM)*****

5) At the end of t_{ch}, OPEN VALVE #3 and watch sample temperature.

6) When T is low enough, TURN OFF V_{ch}.

Charging potential should be turned off immediately at temperature T_o such that $\tau(T_{ch}) << \tau(T_o)$ but continue cooling until the temperature reaches approximately liquid nitrogen temperature.

7) CLOSE VALVES #1 and #3

8) Set heater controller at the beginning of the heating cycle and select a heating rate.TURN ON HEATER CONTROLLER

9) Switch electrode cables from charging circuit to electrometer ciruit - TURN ON ELECTROMETER AND RECORDER

10) At the end of the heating cycle, TURN OFF HEATER, TURN OFF ELECTROMETER, TURN OFF RECORDER.

Full Chargng Test - Slow Cooling

1) Warm sample to 250^{o} K

2) Set controller at beginning of the cooling cycle, choose a cooling rate, and turn on controller.

3) TURN ON V_{ch}.

4) Allow sample to cool to liquid nitrogen temperature at the controlled rate adding liqiud nitrogen as needed to continue cooling.

5) TURN OFF V_{ch} and note sample temperature.

6) Set controller at beginning of the heating cycle and select a heating rate - TURN ON HEATER CONTROLLER.

7) Switch electrode cables from the charging circuit to the electrometer circuit TURN ON ELECTROMETER- TURN ON RECORDER.

8) At the end of the heating cycle TURN OFF THE HEATER, TURN OFF ELECTROMETER, TURN OFF THE RECORDER.

APPENDIX II

II- Inversion Procedures

Programming of the data inversion process may be broken down into four main steps ;

1) Input of data points

2) Creation of the ΔJ vector

3) Calculation of the A matrix

4) Calculation of Δx from either equation 4-1b or 4-4

II-1 Input

The most convenient way to input TSD data to the DEC-20 at this time is creation of a disc data file containing test parameters and data. Temperatures are recorded in digital form as output voltage from thermocouples and calculated using the polynomial reported by the National Bureau of Standards (1974) for type T thermocouples. Data files used to store TSD data in this lab are in the following format. More specific documentation of the programs used in this study may be found in the TSD laboratory.

The first three lines of each file contain descriptive information concerning the test such as the test number, date, sample etc.. These lines are in a general format so that information can be written in any form.

The fourth line of each data file contains specific information about the test such as the number of data pairs, sampling interval, and heating rate.This line is in specific format because these are test parameters to be read and used in calculations.

The remaining lines contain the electrometer current vs. thermocouple voltage data pairs. Appendix IV contains a complete listing of all data files used in this study.

II-2 The ΔJ Vector

The ΔJ vector is formed by, first, calculating the initial estimated value of discharge current

$$j_o(T_i) = j(T_i, E_o, \tau_{oo}, P_{oo})$$

where

E_o = initial estimate of E

τ_{oo} = Initial estimate of τ_o

P_{oo} = Initial estimate of P_o

and then calculating the difference from observed TSD at that temperature.

$$\Delta j_i = j(T_i) - j_o(T_i)$$

Not mentioned in the earlier discussion was the effect of

data point weighting on the inversion. Elements of the ΔJ vector must be weighted with regard to the uncertainty on the data point such that

$$\Delta j_{i\ \text{weighted}} = \Delta j_i / \sigma_i$$

where

σ_i = "i th" data point uncertainty.

In this study all data points are weighted equally with values depending on the current intensity of the particular test. In general, data points are weighted with about 10% of the peak maximum of the test.

$$\sigma_i = j_{max} \times 0.1$$

II-3 The A Matrix

The A matrix (equation 4-1a) is formed by taking numerical derivatives of equation 2-10 with respect to each parameter and evaluating these derivatives at each data point temperature (T_i).

$$A_{ij} = \frac{\partial j_o(T_i)}{\partial x_j} = \frac{\Delta j_o(T_i)}{\Delta x}$$

Then,

$$A_{11} = \frac{[j'_o(T_1, E_o + \Delta E_o, \tau_{oo}, P_o) - j_o(T_1)]}{\Delta E}$$

and

$$A_{32} = \frac{[j'_o(T_3, E_o, \tau_{oo}+\Delta\tau_{oo}, P_{oo}) - j_o(T_3)]}{\Delta\tau_{oo}}$$

A matrix element must also be weighted with regard to the data point uncertainty and parameter uncertainty such that

$$A_{ij\ \text{weighted}} = A_{ij} \times \tau'_j/\sigma_i$$

In this study, parameters for the partially charged TSD curves (peaks A and C) were weighted using uncertainties calculated from initial rise results at varying charging temperatures. Parameter uncertainties for fully charged curves were set at +/- 5% of their initial values. Parameter and data point weighting are discussed in the documentation supplied with inversion programs.

II-4 Calculation of Δx

Calculation of Δx using either equation 4-1b or 4-4a is easily accomplished through the use of International Mathematical Scientific Library (IMSL) subroutimes such as that for matrix inversion (LGINF) or eigenvalue-vector decomposition (EIGRS). Once the A matrix and ΔJ vector have been formed the inversion program involves numerous subroutine calls to form the desired result. Given the Δx vector, the new x's may be found and the resulting $j(T_i)$ calculated. Details of these calculations and of calculating fitting parameters are discussed in program documentation.

APPENDIX III

III-Foil Effects

Determination of the effect of current blocking Teflon foils on TSD is vital for correct interpretation of trapping parameters. In this section, results of TSD test on pure ice samples without current blocking foils are reviewed. These tests were performed on a sample cut from a different column (308/09) of pure ice grown under identical conditions to column 308/7 used for the main body of this work.

Various mechanisms may act at the sample-electrode interface, at one time, resulting in a very strong complex effect on the TSD spectrum. Imperfections in the sample surface may result in air gaps between the sample and electrodes. Townsend Breakdown of the air in these gaps may cause charge to be injected into the surfaces of the sample (see diagram below).

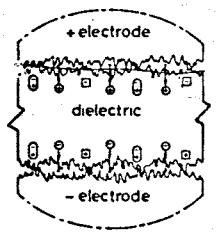

Injected Charges ⊕, ⊙ - Dipoles ⦶ - Ions ⊞, ⊟
from Van Turnhout (1975), p.3

Further, when blocking foils are used, the Maxwell-Wagner effect acting between materials of differing conductivities (Teflon/ice) causes a buildup of charge at the interface (van

Turnhout (1975), p. 138). In the absence of blocking foils, a narrow air gap between the electrode and sample may also act as a (poor) conductor due to Townsend Breakdown.

Townsend Breakdown results in injection of positive and negative charge at the positive and negative electrodes respectively. When blocking electrodes are used, the injected charges are not able to recombine with image charges on the electrodes. If these injected charges are not neutralized through recombination with space charge within the dielectric, a current reversal may result upon heating as these excess charges diffuse throughout the sample. When blocking electrodes are not used, injected charges are free to recombine with image charges at the electrodes and the reversal effect is neutralized.

Results of similar partial charging tests with and without foils are listed on the next page and illustrated in Figures 33-38.

Parameter Summary

Sample 308/09-2 NO FOILS
$\beta = 0.044$ - $T_{ch} = 123°K$ - $V_{ch} = 1500V$

Test	Peak	t_{ch}	E (cal/mole)	τ_o ($\times 10^{-13}$ Sec)	ε_s	Fig
D80	A	2 hr.	7020	28.8	31.3	33
D81	A	3 hr.	7070	29.6	29.9	34
D85	A	6½ hr.	7020 / 7037 ± 24	27.6 / 28.7 ± .8	38.1	35

Parameter Summary (Continued)
Sample 308/09-2 - NO FOILS

Test	Peak	t_{ch}	E (cal/mole)	τ_0 ($\times 10^{-12}$ Sec)	ε_s	Fig
D80	B	2 hr.	7930	4.43	14.9	33
D81	B	3 hr.	7960	4.71	15.5	34
D85	B	6½ hr.	7880	5.13	22.4	35
			7923 ± 33	4.75 ± .3		
D80	C	2 hr.	9550	—	10.48	33
D81	C	3 hr.	9550	—	9.35	34
D85	C	6½ hr.	9600	—	11.27	35
			9567 ± 24			

Parameter Summary

Sample 308/7-1, with foils

$\beta = 0.044$, $T_{ch} = 123^\circ K$, $V_{ch} = 1500 V$

	Peak	t_{ch}	E (cal/mole)	τ_0 ($\times 10^{-12}$ Sec)	ε_s	Fig.
136	A	4 hr.	7256 ± 25.5	33.5 ± .2	23.7	36
139	B	4 hr.	8273 ± 12.5	5.3 ± .03	24.6	37
141	C	4 hr.	9826 ± 17.0	—	9.8	38

These discharge spectra show a consistent reversal at 148° K in tests conducted without foils. Data from tests with, and without foils are compared and generally summarized as follows ;

1) Activation energy is lower with no foils by < 4%.

2) τ_o is lower for A and B peaks with no foils by approximately 10 %, equal for C peaks but still strongly model dependent in inversion (i.e. dependent on initial parameters).

3) ϵ_s with no foils is higher for peaks A and C and lower for peak B.

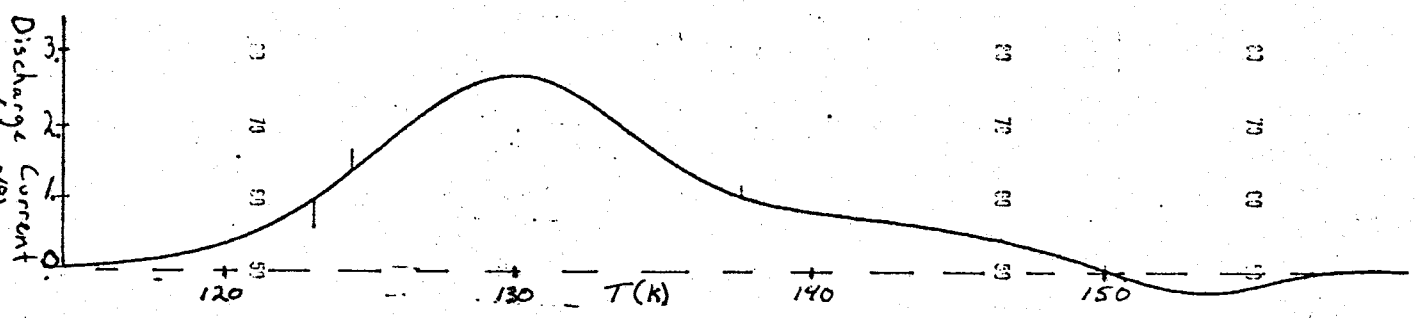

TSD spectrum of test D85
V_{ch} = 1500 V, β = 0.044 °/sec

The appearance of a current reversal without foils is contradictory to the above discussion on foil effects. However, the condition at sample-electrode interfaces may not be considered ideal in either the case of blocking foils or no blocking foils. The interplay of surface effects may result in a very complex TSD response. For example, removal of foils may alter the thickness of the air gap at interfaces

and possibly have the effect of increasing Townsend breakdown while the air gap may still effectively block recombination. This would result in a diffusion current (reversal) without foils. By the same token, the presence of foils may alter both the electrical field distribution and characteristics of the air gap and diminish breakdown and charge injection causing the absence of current reversals with foils.

The effect of blocking foils on the results presented here may not be interpreted accurately until more is known about the condition at the sample-foil-electrode interfaces. Given the theoretical treatment of van Turnhout (1975) a variety of conditions may be modeled and compared with results, possibly resulting in a clearer picture of the sample surface conditions and the effect of foils on TSD. It is unfortunate that an insulating material may not be evaporated on to the sample as is done with metalic electrodes. This would result in a nearly ideal case of a layered dielectric which may be modeled with much greater confidence.

APPENDIX IV

#308/7 (5/28/80) D-62-A 6/17/80

2 hr. chg. at -150. c 3 hr. heating rate

Only coldest peak Tp=-150.5

36 200.044

3.0e-12 5050.
4.0e-12 5030.
6.0e-12 5010.
6.0e-12 4990.
8.0e-12 4970.
9.0e-12 4950.
1.3e-11 4940.
1.6e-11 4915.
2.1e-11 4895.
2.8e-11 4880.
3.6e-11 4860.
4.7e-11 4840.
6.1e-11 4820.
7.6e-11 4800.
9.5e-11 4780.
1.16e-10 4760.
1.38e-10 4740.
1.59e-10 4720.
1.78e-10 4700.
1.93e-10 4680.
1.99e-10 4660.
1.98e-10 4640.
1.88e-10 4620.
1.71e-10 4600.
1.47e-10 4580.
1.2e-10 4560.
9.5e-11 4540.
7.1e-11 4520.
5.2e-11 4500.
3.7e-11 4480.
2.7e-11 4460.
1.9E-11 4435.
1.4e-11 4415.
1.1e-11 4400.
1.0e-11 4380.
8.0e-11 4350.

308/7-3 D68-A 7/1/80

.5 hr. 15 min. chg. at -145. C Vch=1500 V

3 HR. HEATING CYCLE

30 200.044
8.E-12 4960.
1.E-11 4945.
1.4E-11 4930.
1.9E-11 4910.
2.3E-11 4890.
2.9E-11 4870.
3.7E-11 4850.
4.9E-11 4830.
6.1E-11 4810.
7.5E-11 4790.
9.1E-11 4775.
1.09E-10 4750.
1.26E-10 4735.
1.43E-10 4715.
1.56E-10 4695.
1.65E-10 4680.
1.68E-10 4355.
1.64E-10 4635.
1.53E-10 4620.
1.36E-10 4595.
1.16E-10 4575.
9.4E-11 4560.
7.4E-11 4540.
5.4E-11 4520.
3.9E-11 4500.
2.7E-11 4475.
2.E-11 4455.
1.4E-11 4435.
1.1E-11 4410.
8.E-11 4390.

2 HR. 10 MIN CHG. AT -140.5 C Vch=1500 V
3 HR. HEATING CYCLE

27 200.044
9.E-12 4880.
1.2E-11 4860.
1.6E-11 4840.
2.E-11 4820.
2.5E-11 4800.
3.2E-11 4780.
3.8E-11 4760.
4.6E-11 4740.
5.5E-11 4720.
6.3E-11 4700.
7.E-11 4685.
7.5E-11 4665.
7.8E-11 4645.
7.8E-11 4625.
7.5E-11 4605.
7.E-11 4585.
6.2E-11 4565.
5.2E-11 4545.
4.4E-11 4525.
3.5E-11 4505.
2.6E-11 4485.
2.E-11 4465.
1.6E-11 4445.
1.3E-11 4420.
1.1E-11 4400.
1.1E-11 4380.
8.E-12 4360.

308/7-3 D71-A 7/10/80
6 HR. 45 MIN CHG AT -155. C Vch= 1500 V
3 HR. HEATING CYCLE

34 200.044
7.E-12 4990.
9.E-12 4980.
1.1E-11 4960.
1.5E-11 4940.
1.8E-11 4920.
2.4E-11 4900.
3.1E-11 4880.
4.2E-11 4860.
5.5E-11 4840.
7.1E-11 4820.
9.1E-11 4805.
1.15E-10 4790.
1.41E-10 4770.
1.7E-10 4750.
1.99E-10 4730.
2.28E-10 4710.
2.51E-10 4690.
2.67E-10 4670.
2.73E-10 4650.
2.68E-10 4630.
2.49E-10 4610.
2.21E-10 4590.
1.87E-10 4570.
1.5E-10 4550.
1.15E-10 4530.
8.4E-11 4510.
6.E-11 4490.
4.1E-11 4470.
2.9E-11 4450.
2.E-11 4425.
1.5E-11 4405.
1.1E-11 4390.
9.E-12 4360.
8.E-12 4340.

308/7-3 D72 A 7/13/80
17 HR. CHG AT -160 C Vch=1500 V
3 HR. HEATING CYCLE

35 200.044
6.E-12 4965.
1.E-11 4960.
1.2E-11 4940.
1.6E-11 4920.
2.1E-11 4900.
2.5E-11 4880.
3.3E-11 4860.
4.4E-11 4845.
5.7E-11 4825.
7.4E-11 4805.
9.4E-11 4785.
1.18E-10 4765.
1.44E-10 4745.
1.72E-10 4725.
2.01E-10 4710.
2.27E-10 4690.
2.49E-10 4670.
2.63E-10 4650.
2.68E-10 4630.
2.61E-10 4610.
2.44E-10 4590.
2.18E-10 4570.
1.85E-10 4550.
1.5E-10 4530.
1.17E-10 4510.
8.7E-11 4490.
6.4E-11 4470.
4.6E-11 4450.
3.3E-11 4420.
2.3E-11 4405.
1.7E-11 4380.
1.4E-11 4360.
1.2E-11 4340.
1.E-11 4320.
9.E-12 4300.

308/7-3 D73-A 7/18/80
24 HR. CHG. AT -165. C Vch=1500 V
3.HR. HEATING CYCLE

33 200.044
7.E-12 4970.
1.E-11 4950.
1.2E-11 4930.
1.7E-11 4910.
2.2E-11 4895.
2.8E-11 4875.
3.7E-11 4855.
5.E-11 4835.
6.6E-11 4820.
8.5E-11 4795.
1.11E-10 4775.
1.37E-10 4755.
1.68E-10 4735.
1.99E-10 4715.
2.31E-10 4700.
2.56E-10 4680.
2.76E-10 4655.
2.83E-10 4635.
2.77E-10 4620.
2.59E-10 4595.
2.3E-10 4575.
1.93E-10 4555.
1.54E-10 4540.
1.18E-10 4515.
8.6E-11 4495.
6.1E-11 4475.
4.3E-11 4455.
3.1E-11 4435.
2.2E-11 4410.
1.6E-11 4390.
1.2E-11 4370.
1.E-11 4350.
8.E-12 4325.

308/7 D-75 B 7/22/80

35 min chg. at -120 c
3 hr. heating cycle
28 200,046-135.0
4.0e-12 4300.
7.0e-12 4280.
8.0e-12 4260.
9.0e-12 4240.
1.1e-11 4220.
1.4e-11 4205.
1.8e-11 4170.
2.2e-11 4150.
2.7e-11 4130.
3.1e-11 4105.
3.7e-11 4080.
4.5e-11 4060.
5.2e-11 4030.
5.9e-11 4010.
6.7e-11 3990.
7.2e-11 3960.
7.3e-11 3940.
7.0e-11 3910.
6.3e-11 3890.
5.2e-11 3870.
3.9e-11 3840.
2.7e-11 3815.
1.9e-11 3790.
1.3e-11 3760.
1.0e-11 3740.
9.0e-12 3710.
8.0e-12 3690.
7.0e-12 3660.

308/7-3 D76-B 2/23/80

1 hr. 20 min chg at -125. Vch=1500 V

3 hr. heating cycle

```
  26 200.044
7.e-12 4260.
9.e-12 4240.
1.3e-11 4220.
1.5e-11 4200.
1.9e-11 4175.
2.3e-11 4150.
2.9e-11 4130.
3.5e-11 4105.
4.3e-11 4080.
5.2e-11 4060.
6.3e-11 4030.
7.5e-11 4010.
8.5e-11 3990.
9.3e-11 3960.
9.7e-11 3940.
9.4e-11 3910.
8.5e-11 3890.
7.2e-11 3860.
5.5e-11 3840.
4.0e-11 3810.
2.7e-11 3790.
2.e-11 3760.
1.5e-11 3740.
1.2e-11 3710.
1.1e-11 3690.
1.e-11 3660.
```

#308/7 D77B 7/25/80
12 HR. CHG. AT -129 C
3 HR HEATING CYCLE Vch=1500V
28 200.044
7.E-12 4330.
1.E-11 4310.
1.1E-11 4285.
1.3E-11 4265.
1.6E-11 4240.
2.E-11 4220.
2.3E-11 4200.
2.7E-11 4180.
3.3E-11 4155.
4.E-11 4130.
4.8E-11 4110.
5.6E-11 4085.
6.7E-11 4065.
8.E-11 4040.
9.1E-11 4015.
1.03E-10 3995.
1.12E-10 3965.
1.15E-10 3945.
1.1E-10 3915.
9.8E-11 3895.
8.E-11 3865.
6.E-11 3845.
4.1E-11 3820.
2.7E-11 3795.
1.9E-11 3765.
1.4E-11 3745.
1.2E-11 3715.
1.1E-11 3695.
1.E-11 3665.

308/7 F3 8/26/78
FULL CHG. 3 HR HEATING RATE

52 20
4.E-12 4935.
5.E-12 4910.
6.E-12 4895.
8.E-12 4875.
1.E-11 4865.
1.3E-11 4845.
1.6E-11 4825.
1.9E-11 4805.
2.4E-11 4785.
2.9E-11 4775.
3.6E-11 4755.
4.4E-11 4735.
5.3E-11 4715.
6.4E-11 4700.
7.6E-11 4680.
9.1E-11 4665.
1.06E-10 4645.
1.23E-10 4625.
1.40E-10 4610.
1.56E-10 4590.
1.7E-10 4570.
1.8E-10 4550.
1.86E-10 4535.
1.87E-10 4515.
1.83E-10 4495.
1.75E-10 4475.
1.65E-10 4460.
1.55E-10 4440.
1.47E-10 4420.
1.41E-10 4400.
1.35E-10 4380.
1.3E-10 4360.
1.24E-10 4340.
1.17E-10 4320.
1.09E-10 4300.
1.02E-10 4275.
9.4E-11 4250.
8.8E-11 4230.
8.3E-11 4210.
7.4E-11 4170.
7.1E-11 4150.
6.7E-11 4130.
6.2E-11 4110.
5.5E-11 4085.
4.8E-11 4060.
3.9E-11 4040.
3.0E-11 4020.
2.2E-11 3995.
1.5E-11 3970.
1.0E-11 3950.
6.E-12 3930.
4.E-12 3905.

66 200.043
3.E-12 5005.
3.E-12 4985.
4.E-12 4975.
6.E-12 4965.
7.E-12 4945.
9.E-12 4925.
1.2E-11 4905.
1.5E-11 4885.
1.9E-11 4875.
2.4E-11 4855.
2.9E-11 4835.
3.6E-11 4820.
4.4E-11 4805.
5.3E-11 4785.
6.3E-11 4765.
7.6E-11 4750.
9.E-11 4730.
1.05E-10 4710.
1.21E-10 4695.
1.38E-10 4675.
1.54E-10 4655.
1.68E-10 4640.
1.8E-10 4620.
1.88E-10 4600.
1.9E-10 4580.
1.88E-10 4560.
1.81E-10 4540.
1.70E-10 4520.
1.56E-10 4500.
1.43E-10 4480.
1.31E-10 4460.
1.2E-10 4440.
1.12E-10 4420.
1.06E-10 4400.
1.03E-10 4380.
9.8E-11 4360.
9.5E-11 4340.
9.1E-11 4320.
8.7E-11 4300.
8.2E-11 4270.
7.8E-11 4250.
7.3E-11 4230.
7.E-11 4210.
6.8E-11 4185.
6.6E-11 4165.
6.5E-11 4140.
6.3E-11 4120.
6.2E-11 4100.
5.9E-11 4080.
5.6E-11 4050.
5.1E-11 4030.
4.5E-11 4010.
3.9E-11 3980.
3.3E-11 3960.
2.8E-11 3935.
2.4E-11 3910.

2.E-11 3890.
1.7E-11 3870.
1.5E-11 3840.
1.3E-11 3820.
1.1E-11 3790.
9.E-12 3770.
8.E-12 3740.
7.E-12 3720.
5.E-12 3700.
4.E-12 3670.

58 200,044
6.E-12 4940.
8.E-12 4920.
1.E-11 4900.
1.2E-11 4885.
1.6E-11 4870.
2.E-11 4850.
2.5E-11 4835.
3.1E-11 4820.
3.8E-11 4800.
4.6E-11 4785.
5.6E-11 4765.
6.8E-11 4745.
8.1E-11 4725.
9.6E-11 4705.
1.13E-10 4690.
1.30E-10 4670.
1.49E-10 4655.
1.66E-10 4635.
1.81E-10 4615.
1.92E-10 4595.
1.97E-10 4575.
1.96E-10 4555.
1.89E-10 4535.
1.77E-10 4515.
1.62E-10 4495.
1.46E-10 4475.
1.32E-10 4460.
1.21E-10 4440.
1.14E-10 4415.
1.09E-10 4395.
1.04E-10 4355.
1.06E-10 4375.
1.02E-10 4335.
9.9E-11 4315.
9.6E-11 4295.
9.3E-11 4275.
8.9E-11 4255.
8.5E-11 4235.
7.9E-11 4210.
7.2E-11 4185
6.5E-11 4165.
6.1E-11 4145.
5.7E-11 4125.
5.4E-11 4095.
5.1E-11 4075.
4.7E-11 4055.
4.3E-11 4035.
3.8E-11 4005.
3.1E-11 3985.
2.7E-11 3965.
2.3E-11 3935.
1.9E-11 3915.
1.7E-11 3895.
1.4E-11 3865.
1.1E-11 3845.
9.E-12 3825.

7.E-12 3795.
6.E-12 3775.

FULL CHG 3 HR. HEATING CYCLE

60 200.044
5.E-12 4940.
6.E-12 4925.
8.E-12 4910.
1.1E-11 4890.
1.3E-11 4875.
1.7E-11 4860.
2.1E-11 4845.
2.6E-11 4825.
3.1E-11 4810.
3.8E-11 4795.
4.6E-11 4775.
5.6E-11 4765.
6.7E-11 4745.
8.0E-11 4730.
9.5E-11 4605.
1.12E-10 4685.
1.31E-10 4670.
1.50E-10 4650.
1.69E-10 4635.
1.88E-10 4615.
2.02E-10 4595.
2.12E-10 4575.
2.15E-10 4555.
2.11E-10 4535.
2.00E-10 4515.
1.84E-10 4495.
1.65E-10 4475.
1.47E-10 4460.
1.32E-10 4435.
1.20E-10 4415.
1.12E-10 4395.
1.04E-10 4375.
9.9E-11 4355.
9.3E-11 4335.
8.7E-11 4315.
8.2E-11 4290.
7.6E-11 4270.
7.2E-11 4250.
6.8E-11 4230.
6.5E-11 4210.
6.3E-11 4185.
6.3E-11 4160.
6.2E-11 4140.
6.0E-11 4120.
5.9E-11 4095.
5.5E-11 4070.
5.1E-11 4050.
4.6E-11 4030.
4.1E-11 4000.
3.5E-11 3980.
3.0E-11 3960.
2.5E-11 3930.
2.2E-11 3910.
1.9E-11 3890.
1.7E-11 3860.
1.4E-11 3840.

(continued)

```
1.1E-11 3820.
9.E-12 3790.
7.E-12 3770.
6.E-12 3740.
```

3 HR. HEATING RATE FULL CHARGE

```
 56 20
5.E-12 4910.
6.E-12 4890.
7.E-12 4880.
9.E-12 4860.
1.2E-11 4840.
1.6E-11 4825.
1.9E-11 4810.
2.4E-11 4790.
2.9E-11 4770.
3.5E-11 4755.
4.3E-11 4735.
5.2E-11 4720.
6.2E-11 4700.
7.5E-11 4680.
8.8E-11 4665.
1.04E-10 4645.
1.2E-10 4625.
1.36E-10 4605.
1.52E-10 4585.
1.64E-10 4565.
1.74E-10 4550.
1.79E-10 4530.
1.79E-10 4510.
1.75E-10 4490.
1.66E-10 4470.
1.57E-10 4450.
1.47E-10 4430.
1.38E-10 4410.
1.31E-10 4390.
1.24E-10 4370.
1.18E-10 4345.
1.13E-10 4325.
1.07E-10 4305.
1.0E-10 4285.
9.5E-11 4265.
8.9E-11 4245.
8.5E-11 4220.
8.2E-11 4200.
8.E-11 4175.
8.E-11 4155.
8.1E-11 4135.
8.E-11 4110.
7.8E-11 4085.
7.3E-11 4065.
6.7E-11 4045.
5.9E-11 4020.
5.3E-11 3995.
4.6E-11 3975.
4.0E-11 3945.
3.3E-11 3925.
2.6E-11 3900.
2.2E-11 3875.
1.6E-11 3855.
1.3E-11 3830.
1.E-11 3805.
9.E-12 3785.
```

59 200.044
6.E-12 4910.
7.E-12 4890.
9.E-12 4870.
1.1E-11 4860.
1.3E-11 4840.
1.7E-11 4820.
2.0E-11 4800.
2.6E-11 4790.
3.1E-11 4770.
3.8E-11 4750.
4.6E-11 4730.
5.6E-11 4710.
6.7E-11 4690.
8.0E-11 4675.
9.5E-11 4660.
1.11E-10 4640.
1.28E-10 4620.
1.46E-10 4600.
1.64E-10 4580.
1.79E-10 4560.
1.92E-10 4540.
2.00E-10 4520.
2.05E-10 4500.
2.06E-10 4480.
2.03E-10 4460.
1.97E-10 4440.
1.91E-10 4420.
1.85E-10 4400.
1.79E-10 4380.
1.73E-10 4360.
1.67E-10 4335.
1.60E-10 4315.
1.52E-10 4295.
1.45E-10 4275.
1.37E-10 4250.
1.29E-10 4230.
1.20E-10 4210.
1.12E-10 4185.
1.05E-10 4165.
9.9E-11 4140.
9.5E-11 4120.
8.9E-11 4100.
8.1E-11 4075.
7.0E-11 4050.
5.8E-11 4030.
4.8E-11 4005.
3.8E-11 3985.
3.1E-11 3960.
2.5E-11 3940.
2.1E-11 3910.
1.6E-11 3890.
1.2E-11 3870.
9.E-12 3840.
8.E-12 3820.
6.E-12 3795.

FULL CHG. 3 HR. HEATING CYCLE

57 200.044
5.E-12 4955.
6.E-12 4945.
7.E-12 4925.
9.E-12 4905.
1.E-11 4895.
1.3E-11 4875.
1.6E-11 4855.
2.1E-11 4835.
2.5E-11 4825.
3.1E-11 4805.
3.9E-11 4785.
4.7E-11 4765.
4.9E-11 4755.
5.7E-11 4745.
7.E-11 4725.
8.3E-11 4710.
9.8E-11 4695.
1.17E-10 4675.
1.36E-10 4655.
1.57E-10 4635.
1.78E-10 4615.
1.96E-10 4595.
2.11E-10 4575.
2.22E-10 4555.
2.26E-10 4535.
2.24E-10 4515.
2.16E-10 4495.
2.04E-10 4475.
1.91E-10 4455.
1.77E-10 4435.
1.65E-10 4415.
1.55E-10 4395.
1.45E-10 4375.
1.37E-10 4355.
1.29E-10 4335.
1.14E-10 4295.
1.07E-10 4270.
1.01E-10 4245.
9.6E-11 4225.
9.1E-11 4205.
8.9E-11 4185.
8.5E-11 4160.
8.2E-11 4135.
7.9E-11 4115.
7.5E-11 4095.
7.0E-11 4075.
6.3E-11 4045.
5.5E-11 4025.
4.7E-11 4005.
3.7E-11 3985.
3.E-11 3955.
2.2E-11 3935.
1.6E-11 3905.
1.2E-11 3885.
8.E-12 3865.
6.E-12 3835.

4.E-12 3815.

FULL CHG. 12 HR. HEATING CYCLE

36120
8.E-13 5105.
1.3E-12 5080.
1.7E-12 5055.
9.E-13 5030.
2.7E-12 5025.
3.9E-12 5000.
5.3E-12 4970.
7.7E-12 4950.
1.02E-11 4920.
1.35E-114890.
1.79E-11 4855.
2.29E-11 4830.
2.8E-11 4805.
3.5E-11 4775.
4.28E-11 4740.
5.09E-11 4710.
5.89E-11 4680.
6.24E-11 4650.
5.6E-11 4620.
4.02E-11 4590.
2.63E-11 4565.
1.96E-11 4535.
1.59E-11 4505.
1.31E-11 4475.
1.1E-11 4445.
9.2E-12 4415.
8.E-12 4385.
6.9E-12 4355.
5.1E-12 4325.
5.9E-12 4325.
5.E-12 4295.
4.4E-12 4255.
1.2E-12 4255.
4.E-12 4225.
3.6E-12 4195.
3.3E-12 4155.

#308/7 F-17 5/17/80
FULL CHG. 12 HR. HEATING CYCLE

421200.044
5.E-13 5205.
7.E-13 5185.
8.E-13 5160.
8.E-13 5135.
1.1E-12 5110.
1.7E-12 5085.
2.3E-12 5060.
3.2E-12 5030.
4.E-12 5010.
5.4E-12 4980.
7.2E-12 4955.
9.9E-12 4930.
1.29E-11 4900.
1.72E-11 4870.
2.24E-11 4840.
2.77E-11 4810.
3.84E-11 4780.
4.25E-11 4745.
5.1E-11 4715.
5.92E-11 4680.
6.26E-11 4650.
5.63E-11 4620.
4.22E-11 4595.
2.68E-11 4570.
1.97E-11 4535.
1.62E-11 4510.
1.36E-11 4480.
1.17E-11 4450.
1.0E-11 4420.
8.8E-12 4390.
7.3E-12 4360.
6.3E-12 4330.
5.4E-12 4295.
4.7E-12 4265.
4.4E-12 4235.
3.8E-12 4200.
3.5E-12 4165.
3.2E-12 4130.
3.2E-12 4095.
2.9E-12 4065.
2.7E-12 4025.
2.7E-12 3995.

#308/7 F-18 6/3/80
FULL CHG. 3 HR. HEATING CYCLE

40 30
6.E-12 4980.
1.E-11 4935.
1.4E-11 4910.
1.9E-11 4885.
2.8E-11 4855.
3.9E-11 4835.
5.3E-11 4805.
7.3E-11 4775.
9.6E-11 4745.
1.23E-10 4720.
1.51E-10 4690.
1.78E-10 4665.
2.01E-10 4635.
2.14E-10 4605.
2.14E-10 4580.
2.01E-10 4550.
1.73E-10 4520.
1.38E-10 4490.
9.8E-11 4455.
6.3E-11 4420.
3.8E-11 4390.
2.2E-11 4360.
1.4E-11 4330.
1.1E-11 4300.
1.1E-11 4260.
1.4E-11 4230.
1.7E-11 4195.
2.4E-11 4165.
3.3E-11 4130.
4.8E-11 4095.
6.8E-11 4060.
9.3E-11 4025.
1.16E-10 3990.
1.30E-10 3955.
1.25E-10 3920.
1.E-10 3880.
6.4E-11 3845.
3.1E-11 3810.
1.2E-11 3770.
5.E-12 3730.

308/7 (5/28/80) F-19 6/5/80
Full chg. 3 hr. heating rate 32 hr. cooling rate

62 200.044-166.5
4.0e-12 5000.
5.0e-12 4985.
6.0e-12 4970.
7.0e-12 4950.
9.0e-12 4935.
1.2e-11 4915.
1.5e-11 4900.
2.1e-11 4885.
2.5e-11 4865.
3.1e-11 4850.
4.1e-11 4830.
5.2e-11 4810.
6.4e-11 4790.
7.9e-11 4775.
9.6e-11 4750.
1.16e-10 4735.
1.36e-10 4710.
1.56e-10 4695.
1.77e-10 4680.
1.96e-10 4660.
2.12e-10 4640.
2.23e-10 4620.
2.28e-10 4600.
2.26e-10 4580.
2.17e-10 4560.
2.00e-10 4540.
1.78e-10 4520.
1.50e-10 4500.
1.23e-10 4480.
9.6e-11 4460.
7.2e-11 4440.
5.1e-11 4420.
3.6e-11 4395.
2.5e-11 4375.
1.8e-11 4355.
1.3e-11 4335.
1.1e-11 4310.
1.1e-11 4290.
1.2e-11 4270.
1.2e-11 4245.
1.5e-11 4225.
1.8e-11 4200.
2.2e-11 4180.
2.7e-11 4160.
3.4e-11 4135.
4.3e-11 4120.
5.5e-11 4090.
6.8e-11 4070.
8.3e-11 4040.
9.9e-11 4020.
1.15e-10 4000.
1.26e-10 3970.
1.29e-10 3950.
1.25e-10 3930.
1.11e-10 3900.
9.0e-11 3880.

```
6.6e-11 3850.
4.3e-11 3830.
2.5e-11 3800.
1.3e-11 3780.
6.0e-12 3750.
3.0e-12 3730.
```

61 200.044
6.E-12 4990.
7.E-12 4970.
9.E-12 4950.
1.1E-11 4940.
1.4E-11 4920.
1.9E-11 4900.
2.4E-11 4890.
3.1E-11 4870.
4.E-11 4850.
5.2E-11 4830.
6.6E-11 4810.
8.2E-11 4790.
1.02E-10 4775.
1.24E-10 4755.
1.5E-10 4735.
1.76E-10 4715.
2.02E-10 4695.
2.25E-10 4675.
2.44E-10 4655.
2.55E-10 4635.
2.57E-10 4615.
2.49E-10 4595.
2.31E-10 4575.
2.04E-10 4555.
1.72E-10 4535.
1.37E-10 4515.
1.04E-10 4500.
7.6E-11 4475.
5.2E-11 4460.
3.5E-11 4435.
2.3E-11 4415.
1.5E-11 4395.
9.E-12 4375.
6.E-12 4355.
4.E-12 4330.
3.E-12 4310.
2.E-12 4290.
3.E-12 4265.
4.E-12 4245.
4.E-12 4225.
5.E-12 4200.
6.E-12 4180.
9.E-12 4155.
1.2E-11 4135.
1.7E-11 4110.
2.3E-11 4009.
3.E-11 4065.
3.9E-11 4045.
4.9E-11 4020.
6.1E-11 3995.
7.E-11 3975.
7.5E-11 3945.
7.6E-11 3925.
7.1E-11 3895.
6.1E-11 3875.
4.8E-11 3850.

F-21 (Continued)

```
3.4E-11 3825.
2.2E-11 3800.
1.3E-11 3775.
8.E-12 3750.
4.E-12 3725.
```

#307/09-slice 5 D-81 10/11/80
3 hr. charge at -150.5 deg c
NO FOILS 3 hr. heating rate

44 200.044
1.1e-11 4940.
1.0e-11 4920.
1.9e-11 4900.
2.5e-11 4890.
3.2e-11 4870.
4.4e-11 4850.
5.3e-11 4830.
6.9e-11 4810.
8.2e-11 4790.
1.01e-10 4770.
1.18e-10 4750.
1.39e-10 4730.
1.57e-10 4710.
1.75e-10 4690.
1.91e-10 4670.
2.02e-10 4650.
2.1e-10 4630.
2.1e-10 4610.
2.06e-10 4590.
1.97e-10 4570.
1.84e-10 4550.
1.69e-10 4530.
1.52e-10 4510.
1.36e-10 4490.
1.21e-10 4470.
1.08e-10 4450.
9.8e-11 4430.
9.0e-11 4410.
8.4e-11 4390.
7.8E-11 4370.
7.4E-11 4350.
7.7E-11 4320.
6.7E-11 4300.
6.3E-11 4280.
5.5E-11 4260.
5.4E-11 4240.
4.3E-11 4210.
4.7E-11 4190.
3.6E-11 4170.
2.6E-11 4150.
2.0E-11 4120.
1.5E-11 4100.
1.1E-11 4080.
8.E-12 4050.

308/09-SLICE 5 D-80 10/9/80
2 HR. CHARGE AT -150 C
NO FOILS 3 HR. CHARGE

47 200.044
8.E-12 5000.
1.1E-11 4980.
1.0E-11 4960.
1.5E-11 4950.
2.0E-11 4930.
2.6E-11 4910.
3.4E-11 4890.
4.3E-11 4870.
5.4E-11 4850.
6.8E-11 4830.
8.2E-11 4820.
1.01E-10 4800.
1.2E-10 4780.
1.33E-10 4760.
1.53E-10 4740.
1.76E-10 4720.
1.91E-10 4700.
2.03E-10 4680.
2.12E-10 4660.
2.14E-10 4640.
2.10E-10 4620.
1.94E-10 4600.
1.90E-10 4580.
1.7E-10 4560.
1.57E-10 4540.
1.4E-10 4520.
1.21E-10 4500.
1.12E-10 4480.
1.03E-10 4460.
9.2E-11 4430.
8.4E-11 4410.
7.8E-11 4390.
7.5E-11 4370.
7.2E-11 4350.
7.1E-11 4330.
6.3E-11 4310.
6.5E-11 4290.
6.3E-11 4260.
5.8E-11 4240.
5.2E-11 4220.
5.2E-11 4200.
4.3E-11 4180.
3.8E-11 4150.
3.E-11 4130.
2.E-11 4110.
9.2E-12 4080.
4.6E-12 4060.

308/09-SLICE 5 D-85 10/31/80

6 1/2 HR. CHARGE AT -149. C

NO FOILS 3 HR HEATING RATE

```
  49 200.044
1.E-11 5010.
1.3E-11 4990.
1.6E-11 4970.
2.2E-11 4960.
2.6E-11 4940.
3.2E-11 4920.
4.1E-11 4900.
5.1E-11 4880.
6.4E-11 4870.
7.9E-11 4850.
9.7E-11 4830.
1.16E-10 4810.
1.38E-10 4790.
1.60E-10 4770.
1.84E-10 4750.
2.06E-10 4730.
2.27E-10 4710.
2.46E-10 4690.
2.59E-10 4670.
2.68E-10 4650.
2.71E-10 4630.
2.66E-10 4610.
2.55E-10 4590.
2.41E-10 4570.
2.21E-10 4550.
1.99E-10 4530.
1.79E-10 4510.
1.58E-10 4490.
1.39E-10 4470.
1.23E-10 4450.
1.10E-10 4430.
1.0E-10 4410.
9.2E-11 4390.
8.6E-11 4370.
8.2E-11 4350.
7.8E-11 4330.
7.4E-11 4310.
7.1E-11 4280.
6.7E-11 4260.
6.3E-11 4240.
5.9E-11 4220.
5.6E-11 4200.
4.9E-11 4180.
4.3E-11 4150.
3.7E-11 4130.
3.E-11 4110.
2.2E-11 4080.
1.4E-11 4060.
5.E-12 4040.
```

308/7 -1 D-36 11/15/79
4 HR. CHARGE AT -150 C 3 HR HEATING CYCLE
COPPER/TEFLON FOILS

46 200,044
1.3E-11 4855.
1.6E-11 4835.
2.1E-11 4815.
2.5E-11 4800.
3.1E-11 4785.
3.8E-11 4765.
4.6E-11 4745.
5.4E-11 4725.
6.3E-11 4705.
7.4E-11 4695.
8.6E-11 4675.
1.E-10 4655.
1.12E-10 4635.
1.27E-10 4615.
1.39E-10 4595.
1.5E-10 4575.
1.59E-10 4555.
1.65E-10 4535.
1.68E-10 4520.
1.69E-10 4500.
1.67E-10 4485.
1.63E-10 4465.
1.59E-10 4445.
1.55E-10 4420.
1.51E-10 4400.
1.46E-10 4385.
1.41E-10 4360.
1.34E-10 4335.
1.25E-10 4320.
1.16E-10 4295.
1.05E-10 4275.
9.5E-11 4255.
8.5E-11 4235.
7.6E-11 4215.
6.8E-11 4190.
6.1E-11 4170.
5.5E-11 4145.
5.E-11 4125.
4.4E-11 4105.
3.8E-11 4080.
3.2E-11 4055.
2.6E-11 4035.
2.E-11 4015.
1.5E-11 3990.
1.1E-11 3970.
8.E-12 3945.

308/7-1 D-39 11/19/79
4 HR. CHARGE AT -150 C TEFLON/COPPER FOILS
3 HR. HEATING CYCLE

45 200.044
8.E-12 4875.
1.E-11 4855.
1.3E-11 4835.
1.7E-11 4820.
2.1E-11 4805.
2.4E-11 4785.
3.E-11 4765.
3.5E-11 4745.
4.2E-11 4725.
5.E-11 4710.
6.E-11 4695.
7.E-11 4675.
8.1E-11 4655.
9.3E-11 4635.
1.06E-10 4615.
1.19E-10 4595.
1.31E-10 4575.
1.42E-10 4555.
1.5E-10 4535.
1.56E-10 4520.
1.58E-10 4500.
1.59E-10 4480.
1.55E-10 4460.
1.52E-10 4440.
1.47E-10 4420.
1.42E-10 4390.
1.37E-10 4375.
1.32E-10 4355.
1.26E-10 4335.
1.18E-10 4315.
1.1E-10 4295.
1.01E-10 4275.
9.1E-11 4250.
8.0E-11 4225.
7.1E-11 4205.
6.E-11 4185.
5.2E-11 4165.
4.4E-11 4140.
3.7E-11 4120.
3.1E-11 4100.
2.6E-11 4075.
2.1E-11 4050.
1.7E-11 4030.
1.2E-11 4005.
9.E-12 3980.

308/7 -1 D-41 11/30/79
4 HR, HHARGE AT -150 C TEFLON/COPPER FOILS
3 HR HEATING CYCLE

46 200.044
9.E-12 4880.
1.2E-11 4860.
1.5E-11 4845.
1.9E-11 4825.
2.4E-11 4810.
2.8E-11 4790.
3.4E-11 4770.
4.1E-11 4750.
5.1E-11 4730.
5.9E-11 4710.
6.9E-11 4695.
8.0E-11 4675.
9.2E-11 4655.
1.04E-10 4635.
1.18E-10 4620.
1.3E-10 4600.
1.41E-10 4580.
1.49E-10 4560.
1.55E-10 4540.
1.57E-10 4520.
1.57E-10 4500.
1.55E-10 4480.
1.51E-10 4460.
1.46E-10 4440.
1.43E-10 4420.
1.39E-10 4400.
1.36E-10 4380.
1.31E-10 4360.
1.26E-10 4340.
1.21E-10 4320.
1.14E-10 4290.
1.07E-10 4275.
9.9E-11 4250.
9.E-11 4230.
7.9E-11 4210.
6.9E-11 4190.
6.0E-11 4165.
5.1E-11 4145.
4.3E-11 4120.
3.6E-11 4100.
3.E-11 4075.
2.4E-11 4055.
1.8E-11 4030.
1.4E-11 4010.
1.1E-11 3985.
8.E-12 3965.

✓ D-62-A
✓ D 68-A
✓ D 69-A
✓ D 71-A
✓ D 72-A
✓ D 73-A
✓ D75-B
✓ D76-B
✓ D77-B

D-81 ✓
80 ✓
85 ✓
36 ✓
39 ✓
41 ✓

✓ F3
✓ 5
✓ 6
✓ 7
✓ 9
✓ 10
✓ 11
✓ 16
✓ 17
✓ 18
✓ 19
✓ 21

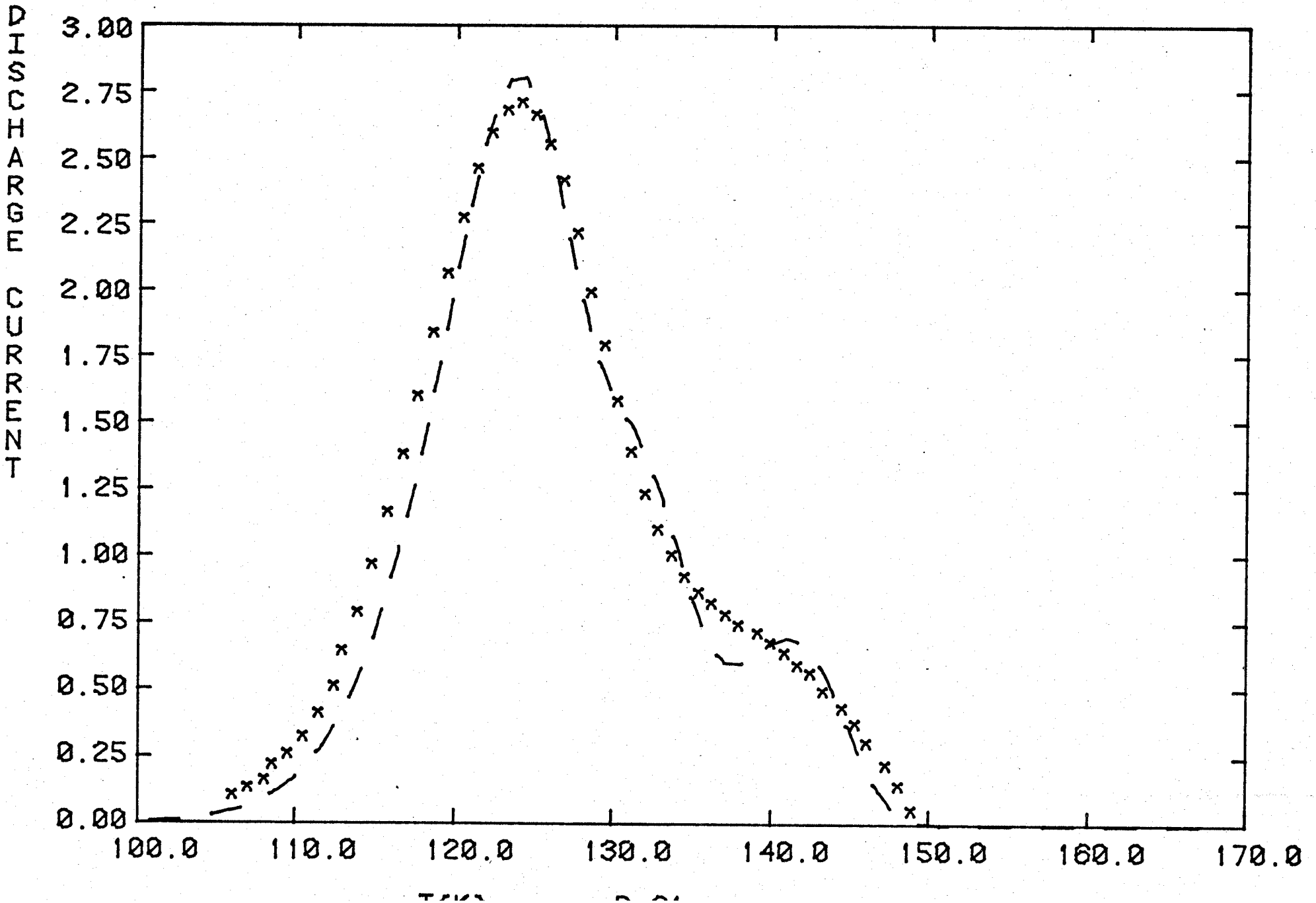
DISCHARGE CURRENT
3.00
2.75
2.50
2.25
2.00
1.75
1.50
1.25
1.00
0.75
0.50
0.25
0.00
100.0
110.0
120.0
130.0
140.0
150.0
160.0
170.0